Manuscript Details

Manuscript number	SG_2018_94_R1
Title	Emplacement modes of the Ladinian plutonic rocks of the Dolomites: insights from Anisotropy of Magnetic Susceptibility
Article type	Original article

Abstract

In the Dolomites (Eastenr Southern Alps, Italy), a diffuse Middle Triassic igneous activity is now present mostly as lava flow and pyroclastic successions, with rare shallow-depth intrusive bodies cropping out at Predazzo, Monzoni and Cima Pape areas. In this work, the emplacement modes of the Predazzo and Monzoni bodies were investigated by means of petrographic and anisotropy of magnetic susceptibility (AMS) data coupled with a field geological study. The presence of intrusive rocks in between these two bodies and the continuity of the metamorphic aureola from west of the Predazzo to east of the Monzoni body suggest that they are parts of a ~20 km wide SW-NE oriented continuous pluton, sub-parallel to Ladinian strike-slip faults. AMS and petrographic data from the Predazzo body are consistent with a multistage ring-dyke emplacement mode, with areas of upward flow of the magma located in the NE and SW part of the intrusion, whereas in the southern sector of the pluton our data suggest prevalently horizontal flows. In general, the Predazzo sheets indicate either upward magma flow or along-strike lateral magma transport, and the round shape suggests no influence of Ladinian tectonic structures. On the contrary, the ENE-WSW elongated shape of the Monzoni body was controlled by the occurrence of strike-slip faults associated with Ladinian-tectonics, the feeder being likely located at the NE edge of the body. However, the absence of deformation at the field- and micro-scale is consistent with a post Ladinian-tectonics timing of emplacement, as for the Predazzo pluton.

Keywords	Dolomites, anisotropy of magnetic susceptibility, pluton, Predazzo, Monzoni, mode of emplacement

Corresponding Author	Eugenio Carminati
Corresponding Author's Institution	Sapienza Università di Roma
Order of Authors	Hassan Abbas, Maria Michail, Francesca Cifelli, massimo mattei, Piero Gianolla, Michele Lustrino, Eugenio Carminati

Suggested reviewers	Carles Soriano, Teresa Román-Berdiel, Nereo Preto, Hannah Pomella

Submission Files Included in this PDF

File Name [File Type]

Abbas-cover letter.doc [Cover Letter]

Abbas et al-reply letter.doc [Response to Reviewers]

Abbas-Highlights.docx [Highlights]

Abbas et al_text and figures-REV.docx [Manuscript File]

Abbas et al_text and figures-REV-changes-highlighted.docx [Supporting File]

To view all the submission files, including those not included in the PDF, click on the manuscript title on your EVISE Homepage, then click 'Download zip file'.

DIPARTIMENTO DI SCIENZE DELLA TERRA
UNIVERSITA' LA SAPIENZA - ROMA

Roma, 9th May 2018

Dear Editor of *Journal of Structural Geology*,

please consider the revised manuscript "**Emplacement modes of the Ladinian plutonic rocks of the Dolomites: insights from Anisotropy of Magnetic Susceptibility** " by Hassan Abbas and coauthors.

Please send correspondence to:

Dr Eugenio Carminati
Dipartimento di Scienze della Terra
Università degli Studi di Roma "La Sapienza"
P.le Aldo Moro 5
I-00185 Roma
Italia

Tel.: ++39-06-49914950
Fax: ++39-06-4454729
Email: eugenio.carminati@uniroma1.it

I thank you in advance for kind attention.

Yours sincerely

Eugenio Carminati

To the kind attention of

Prof. Ian Alsop
Editor of Journal of Structural Geology

Dear Editor,

We thank you and the reviewers (Teresa Román-Berdiel and an anonymous referee) for your efforts to improve the quality of our manuscript, providing constructive criticisms. Below it follows how we answered to the criticisms and suggestions of the reviewer. We fulfilled all the requests. The answers to the reviewers' comments are in bold.

We are confident that this revised version of the manuscript will satisfy the standards required by the Journal of Structural Geology.

Best regards

Eugenio Carminati*

*Corresponding Author contact details

Prof. Eugenio Carminati,
Dipartimento di Scienze della Terra
Sapienza Università di Roma
P.le Aldo Moro, 5
00185 Roma, Italy
Tel ++39(0)649914950
Fax ++39(0)64454729
E-mail: eugenio.carminati@uniroma1.it

Reviewer #1 Teresa Román-Berdiel

In this manuscript, the authors present the structural study of two intrusive bodies by means of AMS analysis and petrographic observations in thin section.

This is a new study based on AMS technique, and its interest lie in the use of AMS to decipher the mode of emplacement of intrusive bodies in the Dolomites. The paper is a new evidence of the validity of the method for unravel the mode of emplacement of igneous bodies with no evidences of strain or mineral preferred orientation in outcrop. The paper is the international interest in the field of AMS technique and for the knowledge of this region of the Alps.

We thank the reviewer for her positive comments.

The article is clear and well organized. However, I do not end up agreeing with the interpretation. There are some points that can be clarified and improved, mainly concerning the illustration of petrographic description. A new figure with photographs of thin sections is necessary to illustrate the petrographic description (section 4.1 and Appendix). Some aspects of the description of the results should also be improved. Do you observe preferred orientation of minerals in thin section? This should be described and showed in some photograph. This is a clue point in the interpretation of AMS results. The mineralogy of the described rocks (Appendix) is dominated by paramagnetic minerals, and the preferred orientation of these minerals must be compared with paramagnetic fabrics obtained. The preferred orientation of paramagnetic minerals must be coherent with the mode of emplacement proposed. Opaque minerals occur as subhedral occupying interstitial position (Appendix). If ferromagnetic and paramagnetic subfabrics do not agree there is most probably that opaque (ferromagnetic) minerals crystallize latter and can be interpreted in other terms, given information regarding a late event in the emplacement process.

We improved the petrographic description, as also asked by reviewer 2, and added a figure (figure 6 in the revised manuscript) showing preferred orientation of minerals.

Description of results about scalar parameters and their relationship (P’, Km) must be described in the result section. I recommended to add the diagram Km-Pj in figure 7.

We added P’-km plot in Figure 7 (T-P’ was removed).

Below I indicate a series of comments that I consider necessary to improve the final presentation of this article. Please see also the annotations made directly in the text.

All the requests were satisfied.

Line 87 - Is “Stava line” in figure 2? It should be.

Stava line has been labelled.

Please use the standard symbol for thrusts in figure 2.

Done

Line 154 - Bellerophon Formation does not appear in figure 3, it should be, if possible.

Done

Line 193 - Stava, Trodena and Cavalase Lines should be in figure 2, if possible.

Stava line has been labelled. We added a simplified tectonic map (Fig. 2a in the revised manuscript) showing Trodena and Cavalese lines, not included in the original Fig. 2 (now 2b).

Line 206 - Can we see radial pattern of Ladinian mafic volcanic dykes in any figure?

The radial pattern can be seen in Fig. 2 around the Predazzo body and in fig. 4a.

I recommended to include a new figure with field photographs showing the main types of rocks sampled and described in sections 2.3 and 2.4

We included new field pics (Figs. 6a and 6b in the revised manuscript) showing the elongated shape of the Monzoni pluton and anisotropic fabric in granite.

Lines 244-251 - Please refer to figures in section 2.5

OK Done

Please add in Table I standard deviation for Km and put all Km values in the same power of 10 (normally 10^{-6} SI).

We added the standard deviation for Km but we didn't use the same power for all the sites because the range of magnetic susceptibility values is too big.

Please add in table caption of Table I "std: standard deviation"

Done

Line 273 - How many thin sections has been analyzed? Please indicate the number.

The number (29) is now indicated.

Line 338 – PR 10? Do you mean PA10?

Yes thanks.

Line 346 - Do you observe preferred orientation of minerals in thin section? This should be described and showed in some photograph.

Yes, we observed preferred orientation of minerals, as shown in the new Fig. 6c,d,e,f and now discussed in the text.

Add “a” and “b” for each part of figures in figures 4 and 5.

We corrected the figures adding “a” and “b”

In figure 5 – Please add “Monzoni” in the map Hassan, please correct the figures

We added “Monzoni” in the map.

In figure 8 there are two “i” and the “l” is missing.

OK, corrected

In figure 9 add a hyphen to separate the site number from the sample number.

Done

In general, I advise to refer to the figures more precisely in the text.

Thanks to the suggestions of the reviewer we quoted the figures mor precisely.

Homogenize when writing the name of monzonitic units. Always write with uppercase or lowercase, in section 2 it is write in lowercase, in section 4 it is write in uppercase.

OK, done

Homogenize also: M1, M2, M3 or 1, 2, 3 (in section 2 it is write monzonitic unit M1, M2, M3; in section 4 it is write Monzonitic Unit 1, 2, 3; in figure 4 it is write Monzonitic unit 1, 2, 3).

OK, done

Lines 427-429 – Author explain that in samples where the HF-paramagnetic fraction is significant (>50%) there is a good correlation between low-field and high-field (ferromagnetic and paramagnetic) magnetic ellipsoids. The high-field paramagnetic sub-fabric obtained in samples where paramagnetic fraction is lower must be also interpreted in terms of emplacement mode.

Unfortunately, in samples where the paramagnetic fraction is very low, its orientation cannot be determined with the necessary accuracy (this is now specified in the text). Unfortunately, the request of the reviewer cannot be fulfilled.

Line 451 – Do you refer to Monzonitic unit 3? Does site PA11 belong to the Predazzo pluton?

Yes, it belongs to the Predazzo pluton. The text is now corrected accordingly.

Line 517 - It is the first time do you described results about P parameter. This information must be described in results section.

We added a sentence in text (result section).

Table 1 - Use one of the two scalar parameters (P or Pj), preferably Pj. One is enough.

We removed P (and related standard deviation) from the table

Line 521 - Information about relationship between Km and Pj must be described in results section before.

We added a sentence in text (results section).

I recommended to add the diagram Km-Pj in figure 7.

Done

Replace P' by Pj in diagram Pj-T of figure 7.

Done

Line 523 – "…the orientation of dykes (mainly trending NNW-SSE) crosscutting intrusive rocks …" In section 2.3 you described mainly radial pattern for dykes, please clarity.

We have clarified the text. The radial pattern was postulated by Doglioni (1983). This is now clearly explained. As shown in Fig. 4, the dykes around the Predazzo pluton show variable orientations, with a prevalence of NNW-SSE oriented. This is our observation, as specified in the text.

531-534 –A final figure showing a scketch of the emplacement model can help.

A final figure with the emplacement models have been added (new Fig. 11).

Reviewer #2

Dear authors, dear editors

I went carefully throughout the manuscript entitled "Emplacement modes of the Ladinian plutonic rocks of the Dolomites: insights from Anisotropy of Magnetic Susceptibility", focusing mainly on regional geology, correlation and the stratigraphy related to this study. My main research field is not structural geology nor it is igneous petrology, thus, I cannot comment too much on these two aspects.
This works is relevant with respect to a long-lasting debate on the nature of Triassic syndepositional tectonics and volcanism in the Dolomites. Despite decades of studies, this debate is far from settled, and the application of a new method of investigation (the study of magnetic anisotropies in plutonic rocks) brought to a true and welcome addition of completely new data.
With this new approach, the authors were able to pin down firmly that (1) the emplacement of the plutons followed the main Triassic tectonic phase, and (2) there where no strike-slip movements along the main Triassic tectonic lineage since the Late Ladinian (age of plutons emplacement). In my view, these results are very relevant for the reconstruction of the geologic history in a key area for the Triassic, and bear relevance for the still largely incomplete understanding we have of the geodynamic evolution of the western Tethys area during the Mesozoic.
Overall, I found the manuscript well written and easy to read. I have annotated some inconsistencies or formal problems in the way biostratigraphic or lithostratigraphic units are described, but these are things that can be easily fixed. Instances of incorrect nomenclature are marked in the commented manuscript.
We thank the reviewer for his/her positive comments.

In terms of the overall manuscript organization, I have only a few comments.
(1) meaning of Ladinian tectonics.
In the introduction, a nice, complete and synthetic explanation of the many ways the Triassic syndepositional tectonic structures of the Dolomites were interpreted is given. Later on (chapter 2.2 Ladinian tectonics in the Dolomites) only the sinistral strike-slip interpretation is considered as a base for data interpretation. This is illogical and at the same time hard to follow. If it is the author's point that only this interpretation of the Ladinian tectonics of the Dolomites is acceptable, it must be discussed somewhere, and other models should be excluded with some argumentation. If otherwise all other interpretations are outdated, there would have be no point in listing them in the introduction, and the whole problem could be dismissed by means of a few references.
This is quite important for the logical flux of the text. Later on (e.g., line 498), locally extensional features (open fractures filled by magmatic dykes) are related to strike-slip tectonics, but the reader cannot understand why other possible tectonic models are being discarded at this point, where no direct evidence of strike-slip is given. Other similar instances occur later in the text.
We agree with the reviewer. In the introduction, after introducing all the proposed models, we explain that models involving subduction (2,4,9) are not coherent with the geological context of the Southern Alps that shows no evidence of volcanic arcs or oceanic subduction. The other models are consistent with geodynamic scenarios involving extensional tectonics, either controlled by rifting or strike-slip tectonics. The recognition of Middle Triassic NE-SW strike-slip faults in the Dolomites (e.g., Doglioni 1984a) testifies for the importance of wrench tectonics in this period. This should help the reader to understand the following of the paper.

(2) Separation of data and discussions
Albeit a clear separation of background information, data and interpretations is kept in the manuscript, some mixing sneaked in into the discussions.
- The opening statements ("The AMS technique provides a quick and accurate determination...") may better fit into the introductory or methods chapters.
We agree. The statement has been moved to the methods section.

- Microstructures are described as purely magmatic in the discussion as a premise to the interpretation of magnetic foliations – lineations, but these microstructures are not shown and the reader could not understand why they should be magmatic and not younger. Information on this may be inferred indirectly from the sample descriptions in the appendix, but this description and inference should be in part moved into the main text, along with a selection of images from thin sections.
As also suggested by reviewer 1 we better explained this point (moving some info from appendix to text in the results section) and added a figure (Fig. 6 in the revised manuscript) including photographs of magmatic structures at the meso- and micro-scale.

In summary, this is a welcome and new contribution to the understanding of the Western Tethys region. This region was tectonically active for hundreds of million years between the Varisican and Alpine orogeneses, but so far there isn't a universally accepted geodynamic model. This work provides strong evidence about the temporal relationships between magmatic activity and tectonism. My evaluation of the manuscript is overall positive.
Thanks to the reviewer for the time spent evaluating our manuscript and providing constructive criticisms.

- Emplacement of Triassic Predazzo and Monzoni plutons (Dolomites) is investigated
- Petrographic and anisotropy of magnetic susceptibility (AMS) data are used
- Middle Triassic structures controlled plutons emplacement modes
- Predazzo body was emplaced as a multistage ring-dyke complex
- Monzoni emplacement was controlled by a Ladinian strike-slip fault

Emplacement modes of the Ladinian plutonic rocks of the Dolomites: insights from Anisotropy of Magnetic Susceptibility

Hassan Abbas [1], Maria Michail [2], Francesca Cifelli [3], Massimo Mattei [3], Piero Gianolla [2], Michele Lustrino [1,4], Eugenio Carminati [1]

1) Dipartimento di Scienze della Terra, Sapienza Università di RomaP.le A. Moro 5, 00185, Roma, Italy

2) Dipartimento di Fisica e Scienze della Terra, Università degli studi di Ferrara, Via Saragat 1, 44122, Ferrara, Italy

3) Dipartimento di Scienze, Università di Roma Tre, Largo San Leonardo Murialdo 1, 00146, Roma, Italy

4) CNR - Istituto di Geologia Ambientale e Geoingegneria, P.le A. Moro, 5, 00185 Roma, Italy

Corresponding author:

Prof. Dr Eugenio Carminati

Dipartimento di Scienze della Terra

Università degli Studi di Roma "La Sapienza"

P.le Aldo Moro 5

I-00185 Roma

Italia

Tel.: ++39-06-49914950

Fax: ++39-06-4454729

Email: eugenio.carminati@uniroma1.it

Abstract

In the Dolomites (Eastenr Southern Alps, Italy), a diffuse Middle Triassic igneous activity is now present mostly as lava flow and pyroclastic successions, with rare shallow-depth intrusive bodies cropping out at Predazzo, Monzoni and Cima Pape areas. In this work, the emplacement modes of the Predazzo and Monzoni bodies were investigated by means of petrographic and anisotropy of magnetic susceptibility (AMS) data coupled with a field geological study. The presence of intrusive rocks in between these two bodies and the continuity of the metamorphic aureola from west of the Predazzo to east of the Monzoni body suggest that they are parts of a ~20 km wide SW-NE oriented continuous pluton, sub-parallel to Ladinian strike-slip faults.

AMS and petrographic data from the Predazzo body are consistent with a multistage ring-dyke emplacement mode, with areas of upward flow of the magma located in the NE and SW part of the intrusion, whereas in the southern sector of the pluton our data suggest prevalently horizontal flows. In general, the Predazzo sheets indicate either upward magma flow or along-strike lateral magma transport, and the round shape suggests no influence of Ladinian tectonic structures.

On the contrary, the ENE-WSW elongated shape of the Monzoni body was controlled by the occurrence of strike-slip faults associated with Ladinian-tectonics, the feeder being likely located at the NE edge of the body. However, the absence of deformation at the field- and micro-scale is consistent with a post Ladinian-tectonics timing of emplacement, as for the Predazzo pluton.

Keywords: Dolomites, anisotropy of magnetic susceptibility, pluton, Predazzo, Monzoni, mode of emplacement

1. Introduction

The Middle Triassic igneous activity in the Dolomites (eastern Southern Alps, Italy; Figs. 1 and 2) is well known from nearly two centuries (e.g., von Richthofen, 1860; Hansel, 1878). The Dolomites represent a worldwide reference area for the relationships between magmatism, sedimentation and tectonics (e.g., Ogilvie-Gordon, 1902, 1903; Hörnes, 1912; Penck, 1911; Vardabasso, 1929, 1930; Leonardi, 1967; Castellarin et al., 1982, 1982b; Visonà, 1997). The igneous activity of the Dolomites is part of a more widespread magmatism developed during Middle and early Late Triassic in the western Tethys comprising the Southern Alps, Dinarides, Transdanubian Range and Austroalpine (Lucchini et al., 1982). In the Dolomites area, Middle Triassic igneous rocks are mostly pyroclastic, but abundant submarine and subaerial lava and dyke swarms also occur, with magma chambers eroded to shallow-depth intrusive body levels, cropping out at Predazzo, Monzoni and Cima Pape (Fig. 2).

Several contrasting geodynamic/tectonic models were proposed to explain Middle Triassic igneous activity in the Southern Alps: 1) An aborted continental rifting, based on the association of extensional structures and volcanism (Bechstädt et al., 1977); 2) Northward subduction and delamination of lower continental crust in the upper mantle, based on the calcalkaline and shoshonitic magmatic association and on local compressional structures of Middle Triassic age (Castellarin et al., 1980, 1988; Casetta et al., 2017); 3) Sinistral strike-slip tectonics associated with local compressional and extensional structures ("rhomb-horsts" and "pull-apart basins") generating magma extrusion and subsidence as result of the collapse of magma chamber roofs (Blendinger, 1985; Doglioni, 1987, 1988); 4) Marginal back-arc basin associated with the post-Variscan evolution of the Alpine sector (Marinelli et al. 1980; Viel, 1982); 5) Partial melting of a mantle source modified during the preceding Variscan orogeny and contaminated by the incorporation of large portions of crustal material (Crisci et al., 1984; Sloman, 1989; Bonadiman et al., 1994); 6) Intra-Pangea dextral megashear system with lithosphere-scale extension enabling hybridization between mantle melts and lower crust lithologies (Brandner and Keim, 2011); 7) Rifting related with the opening of the Neotethys (Beltran-Trivinõ et al., 2016; Brandner et al., 2016); 8) Active upwelling of hot asthenospheric mantle due to the insulating thermal effect of the huge Pangea landmass (Stahle et al., 2001); 9) Subduction of a small Permian back-arc oceanic (Garzanti 1985; Zanetti et al. 2013). The models involving subduction (2,4,9) are not coherent with the geological context of the Southern Alps that shows no evidence of volcanic arcs or oceanic subduction. The other models are consistent with geodynamic scenarios involving extensional tectonics, either controlled by rifting or strike-slip tectonics. The recognition of Middle Triassic NE-SW strike-slip faults in the Dolomites (e.g., Doglioni 1984a) testifies for the importance of wrench tectonics in this period.

The Predazzo, Monzoni and Cima Pape Middle Triassic intrusive bodies in the Dolomites crop out close to Middle Triassic NE-SW strike-slip faults (e.g. Stava line; Fig. 2), suggesting a potential role for strike-slip tectonics in the emplacement of these plutons. The generation, ascent and emplacement of magma through the crust and its relation to strike-slip faulting are still matter of debate (Castro 1987; Tikoff and Teyssier 1992; Paterson and Fowler 1993; Román-Berdiel et al. 1997; Rosenberg 2004). The emplacement of intrusive bodies can be considered either as controlled by regional tectonics (syntectonic) if the magmatic fabric is consistent with the regional strain field, or caused by the internal dynamics of the magma chamber if the magmatic fabric patterns are independent from the regional tectonic structures (Hutton, 1988; Paterson et al., 1998; Rosenberg, 2004).

In the past years, several structural studies on intrusive bodies have been carried out using the anisotropy of magnetic susceptibility (AMS) technique (e.g., Van der Voo and Klootwijk 1972; Bouchez et al. 1990; Raposo and Gastal 2009, Cifelli et al., 2012). The magnetic fabric in a pluton is affected by several factors, such as the flow of the magma, the changes in its effective viscosity and the finite deformation it undergoes before complete crystallization. Assuming a direct relationship between mineral and magnetic fabrics (e.g., Graham 1954), the analysis of the AMS in igneous bodies can be used to define the relationship between magma emplacement and tectonics.

This is particularly crucial for rocks that often appear isotropic and where magmatic foliation and lineation are difficult to observe and measure at the outcrop scale, such as granites (e.g., Knight and Walker, 1988, Tarling and Hrouda 1993).

In this study, we investigate the space and time relationship between the Ladinian Predazzo and Monzoni plutons and Middle Triassic strike-slip faulting in the Dolomites using AMS techniques, coupled with petrographic and field studies. In addition to this regional significance, our work can contribute to the understanding of magma migration and emplacement in the upper crust. A few exposed subvolcanic and caldera-related plutons have been reported and magma-plumbing systems of active volcanic areas cannot be directly studied. Therefore, developing and testing models for the emplacement mechanisms of the ancient exposed sheet intrusions can contribute to the assessment of volcanic hazard and risk in active volcanic areas (Sparks, 2003; Tibaldi and Pasquarè, 2008; Cashman and Sparks, 2013).

2. Geological setting

The Dolomites (Figs. 1 and 2) are located in the central-eastern portion of the Southern Alps, a south-verging fold-and-thrust belt that belongs to the much larger Alpine Orogeny (Carminati et al., 2010b; Handy et al., 2010). The Southern Alps (Fig. 1) are located south of the dextral Neogene Periadriatic Line (also known as Insubric Line) and represent the retro-wedge of the double-vergent Alpine Chain (Doglioni, 1987; Castellarin et al., 1998; Castellarin and Cantelli, 2000; Bosellini et al., 2003; Doglioni and Carminati, 2008). The Southern Alps consist of a well-preserved Mesozoic passive continental margin inverted during the Alpine orogeny (Doglioni, 1987, 2007; Handy et al., 2010).

The area of the Dolomites testify several tectonic and magmatic events recorded in the stratigraphic succession, including: 1) Permian extensional tectonics and massive acid magmatism (Barth et al., 1993; Schaltegger and Brack, 2007; Visonà et al., 2007; Brandner et al., 2016) that induced a lithospheric anisotropy that significantly influenced the Triassic and Alpine evolution; 2)

Middle Triassic tectonics, associated with differential subsidence and uplift and diffuse magmatic events during the late Ladinian (Fig. 3); 3) A rifting, started in the Late Triassic (Fig. 3), evolved into the western Tethys spreading during Early Jurassic times (Carminati et al., 2010); 4) Several superimposed phases of compressional Alpine deformation including the Eo-Alpine, Mesoalpine and Neoalpine phases (Castellarin et al., 2004, 2006).

The dolomitic area was a wide shallow sea during Late Permian and Early Triassic times, but started to differentiate at the beginning of early-middle Anisian (Brandner, 1984; Doglioni, 1984a, 1987; Masetti and Trombetta, 1998; Bosellini et al., 2003). Later, a sudden increase in subsidence combined with a strong sea level rise (Gianolla et al., 1998) drove to a general deepening, associated with the formation of high-relief carbonate buildups and retreat of the siliciclastic shoreline (De Zanche et al., 1993; Brack et al., 2007; Stefani et al., 2010; Marangon et al., 2011). Subsidence rates reached a climax during late Anisian, when the paleogeography of the Dolomites featured numerous small isolated microbial carbonate platforms (Sciliar Formation) surrounded by a deep basin (Buchenstein Formation). During Middle Triassic (Ladinian) the Dolomites witnessed a short-lived massive magmatic event, associated with a strong and localized tectonic activity (Assereto et al., 1977; Viel, 1979; Bosellini et al., 1982; Castellarin et al. 1988). Magmatic edifices such as Predazzo, Monzoni and Cima Pape (Fig. 2; Castellarin et al., 1982b; Sarti and Ardizzoni, 1984), now eroded to subvolcanic to epi-pluton levels, developed during significant tectonic displacement and huge accumulation of megabreccia and chaotic mass-flow deposits (Caotico Eterogeneo, Fernazza Formation). The volcanic sequence (both submarine pillow lava and pillow breccias and subaerial lava flows) is composed of alkali olivine basalt to latite association (Castellarin et al., 1982b; Visona, 1997) and huge volumes of tuffs and volcaniclastics (Fernazza Formation). Rare quartz syenitic and much more common shoshonitic dyke swarms cut the sedimentary cover and intrude the magmatic edifices (Vardabasso, 1930; Castellarin et al, 1982b; Doglioni, 1983). Volcanic activity is also associated with the formation of evaporitic diapirs (sourced in the Upper Permian evaporitic Bellerophon Formation) that deform sedimentary covers in areas adjacent to volcanic centers. The syn-volcanic age of these structures is documented by the fact that they are often cut by the magmatic dykes (Castellarin et al., 1998b). The volcanic activity ceased in upper Ladinian time and large volumes of volcanic material were dismantled and deposited as delta and turbiditic sequences in the surrounding basins (Wengen Formation). From late Ladinian to early Carnian, the subsidence rate decreased, resulting in the progradation of the southern shoreline and a general shallowing of the basins. This regressive trend culminated in the late Carnian, with a strong north-eastward shift of the coastline and complete flattening of the palaeotopography restoring a relative homogeneity in sedimentary palaeoenvironments, as documented by the Heiligkreuz and Travenanzes Formations (Stefani et al., 2010). A new transgression in the latest Carnian allowed the deposition of the thick peritidal succession of the Dolomia Principale (Stefani et al., 2010), which records a huge regional platform that extended for hundreds of kilometres from north to south and east to west. Widespread carbonate platforms then characterised the Southern Alps for several million years, from the late Carnian to (at least) the late Norian.

2.1 Age and duration of the Ladinian magmatic event.

The age of the igneous activity is well constrained by biostratigraphy and geochronology. The first tephra horizon (Fig. 3) with a mafic mineral association (clinopyroxene, plagioclase and olivine) is recorded in the Acquatona Fm. (*longobardicum* ammonoid subzone;Viel., 1979; De Zanche and Gianolla, 1995; Gianolla et al., 1998) and in the coeval Buchenstein Fm. (*sensu* Brack amd Rieber, 1993)). The main phase of volcanic activity is recorded by the Fernazza Fm. (*neumayri* and early *regoledanus* ammonoid subzones) while the often unconformably overlaid post volcanic unit (Wengen Fm.) is assigned to the *regoledanus* ammonoid zone (Stefani et al., 2010; Mietto et al., 2012). Absolute ages from ash layers of the Seceda section (Brack et al., 1996, 1997; Brack and Muttoni, 2000; Wotzlaw et al., 2018) suggest that the first evidence of mafic activity (tuffs, lava flows or submarine debris flow with lava blocks) is younger than 239.04 ± 0.04 Ma (U-Pb geochronology, Wotzlaw et al., 2018) and possibly coeval with the Upper Pietra Verde volcaniclastics, where an ash layer (close to the *longobardicum/neumayri* subzones boundary) showed an age of 238.0 ± 0.05 Ma (Mundil et al. 1996). The age of the termination of the paroxysmal effusive phase, is given by a tuff from the area of Alpe di Siusi (Mietto et al., 2012), where an ash layer, few meters above the top of the pillow-lava, gives an age of 237.77 ± 0.05 Ma (U-Pb geochronology).

These ages confine the duration of the paroxysmal phase of Ladinian volcanism in the Dolomites to a time interval no more than 0.7 Myr long (considering all analytical errors) and are in agreement with the absolute age from the Predazzo intrusion, where zircons from the granitic phase were dated to 237.3 ± 1.0 Ma (Mundil, 1996; Brack et al., 1997) and thus confirming a short-lived Upper Ladinian magmatic Event.

2.2 Ladinian tectonics in the Dolomites

During Middle Triassic time, the Dolomites were affected by N 70°-90°E trending strike-slip faulting (along the Stava, Trodena and Cavalase Lines), which locally was associated with transtensional and transpressional structures. These faults cut basement and sedimentary succession up to lower-middle Ladinian rocks (Doglioni, 1984b; Doglioni, 1987; Doglioni and Carminati, 2008). These structures are concentrated along the alignment of the Stava Line – northern limb of the Cima Bocche Anticline – where flower structures suggest a sinistral kinematics.

Middle Triassic compressional structures were locally documented in the Dolomites and consist of folds and reverse faults (Bechstadt et al., 1977, Pisa et al., 1980, Bosellini et al., 1982; Castellarin et al., 1982; Doglioni 1982, 1984a, 1984b, 1985, 1987; Doglioni and Carminati, 2008). In addition, diapiric structures (originating from the Upper Permian evaporitic Bellerophon Fm.) elongated along N70E axis and dated to the Middle Triassic crop out in the central Dolomites (Doglioni, 1984a). These Middle Triassic compressional structures were interpreted as related to N70E sinistral transpressional tectonics (Doglioni 1984a, 1984b, 1987, 2007), resulting from the sinistral relative movement between Africa and Europe (Doglioni 1984b). According to Doglioni (1983) Ladinian mafic volcanic dykes in Dolomites show a radial pattern, which was interpreted as related to a domal uplift induced by coeval magmatism, possibly inheriting previous structures.

2.3 The Predazzo intrusive complex

The Predazzo intrusive complex (Fig. 4) is ring-shaped, ~4 km in diameter and covers an area of ~13 km^2. It has been subdivided into four intrusive units on the basis of magma chemistry, geometry and relative geochronology (Menegazzo et al. 1995; Visonà 1997). Monzonitic unit M1 represents the first intruded unit and forms the outer part of the ring with mainly monzonitic composition associated with ultramafic rock types (pyroxenites). These ultramafic bodies are generally small, tabular and vertical with sinuous sharp contacts. Monzonitic unit M2 is intruded into the Middle Triassic volcanic rocks and into the Monzonitic unit M1 and cut them with short dykes. This unit crops out in the western part of the igneous complex and is mainly composed of quartz monzonite with subordinate leuco-quartz monzonite and quartz monzodiorite. In more recent studies, M1 and M2 units were merged into a single shoshonitic silica-saturated (SS) series (Casetta et al., 2017). Monzonitic unit M3 is mainly located in the eastern part of the pluton and intrudes both volcanic rocks and Monzonitic unit M1. It consists of monzodiorite to syenite, both quartz- or foid-bearing. The granite unit is located in the central part of the pluton and cuts both volcanic rocks and Monzonitic units M1 and M2. It consists of two separate lithotypes: a) biotite granite, b) tourmaline leuco-granite (Visonà, 1997). In Fig. 4 we observe variably (mainly NNW-SSE) oriented systems of basaltic to trachytic dykes that cut the entire intrusive complex together with the surrounding volcanic products, which in total cover an area of ~25 km^2 (Casetta et al., 2017).

2.4 The Monzoni intrusive complex

The Monzoni intrusive complex (Fig. 5and 6), located 8 km to the NE of the Predazzo complex (2) is a NE-SW elongated pluton with a length of <5 km covering an area of ~8 km^2. The Monzoni pluton played a central role not only for the study of the Middle Triassic magmatism but also in the development of petrography, being the type locality for monzonitic rocks (Brogger, 1895). The intrusion comprises a series of basic to intermediate plutonic rocks, which consist of gabbroic rocks (gabbro, olivine gabbro, monzogabbro), cropping out in the north-eastern part of the complex together with clinopyroxenite, while monzonites and monzodiorites constitute the western part of the intrusion (Del Monte et al., 1967; Bonadiman et al., 1994; Gallien et al., 2007) (Fig. 5). The Monzoni complex and its thermo-metamorphosed Permian to Triassic host-rocks are cut by quartz syenitic and shoshonitic dyke swarms (Bonadiman et al., 1994).

2.5 Intrusions' host rocks

The country rocks of the Ladinian plutons include (Castellarin et al, 1982b) lower Permian acidic volcanic rocks of the Athesian Volcanic Group (mostly rhyolites; Marocchi et al., 2008), a succession of volcanites up to >2 km thick, the Upper Permian fluvial red beds of Val Gardena Sandstones (~100 m thick; Figs. 4, 5), the Upper Permian marls and evaporites of the Bellerophon Fm. (~300 m; Fig. 4), the Lower Triassic clastic-carbonate Werfen Fm. (~280-500 m; Figs. 3, 4), the middle Anisian mixed carbonate-siliciclastics units (from Richthofen to Contrin Fm.; ~150-200 m; Figs. 3, 5), the Sciliar carbonate platform (~800 m) and the mainly cherty limestones of Buchenstein Fm (max 80 m).

The sedimentary cover is overprinted by contact metamorphism around the plutons (Vardabasso, 1929,1930; Ferry, et al., 2002, Gallien, et al., 2007), and exhibit strong evidence of regional tectonic deformation. The area around the intrusions is characterized also by significant collapses of the sedimentary cover (Vardabasso, 1930; Castellarin et al., 1982b) with vertical displacements of several hundred meters (e.g., Monte Agnello area) and platform-block tilting (e.g., Vallaccia area).

3. Sampling and Methods

3.1 Sampling

Sampling for petrographic and AMS analyses was carried out both in the Predazzo and Monzoni plutons (Table 1). In the Predazzo intrusive body, 14 sites were sampled and 107 cylindrical cores were collected for AMS analysis (Fig. 4a). In the Monzoni intrusive body, 10 sites were sampled for a total of 84 cylindrical cores (Fig. 5a). At each site, cores were drilled using an ASC 280E petrol-powered portable drill and oriented *in situ* by a magnetic compass, corrected to account for a local ~2° magnetic declination according to the NOAA National Geophysical data center. The geographic distribution of the sampling was influenced by the difficulty to find accessible outcrops in many areas, preventing the possibility to make a homogeneously distributed sampling throughout the two intrusive bodies.

3.2 Petrographic analysis

The collected samples were cut with a diamond-disc saw to obtain 29 thin sections for petrographic study and the reminder parts were grounded in a steel mill to about mm-scale fragments. The petrographic description of the thin sections was accomplished using an optical polarizing microscope.

3.3 Magnetic mineralogy

The AMS technique provides a quick and accurate determination of igneous rock fabric. The magnetic fabric (lineation and foliation) data obtained from AMS measurement can record the primary magma flow in magmatic sheet intrusions (Polteau et al., 2008; Petronis et al., 2013, Andersson et al., 2016; Magee et al., 2016), although magnetic fabric data are sometimes complex and in some cases subject of controversy. The precise knowledge of the magnetic mineralogy is an important aspect to use AMS for tectonic purposes because the preferred orientation of different magnetic minerals reflects the deformation history of the rock (e.g., Rochette et al. 1992; Hrouda et al. 1997). Magnetic mineralogy analyses were carried out in order to characterize which are the main magnetic minerals in the sampled sites. The variation of magnetic susceptibility with temperature was measured on powders from 24 representative samples, one for each site, by means of the same Agico KLY-3 Kappabridge used for LF-AMS measurements, equipped with a CS-2 furnace, at the paleomagnetic laboratory of the Department of Sciences of Roma Tre University. Samples were heated up to 700 °C and cooled back to 40 °C to estimate the Curie/Néel range of temperatures, according to the inverse susceptibility method proposed by Petrovský and Kapička (2006), and to examine any possible mineralogical change associated to the heating process in air. Moreover, the hysteresis properties of powders from 21 representative samples were measured on a Princeton Measurements Corporation 3900 vibrating sample magnetometer (VSM), in field up to 1 T. The powders have been placed in pharmaceutical gel caps suitable for vibrating in the VSM, in order to determine, after subtracting the high field linear trend, the coercive force (Bc), the saturation remanent magnetization (Mrs), as well as the saturation magnetization (Ms). The coercivity of remanence (Bcr) values have been extrapolated from backfield remagnetization curves up to -1 T, following forward magnetization in a +1 T field. These measurements were carried out in the Istituto Nazionale di Geofisica e Vulcanologia (INGV, Rome).

3.4 Anisotropy of low-field magnetic susceptibility (LF-AMS)

AMS is defined by a second rank tensor and represented geometrically by an ellipsoid in which the greatest intensity of magnetization is induced along the long axis k_1 and the weakest intensity along the short axis k_3 (with the principal axes $k_1 > k_2 > k_3$). Since the pioneering work of Graham (1954), a close correlation between the directions of the main axes of AMS ellipsoid (k_1,k_2,k_3) and the petrofabric strain axes (λ_1,λ_2,λ_3) has been widely demonstrated. Several parameters have been defined both for the quantification of the magnitude of anisotropy and for defining the shape of the ellipsoid (Table; Jelinek, 1981; Hrouda, 1982). The mean susceptibility values k_m have been computed as $k_m = (k_1+k_2+k_3)/3$. The magnetic lineation is computed by L (k_1/k_3) and has an orientation defined by the orientation of k_1, while the magnetic foliation is computed by F (k_2/k_3) and it is defined as the plane perpendicular to k_3. T is the shape parameter and range from -1 (perfectly prolate ellipsoid with L >>F) to +1 (perfectly oblate ellipsoid with F >>L) with zero values corresponding to a triaxial shape (F ~ L). The anisotropy degree is computed by the parameter Pj (Jelinek, 1981), which is obtained considering all the three principal susceptibility values.

Measurement of the anisotropy of low-field magnetic susceptibility (LF-AMS) represents a rapid and non-destructive technique for the characterisation of the mineral fabric in rocks (Hrouda, 1982). In this study, the LF-AMS was measured on about 200 specimens, with an Agico KLY-3S susceptibility bridge (Jelínek and Pokorný, 1997) in the paleomagnetic laboratory of the Department of Sciences of Roma Tre University. The anisotropy measurements at both the specimen and the site scale were evaluated using Jelínek's statistics (Jelinek, 1977).

3.5 Anisotropy of high-field magnetic susceptibility (HF-AMS)

As the LF-AMS is the sum of the contribution from all minerals, which include ferromagnetic, paramagnetic and diamagnetic phases (Rochette et al., 1983), we measured high-field AMS (HF-AMS) on 13 selected samples in order to discriminate the relative contribution of ferromagnetic and paramagnetic minerals to the magnetic anisotropy (e.g., Martin Hernandez and Hirt, 2001). HF-AMS measurements were carried out, using magnetic fields up to 1500 mT. These fields are strong enough to saturate all ferromagnetic minerals except hematite (not present in the analyzed samples), and allow the separation of paramagnetic and ferromagnetic contribution to the magnetic anisotropy (e.g., Hrouda and Jelínek, 1990). Measurements were made with a high-field torque magnetometer (Bergmüller et al., 1994) in the Laboratory of Natural Magnetism of the Institute of Geophysics ETH in Zürich.

4. Results

4.1. Petrographic description

A complete petrographic description of the samples (Table 1) is provided in Appendix A. Here a summary is presented.

In the Predazzo pluton, lithologies vary from cumulitic clinopyroxenite (samples PA12, PA11a, b, c) to cumulitic gabbro (PA10), diorites (PA06), monzonite (PA02, PA10), monzodiorite (PA08, PA14c, PA09), monzogabbro (PA12) albitized granite (PA01, PA04, PA05, PA17) and biotite granite (PA07, PA03, PA13). We found evidence of hydrothermal alteration in samples from the northern part of granite body of the Predazzo pluton (PA01, PA04, PA05, and PA17).

The samples from Monzoni pluton are classified into two main groups: gabbroic rocks and monzonites. Gabbroic rocks are mainly located in the north-eastern sector of the pluton and consist of monzogabbros (PA21), non-cumulitic gabbros (PA16) cumulitic gabbros (PA15) and olivine gabbros (PA20, PA18). Monzonites (PA22, PA22a, PA23, PA24) are mainly located in the south-western sector of the pluton and represent the most widespread rock type.

As accurately described in the appendix, the samples from both plutons show purely magmatic structures (for most of lithologies hypidiomorphic inequigranular medium- to coarse-grained textures with anhedral, to euhedral crystals) with undeformed feldspar, clinopyroxene, and amphibole. In few cases, kinked biotite occurs. Quartz does not show any or very limited undulatory extinction, and no or rare sub-grains.

4.2 Magnetic fabric results

The magnetic susceptibility and main anisotropy parameters of the analyzed sites are listed in Table 1. The orientation of the magnetic foliation and magnetic lineation has been reported in pre-tilting coordinates, on the base of the regional structural evolution and geological mapping, which show a 10° of tilting toward NE in the Predazzo area and 15° toward N in the Monzoni area. In the Predazzo pluton, a bimodal distribution of k_m values is observed, which reflects the lithological differences of the analyzed samples (Table 1). Samples taken from granites show low values, in the range of E^{-03}-E^{-05} SI, whereas samples from clinopyroxenites, gabbros and diorites show higher values (up to 1.63 E^{-01} SI), qualitatively suggesting a major contribution of ferromagnetic minerals to the magnetic susceptibility in these latter lithologies. These data are consistent with the occurrence of magmatic foliation (Fig. 6b) both at meso- and micro-scale. In the Monzoni pluton, monzonites and gabbroic rocks show similar values of k_m, in the range of E^{-02} SI, suggesting a strong contribution of ferromagnetic minerals (Table 1) consistent with preferred orientation of minerals observed in thin sections (Fig. 6c,d,e,f). The susceptibility *vs.* temperature heating-cooling curves indicate that low-Ti content titanomagnetite and magnetite are the main ferromagnetic minerals both in the Pradazzo and Monzoni intrusive bodies. A slight to moderate step around 350 °C is attributed to the presence of a small amount of maghemite which converted to hematite as confirmed by the slightly lower susceptibilities recorded along the cooling curves (Fig. 7 a-d). Also, a well-defined Hopkinson peak has been recorded in few samples, before a sudden drop in susceptibility which might correspond to a partially oxidized titanomagnetite (Fig. 7 c and d). Hysteresis loops (Fig. 7 e-h), isothermal remanent magnetization (IRM) acquisition curves and backfield applications are well defined, due to the relatively high values of the concentration dependent magnetic parameters. The results are mainly consistent with a prevailing low-coercivity component, as evidenced by Bcr values, which are lower than 40 mT (Fig. 7 i-l).

In most of the sites, the magnetic foliation is well developed and its values (F) are greater than those of the magnetic lineation (L; Table 1 and Fig. 8). Magnetic shape factors (T) in most of the samples show a dominant oblate shape, and for few samples, it shows prolate and triaxial shape (Table 1). The degree of anisotropy (Pj) values do not show significant difference between monzonite and granites and vary between 1.01 and 1.15 (Fig. 8b Table 1).

In the Predazzo intrusives, the Monzonitic Unit M1 has been sampled in different sites along the southern (PA08, PA09, PA10), the south-western (PA06) and north-western (PA02) borders of the plutonic body (Fig. 4a). In all these sites AMS shows a well-defined magnetic foliation, which ranges from moderately dipping (25°) to vertical (89°) and strikes almost parallel to the intrusive borders. In particular the magnetic foliation is oriented WSW-ENE at sites PA08, PA09, and PA10, WNW-ESE at site PA06, and N-S at site PA02 (Figs. 4b and 9a, e, f). Furthermore, we sampled a site (PA12) in one of the mafic bodies that outcrop along the western part of the intrusive. The magnetic foliation dips outward the intrusive body at sites PA02, PA09 and PA10 and toward the boundary within Monzonitic Unit M2 at sites PA06, PA08 and in the mafic body site PA12. The magnetic lineation shows gentle to sub-horizontal dipping, and is variably oriented respect to the intrusive body, ranging from sub parallel to the boundary (PA02, PA06, PA08, PA09) to orthogonal to it (PA10) to disperse around a great circle (PA12). The Monzonitic Unit M3 has been sampled at one site (PA11), located in the eastern part of the intrusive. In this site, magnetic foliation is very well defined and is sub-vertical with a WSW-ENE direction, parallel to the elongation of this unit. Magnetic lineation is also well defined and sub-vertical (Figs. 4b and 9d).

The granite intrusion has been sampled in 7 sites, located in the north-western (PA01, PA04, PA05 and PA17), in the south and south-western (PA03, PA07 and PA08) boundaries of the body (Fig. 4a). The magnetic foliation is well defined in all the sites, but in site PA01 where it shows a significant dispersion around an E-W direction. In the north-western part of the intrusion magnetic foliation is oriented NNE-SSW at sites PA04 and PA05, where it is sub-vertical and dips toward the internal and the external border of the intrusive body, respectively (Figs. 4b and 9b, c), whereas at site PA17 the magnetic foliation is E-W oriented and dips toward the north. In the south-western part of the granitic body, the magnetic foliation is also parallel to the border of the intrusion, being W-E oriented at site PA03 and NW-SE at site PA07. In both sites, the foliation is dipping toward the external part of the intrusion. The magnetic lineation is very poorly defined at sites PA01 and PA07, whereas is sub-vertical at sites PA04 and PA05. At sites PA03 and PA17 the magnetic lineation is poorly grouped with a sub-horizontal E-W orientation (Figs. 4 and 9a-f).

In the Monzoni pluton we sampled mafic rocks in the eastern part of the intrusive, and monzonite units in the western part of the body (Fig. 5a). In the monzonite sites (PA22, PA23, and PA24), the magnetic foliation is well defined, with a W-E orientation and a sub-vertical attitude. In these sites, the magnetic lineation is well defined and mostly shows sub-vertical dip (Figs. 5b and 9j). In the mafic units, the magnetic foliation is well defined and varies from gently dipping toward the SE (PA18) to a sub-horizontal attitude (PA19, PA20, PA21). In all these sites, the magnetic lineation is well defined with a WNW-ESE orientation (Figs 5b and 9i, k, l). At sites located in the eastern part of the pluton, the magnetic foliation is well defined at sites PA15 and PA16, where it shows a NE-SW orientation and a step dipping to NW. At site PA14 the magnetic foliation is poorly defined, being dispersed in a E-W direction. Magnetic lineation is well defined at sites PA14 and PA16, where it is sub-horizontal and N-S oriented respectively, whereas it is poorly defined at site PA15. (Figs. 5b and 9g-h).

HF-AMS measurements indicate that, for most of the samples, the observed magnetic fabric is dominated by the ferromagnetic component (Fig. 10) in most of the sites and a very good correspondence between the orientation of the principal axes of the ellipsoid at low-field and those of the ferromagnetic ellipsoid in high-field exists. This suggests that the magnetic fabric can be described in terms of the orientation of the ferromagnetic minerals. In samples where the HF-paramagnetic fraction is significant (>50%), there is a good correlation between low-field and high-field (ferromagnetic and paramagnetic) magnetic ellipsoids, whereas when the paramagnetic fraction is very low its orientation cannot be determined with the necessary accuracy (Fig. 10d).

5. Discussion

Magnetic fabric in intrusions can be purely magmatic (related to internal magma chamber processes, such as convection, magma surges, and dyke injection) or it can be the result of regional deformation (syn- to post-tectonic strain) or a combination of these two processes (Paterson et al., 1998). In the Predazzo and Monzoni bodies, thin section analyses show that the microstructures are purely magmatic (i.e., just after the complete crystallization of magma). The absence of evident solid-state deformation suggests that the magnetic fabric is not related to tectonic deformation after cooling, but it rather developed during magma emplacement and cooling (Büttner, 1999). Hydrothermal fluids can also modify the magnetic fabric orientation and parameters acquired during magma emplacement and cooling, thus complicating the interpretation of magnetic fabric data (e.g. Just et al. 2004; Petronis et al. 2011; Nédélec et al. 2015; Tomek et al., 2017). Although some samples from the northern part of the Predazzo granite body (PA01, PA04, PA05, and PA17) showed evidence of hydrothermal alteration, in most of these sites magnetic foliations are generally tangent to the ring shape of the pluton. This suggests that hydrothermal alteration had no or minor effect on the magnetic fabric, with the exception of sample PA17, that is strongly hydrothermally altered and fractured and show a distinctive magnetic fabric. Therefore, site PA17 will be no longer considered in the discussion of the emplacement mode of the Predazzo pluton. Samples from site PA11, belonging to Monzontic Unit M3 of the Predazzo body, are highly altered and transformed as a result of hydrothermal solutions. However, the magnetic fabric orientation is concordant with NE-SW elongation shape of Monzontic Unit M3 and shows well-clustered magnetic fabric. The compatibility of the magnetic fabric with the elongation shape of this unit could be explained as the hydrothermal fluid was likely coeval with the emplacement as a single event (e.g. Nédélec et al., 2015). Moreover, the NE-SW orientation of the magnetic fabric and elongation of the Monzonitic Unit M3 suggests that the emplacement of this unit was controlled by NE-SW Middle Triassic (Ladinian) tectonic structures.

In the following, the Predazzo and Monzoni plutons will be discussed separately. However, Figure 2 shows that these intrusive bodies may be parts of a single large and rather continuous body, as suggested by the outcrop of a small volume of intrusive rocks between the plutons and by the continuity of a metamorphic aureola from west of the Predazzo body to the Monzoni body. The emplacement of Ladinian intrusive bodies likely occurred along a fractured zone associated with previous strike-slip tectonics (Fig. 11a), as suggested by the parallelism between Ladinian intrusives and Middle Triassic faults (e.g., Stava-Trodena line, Fig. 2b).

The Predazzo and Monzoni plutonic rocks show distinct shapes, the first being roughly round shaped and characterized by ring type successive intrusions, the second being markedly NE-SW elongated, sub-parallel to the Middle Triassic Stava-Trodena line. Similarly, the AMS analyses show markedly different results for the two intrusive bodies, suggesting different emplacement modes. Both the Predazzo and Monzoni bodies are the result of multiple intrusions, as indicated by the variety of lithologies described above (see also appendix A).

5.1 Emplacement mode of the Predazzo pluton

In the Predazzo body, AMS has been measured in the different intrusive bodies that form the pluton, showing distinctive pattern of magnetic fabric. The Monzonitic Units M1 and M2, that represent the older portion of the pluton, are characterized by an annular ellipsoidal shape, gently elongated in a ENE-WSW direction. In this body, the magnetic foliation is generally oriented parallel to the borders of the intrusion (i.e., parallel to its perimeter). In sites that are located along the external rim, the foliations are predominantly steeply or shallowly radially dipping away from the pluton. On the contrary, in sites located along the internal rim of the annular intrusion the foliations radially dip towards the centre of the pluton. The magnetic lineation is generally gently dipping to sub-horizontal and parallel to the border of the intrusion. In the granite body the magnetic foliation is almost parallel to the rims of the pluton and dips away from the intrusion, whereas the magnetic lineation varies from sub-vertical to sub-horizontal. The rough ring shape of the Predazzo multistage intrusive complex and the presence of volcanic rocks at the centre of the ring (suggesting a caldera collapse of this area), led Castellarin et al. (1982b) to suggest a ring dyke emplacement mode. Ring dykes are cylindrical sheet intrusions occurring at subvolcanic level characterized by outward-dipping walls on all sides. They are due to magma ascent along steep outward-dipping ring fractures, induced by the collapse of the central block subsidence (e.g., O'Driscoll et al., 2006). The development of caldera ring-faults and the related subsidence of a central block are the main structural processes that permit the intrusion of ring-dikes (Roche et al., 2000).

Our AMS data are consistent with the ring dyke emplacement mode. In particular magnetic foliation in the Monzonitic units is dominantly oblate and consistently parallel to the boundaries of the intrusion and prevalently dips away from the intrusion. Only in places, where sites have been sampled close to the internal boundary of the Monzonitic units, the foliation is very steep and dipping toward the internal rim, describing a symmetrical pattern of the magnetic foliation respect to the dike rims. This geometry has been widely recognized in volcanic dykes, where it has been interpreted as related to imbrication of the magnetic foliation along the dyke margins, related to upward flow of the magma (Aubourg et al., 2002). In this mechanism, the horizontal magnetic lineation can be interpreted as an intersection lineation between differently oriented foliation planes , which is oriented orthogonal to the magma flow. In sites far from the pluton margins (e.g. PA11), the steep lineations associated with steeply dipping foliations are likely related to ascent paths of magma, in particular with laminar flow and wall friction during injection (Andersson et al., 2016). On the other hand, in sites far from the intrusive rims (e.g. PA02) the occurrence of sub-horizontal lineations (tangential to the shape of the pluton) could be related to lateral flow of magma induced by "roll-over" at propagating sheet tips (Emeleus et al., 2012; Andersson et al., 2016) or to semi-chaotic particle movement during ring fissure flow, as observed in analogue models (Kennedy et al., 2008). The occurrence in some samples of magmatic layering steeply dipping inward and magnetic lineations plunging toward the centre of the intrusion suggests that the shape of the walls was not as regular (i.e., constantly outward dipping) as assumed in ring dyke models (complex flow due to complex sheet geometry of Andersson et al., 2016). The steep attitude of inward dipping foliations is not consistent with a lopolithic geometry of the Predazzo intrusion.

The degree of anisotropy (Pj) varies between 1.01 and 1.15 and is not controlled by lithology (i.e., low and high values are found both in monzonites and granites). More remarkably, the values do not show a pattern (e.g., high values aligned along WSW-ENE directions, typical of Ladinian tectonics) but are rather randomly distributed. This confirms a primary (i.e., emplacement-related) nature of magnetic anisotropy. Moreover, the nonlinear relationship between Km and Pj supports that the obtained low Pj values indicate the existence of low strain during the emplacement.

Finally, also the orientation of dykes (mainly trending NNW-SSE) crosscutting intrusive rocks is at odds with sinistral strike slip tectonics along WSW-ENE structures, that would be rather associated with NE-SW trending dilational (extensional) structure. NE-SW trending dykes are rather found in the host rocks of the pluton, suggesting that they utilized previous extensional structures associated with sinistral strike-slip faulting. Thus, their emplacement and the emplacement of the pluton were post-tectonics.

In summary, field petrographic and AMS data are consistent with a multistage ring dyke emplacement mode, similar to the piston floor subsidence mechanism (Tomek et al., 2014), likely post-tectonics. The Predazzo sheets were emplaced via prevalent updip magma flow associated with local along-strike lateral magma transport (Fig. 11b).

5.1 Emplacement mode of the Monzoni pluton

The shape of the Monzoni pluton was clearly controlled by Middle Triassic tectonics, being it elongated WSW-ENE, parallel to the Stava-Trodena strike-slip fault. It remains to be discussed whether this control was direct (syn-tectonic emplacement of the pluton) or indirect (emplacement along pre-existing tectonic structures). The host rocks of the Monzoni pluton are affected on all sides by contact metamorphism. This suggests that the host rock-pluton contacts are primary, thus no or very poorly affected by post-emplacement tectonics.

Comparing magnetic and deformation fabrics in the pluton with strain markers in the country rocks one can determine whether the magnetic fabric in pluton is primary or reflects regional tectonic strain (Benn et al., 1998, 2001; Talbot et al., 2005; Raposo et al., 2012). Three different areas, with distinct magnetic fabric can be recognized in the Monzoni body. In the NW side, the magnetic foliation is well defined, sub-vertical, and parallel to the E-W oriented boundaries of the igneous body in this area, with a very steep magnetic lineation. Along the NE side of the intrusive body the magnetic foliation and magnetic lineation vary from very gently dipping to sub-horizontal. Along the SE side the magnetic foliation is almost parallel to the boundary of the intrusive and gently to strongly dipping toward the internal part of the pluton, whereas the magnetic lineation is prevalently gently plunging.

Our AMS results suggest that the magnetic fabric in Monzoni pluton was not directly controlled by Middle Triassic or post-tectonic deformation. This conclusion is supported by the absence of solid state deformation, by the general steeply magnetic fabric on the two sides of the pluton with absence of the NE-SW horizontal magnetic lineation and by the low degree of anisotropy (Pj), suggesting that magnetic fabric developed during magma emplacement and cooling and was likely controlled by the shape of the magma chamber.

The magnetic fabric can be read in terms of direction of flow and can help to infer the location and geometry of the feeding or root zones for magmatic bodies (e.g., Marre, 1986; Djouadi et al., 1997; Callot et al., 2001; Petronis et al., 2005; O'Driscoll et al., 2006; Maes et al., 2007). Magma originating from a planar dyke generates a parallel flow pattern with lineations pointing to opposing, but consistent directions, on either side of the dyke (Knight and Walker, 1988; Ernst and Baragar, 1992; Maes et al., 2007). Generally, the magnetic lineation, which represents the magma flow, plunges toward the magma source (Knight and Walker, 1988; Ernst and Baragar, 1992; Maes et al., 2007). In case of magma fed from a sub-vertical conduit, radial magma flow pattern is expected. Multiple feeders can produce more complex patterns of magma flow (Maes et al., 2007). In the Monzoni pluton, the magnetic lineations converge towards the north-eastern part of the pluton (PA15, PA16, PA18, PA22, PA23, and PA24), suggesting that the root zone was not located at the centre of the pluton but rather towards NE. This interpretation is also consistent with the magmatic evolution of the pluton. Indeed, the most evolved rocks are located at the south-western edge of the pluton, while the less evolved rocks are located at the north-eastern part of the pluton.

In the Monzoni pluton, steep to moderate foliations and lineations at the western and eastern borders of the pluton leave space to shallowly dipping fabric in its intermediate parts. This fabric may have been induced by shear of magma along the host-rocks at the top of the pluton. This inference is in agreement with field host-rocks above the pluton, in agreement with geological observations that allow to infer that the top boundary of the pluton was located just above the mountain peaks in the central part of the pluton (Castellarin et al., 1982b).

In summary, field, petrographic and AMS data and the ENE-WSW elongated shape indicate that the site and shape of the Monzoni pluton was controlled by strike-slip faults associated with Ladinian-tectonics. However, the absence of deformation at the field- and micro- scale is consistent with a post Ladinian-tectonics timing of emplacement, as for the Predazzo body.

6. Conclusions

Petrographic and AMS data, coupled with field geological data allowed us to investigate the emplacement modes of the Predazzo and Monzoni bodies. Although these plutons are considered in the literature as separated bodies, the outcrop of a small volume of intrusive rocks between the bodies and the continuity of metamorphic aureola from west of the Predazzo body to east of the Monzoni body suggest that they are parts of a ~20 km long SW-NE oriented continuous pluton, sub-parallel to Ladinian strike-slip faults. However, our results suggest a variable control of Ladinian tectonic structures on the emplacement modes of the two bodies.

AMS and petrographic data from the Predazzo body are consistent with a multistage ring dyke emplacement mode, with areas of upward flow of the magma located in the NE and SW part of the intrusion, whereas in the southern part of the pluton our data suggest prevalently horizontal flows. Generally, the Predazzo sheets were emplaced via either updip magma flow or along-strike lateral magma transport, and the round shape suggests no influence of Ladinian tectonic structures.

On the contrary, the ENE-WSW elongated shape of the Monzoni body was controlled by the occurrence of strike-slip faults associated with Ladinian-tectonics, the feeder being likely located at the NE edge of the body. However, the absence of deformation at the field- and micro- scale is consistent with a post Ladinian-tectonics timing of emplacement, as for the Predazzo pluton.

Acknowledgements

The Editor (Ian Alsop) and two reviewers (Teresa Román-Berdiel and an anonymous referee) are warmely thanked for their constructive criticisms. Financial support from PRIN2015-Project 2015EC9PJ5_001 and Progetti di Ateneo Sapienza 2017 (E. Carminati) is acknowledged. Marcello Caggiati and Massimo Coltorti provided invaluable help in the field. Aldo Winkler and Ann Marie Hirt are warmly thanked for doing hysteresis and HF-AMS measurements, respectively. The Trento province is thanked for providing permissions for sampling in the Dolomites, that are an UNESCO protected site. Erasmus Mundus European Commission is acknowledged for providing financial support the PhD program project of Hassan Abbas in the framework of EU METALIC II project (Erasmus Mundus Action 2).

Appendix A

Petrographic description

Predazzo pluton

Clinopyroxenite (PA12, PR11a, b, c)

Clinopyroxenites show a typical hypidiomorphic inequigranular medium- to coarse grained cumulitic texture. Cumulitic phase (clinopyroxene) accounts for more than ~65% of the rock with usually subhedral, fresh and rarely twinned crystals. Clinopyroxene is mainly medium grained (~3 mm) but a few reach larger dimensions, up to ~6 mm. The intercumulus phases consist of subhedral fine- to medium-grained opaques (~0.3-1.3 mm; ~15%), sometimes included in larger biotite crystals, anhedral to subhedral biotite (~13%) with an average size of ~4 mm and anhedral to subhedral small (~1 mm) plagioclase (~7%). In few cases biotites are partly chloritized, while plagioclases are usually partially sericitized. Fine-grained opaques, biotite and plagioclase are also found included in the clinopyroxene oikocrysts (poikilitic). Apatite and zircon are the common accessory minerals usually found as tiny grains included in clinopyroxene and biotite.

Cumulitic gabbro (PA 10)

The cumulitic gabbro is medium-grained with hypidiomorphic inequigranular texture. The cumulitic phases are plagioclase (~50%), clinopyroxene (~36%) and opaques (~10%). Subhedral to euhedral medium-grained (~3 mm) plagioclase is highly altered to sericite with cores more altered than rims. Clinopyroxene is subhedral medium grained (~2 mm), highly fractured, slightly altered and usually twinned. Opaques occurs as subhedral to anhedral fine grained (<1 mm) and usually found in clusters with clinopyroxene or included in clinopyroxene and biotite. The intercumulus phases (~4%) consist of anhedral to subhedral fine grained (<1 mm) biotite and plagioclase. Biotite and plagioclase also occur as anhedral small grains included in the clinopyroxenes. Apatite is a common accessory mineral occurring as minute inclusion in clinopyroxene and biotite.

Diorite (PA06)

The diorite is characterized by hypidiomorphic inequigranular with medium- to fine-grained texture. The rock is composed of plagioclase (~60%), amphibole (~15%), biotite (~10%), clinopyroxene (~10%), plus smaller amounts of K-feldspar, opaques, quartz and accessory minerals. Plagioclase occurs as slightly sericitized tabular to equant subhedral crystals with an average size of ~1.5 mm. Anhedral to subhedral amphibole, biotite and clinopyroxene occur as small (~1 mm) interstitial clusters, together with subhedral fine-grained opaques, usually found as inclusion in these minerals. Clinopyroxene is generally replaced to different degrees to amphibole. Most of the biotite crystals are slightly to moderately altered to chlorite. K-feldspar and quartz (<1 mm) occur as anhedral intergranular crystals in between plagioclase laths. Apatite and rare zircon are present as small inclusions mainly within plagioclase and clinopyroxene.

Monzonites (PA02, PA10), monzodiorites (PA08, PR14c, PA09) and monzogabbro (PR12)

These three types of rocks generally share the same petrographic features, being different only for the relative K-feldspar/plagioclase ratio. The amount of mafic minerals increases from monzonites to monzodiorites and monzogabbros. This rock group shows hypidiomorphic inequigranular texture. Monzonite and monzogabbros are medium-grained, while monzodiorites are medium- to fine-grained. The rocks are poikilitic, with big anhedral K-feldspars including other minerals.

The rocks are generally composed, in order of abundance, of plagioclase, K-feldspar, clinopyroxene, amphibole, biotite, quartz, opaques, orthopyroxene and accessory minerals. Plagioclase is usually euhedral with variable grain size (~0.5-3 mm) and sometimes zoned, with cores always more altered than the rims (i.e. sericitized and saussuritized). Few crystals show combined pericline and albite twining. Alkali feldspar (~1-4 mm) occurs as anhedral irregular grains characterized by perthitic exsolution. Clinopyroxene is subhedral with medium size (~1-2 mm), sometimes twined and in most cases found in clusters. The clinopyroxene crystals are partially to completely altered to amphibole (uralitization). Amphibole is anhedral to subhedral (~0.5-1.5 mm) and mostly found along the margin of clinopyroxene. Biotite occurs as subhedral to anhedral crystals with different grain size (~2-0.5mm) and often found in clusters. In some cases, large biotite crystals are poikilitic for the presence of opaque mineral inclusions. The biotite state generally is good but, in some cases, it is partly altered into chlorite. Anhedral quartz is fine- to medium-grained (~1.5-0.3 mm) and occurs as interstitial phase. Orthopyroxene is subhedral to anhedral and are usually found in few percent and recorded not in all the thin sections. Also, orthopyroxenes show alteration to amphibole with various degrees. Opaques are small subhedral grains usually included in the other mafic minerals or occupying interstitial areas. The accessory minerals are apatite, zircon and sphene, observed as inclusions or along mineral boundaries.

Granite group (PA01, PA03, PA04, PA05, PA07, PA13, PA17)

The samples exhibit hypidiomorphic inequigranular texture. In a few cases, granophyric texture is also recorded. The granite rocks are classified into two main groups: albitized granite (affected by hydrothermal alteration) and biotite granite.

In the first group biotite is completely transformed mainly to sericite and minor chlorite (PA01, PA04, PA05, PA17), while in the second group biotite is generally found in a good state of preservation (PA07, PA03, PA13). The biotite granite group is characterized by the presence of microgranular quartz usually forming aggregates around feldspar crystals.

The rocks are made up, in order of abundance, of K-feldspar, quartz and plagioclase with minor biotite, muscovite, chlorite and rare amphibole.

K-feldspar occurs as subhedral medium grained (~2-4 mm) crystals characterized by perthitic exsolution lamellae. Carlsbad twining is common and the crystals usually shows minor alteration.

Quartz mainly occurs in anhedral grains (~1-3 mm) but is also sometimes found in the interstitial areas (<0.5 mm) or forming aggregates around feldspar crystals. Quartz crystal shows no or incipient undulatory extinction. Plagioclase is subhedral medium grained (~1-3 mm), sometimes zoned and usually show albite twinning. In biotite granite, most of the plagioclase crystals are slightly to moderately altered (sericitized and saussuritized), with the cores more altered than the rims. On the other hand, in albitized granite plagioclase is completely transformed having lost completely its anorthite component. Biotite is present as subhedral platy crystals (~0.5-2 mm) and usually forms clusters of numerous crystals. Biotite is partially to completely altered to chlorite and sericite. Sericite occurs as anhedral to subhedral (~1-2 mm) pseudomorphs after biotite and is commonly associated with chlorite. Chlorite is subhedral to anhedral (~0.5-2 mm) pseudomorphs after biotite. Rare amphibole crystals have been recorded in the second group. Accessory minerals are zircon, apatite, fluorite, iron oxide and monazite.

Monzonite to Syenite? (PA11)

This sample is strongly affected by hydrothermal alteration and a precise classification cannot be conducted.

Monzoni pluton

The samples from Monzoni pluton have been classified into two main groups: Gabbroic Rock (olivine-gabbros, gabbros, monzogabbros), mainly located at the northeastern part of Monzoni pluton, and monzogabbros (PA21).

These rocks are medium- to coarse-grained with hypidiomorphic inequigranular texture. The rocks are composed, in order of abundance, of plagioclase, clinopyroxene, K-feldspar, opaques, olivine, biotite and accessory minerals.

Plagioclase is the most abundant phase. It is euhedral to subhedral medium-grained (~1-4 mm), always twinned, rarely zoned and mostly unaltered. Clinopyroxene is represented by subhedral medium- to coarse-grained (~1-5 mm) unaltered crystals. K-feldspar is anhedral to subhedral medium- to fine-grained (~0.5-4 mm), unaltered, untwined, usually occupying the interstitial areas and in some cases as oikocryst, including the other minerals (poikilitic texture). Opaques are subhedral fine- to medium-grained (~0.2-1.3 mm), mainly included within other minerals (biotite, clinopyroxene and olivine) or occupying interstitial areas. Olivine is subhedral medium-grained (~1-5 mm), usually unaltered and fractured. Biotite is anhedral to subhedral fine- to medium-grained and unaltered, occupying the interstitial areas between the early crystallized minerals.

Gabbro (non-cumulitic) PA 16. This rock exhibits coarse-grained with hypidiomorphic inequigranular texture. It is made up with plagioclase, clinopyroxene, opaque, biotite and accessory minerals (in order of occurrence). Plagioclase is euhedral medium- to coarse-grained (~2-5 mm), usually found in good state or showing slight alteration to sericite and is usually twinned. Clinopyroxene is subhedral medium- to coarse-grained (~2-6 mm), unaltered, rarely twinned, with ophitic and subopthic texture (plagioclase partially or completely enclosed by clinopyroxene). Opaques are subhedral fine- to medium-grained (~0.3-1.3 mm), occupying the interstitial areas or included within the biotite and clinopyroxene. Biotite is anhedral to subhedral, fine- to medium-grained (~0.5-2.5 mm), unaltered, and interstitial.

Gabbro (cumulitic) PA15. This rock is coarse-grained with cumulitic texture. Cumulus phases are mainly clinopyroxene with minor olivine. Intercumulus phases are primarily plagioclase and biotite with minor opaque oxides. Clinopyroxene is euhedral to subhedral coarse- to medium-grained (~2-8 mm), rarely twinned and sometimes slightly zoned. Olivine is subhedral medium-grained (~1-3 mm) and usually found in good state with fracture. It is slightly altered to iddingsite particularly along the fractures. Plagioclase is euhedral to subhedral medium-grained (~1-2 mm), slightly altered to sericite and always twinned. Biotite is subhedral to anhedral medium- to fine-grained (~0.5-2 mm) and in a few cases is slightly chloritized. Opaques are subhedral fine- to medium-grained (~0.1-1.5 mm). They occur both as interstitial phases or included within clinopyroxene and biotite.

Olivine gabbro (PA20, PA18). These rocks are medium- to coarse-grained. Cumulus phases are represented by clinopyroxene, plagioclase, and olivine. Clinopyroxenes occurs as subhedral medium- to coarse-grained (~ 2-6 mm), unaltered and usually untwined. Clinopyroxene oikocrysts usually include small crystals from opaques, plagioclase, olivine and biotite. Olivine crystals are subhedral medium-grained (~ 1-2.5 mm). Olivine in sample PA20 is fresh and fractured, whereas in sample PA18, it is completely altered to secondary minerals (iddingsite, bowlingite and celadonite). Plagioclase is euhedral to subhedral medium-grained (~ 1-2.5 mm), rarely zoned, and always showing twining. Plagioclase is fresh in sample PA20 and slightly altered in PA18. Intercumulus phases are composed of plagioclase, biotite, opaques, and K-feldspar. Plagioclase occurs as fresh subhedral fine-grained (~ 1 mm). Biotite is fresh medium-grained (~ 1-3 mm), subhedral or sometimes anhedral, when occupying interstitial positions. Opaques occur as subhedral fine- to medium-grained (~ 0.5-1.3 mm), and commonly are interstitial phases or are included in clinopyroxene, biotite and olivine. K-feldspar is clear anhedral fine- to medium-grained (~ 0.5-1.5 mm) and is usually found as interstitial crystals between the early crystallized minerals.

Monzonite (PA22, 22A, 23, 24). These rocks are mainly located in the south-western sector of Monzoni pluton and represent the most widespread rock type. These rocks are medium- to fine-grained and exhibit hypidiomorphic inequigranular texture. The rocks are composed, in order of abundance, of plagioclase, K-feldspar, biotite, clinopyroxene, amphibole, opaques, quartz and accessory minerals.

Plagioclase represents the most abundant phase with euhedral to subhedral tabular laths with variable grain size (up to 4 mm), usually twinned. Plagioclase crystals generally show slight to moderate degrees of alteration (sericitization). K-feldspar occurs as anhedral to subhedral, rarely perthitic, untwined with variable size (up to 5 mm) and is usually found in a good state or in some cases slightly sericitized. K-feldspar oikocrysts usually include other minerals in a poikilitic relation. Clinopyroxene is subhedral to anhedral fine- to medium-grained (up to 2 mm), usually showing different degrees of alteration to amphibole (uralitization). Biotite is subhedral to anhedral fine- to medium-grained (up to 3 mm), generally found in good state or sometimes showing slight to moderate alteration to chlorite. Quartz occurs as fine interstitial grains between the early crystallized minerals. Opaques are subhedral to anhedral fine-grained (~0.2-1 mm), and occupy the irregular interstices in between the other minerals or are included within K-feldspar. Orthopyroxene is rarely found with anhedral to subhedral medium-grained. Sample PA24 is highly altered compared to the other Monzonite samples.

References

Andersson, M., Almqvist, B.S.G., Burchardt, S., Troll, V.R., Malehmir, A., Snowball, I., Kübler, L., 2016. Magma transport in sheet intrusions of the Alnö carbonatite complex, central Sweden. Sci. Rep. 6, 1–13. doi:10.1038/srep27635.

Assereto, R.L., Brusca, C., Gaetani, M., Jadoul, F., 1977. The Pb-Zn mineralization in the Triassic of the Dolomites Geological history and genetic interpretations. L'Industria Mineraria 28, 1–34.

Aubourg, C., Giordano, G., Mattei M., Speranza, F., 2002. Magma flow in rhyolitic dikes inferred from magnetic fabric analysis (Ponza Island, W Italy). Physics and Chemistry of the Earth, 27, 1263-1272.

Balini, M., Lucas, S.G., Jenks, J.F., Spielmann, J.A., 2010. Triassic ammonoid biostratigraphy: an overview. Geol. Soc. (Lond.) Spec. Publ. 334, 221–262.

Barth, S., Oberli, F., Meier, M., Blattner, P., Bargossi, G.M., Di Battistini, G., 1993. The evolution of a calc-alkaline basic to silicic magma system: Geochemical and Rb-Sr, Sm-Nd, and $^{18}O/^{16}O$ isotopic evidence from the Late Hercynian Atesina-Cima d'Asta volcano-plutonic complex, northern Italy. Geochim. Cosmochim. Acta 57, 4285–4300.

Bechstadt, T., Brandner, R., Mostler, H., Schmidt, K., 1977. Aborted rifting in the Triassic of the Eastern and Southern Alps. N. Jb. Geol. Palaont. Abh. 156, 157-178.

Beltrán-Triviño, A., Winkler, W., von Quadt, A., Gallhofer, D., 2016. Triassic magmatism on the transition from Variscan to Alpine cycles: evidence from U–Pb, Hf, and geochemistry of detrital minerals. Swiss J. Geosci. 109, 309–328. doi:10.1007/s00015-016-0234-3.

Benn, K., Ham, N.M., Pignotta, G.S., Bleeker, W., 1998. Emplacement and deformation of granites during transpression: Magnetic fabrics of the Archean Sparrow pluton, Slave Province, Canada. J. Struct. Geol. 20, 1247–1259. doi:10.1016/S0191-8141(98)00065-0.

Benn, K., Paterson, S.R., Lund, S.P., Pignotta, G.S., Kruse, S., 2001. Magmatic fabrics in batholiths as markers of regional strains and plate kinematics: Example of cretaceous Mt. Stuart batholith.

Phys. Chem. Earth, Part A Solid Earth Geod. 26, 343–354. doi:10.1016/S1464-1895(01)00064-3.

Bergmüller, F., Bärlocher, C., Geyer, B., Grieder, M., Heller, F., & Zweifel, P., 1994. A torque magnetometer for measurements of the high-field anisotropy of rocks and crystals. Measurement Science and Technology. 5, 1466-1470.

Bigi, G., Cosentino, D., Parrotto, M., Sartori, R., Scandone, P., 1990. Structural model of Italy, Scale 1:500.000, C.N.R. Progetto Finalizzato Geodinamica.

Blendinger, W., 1985. Middle Triassic strike-slip tectonics and igneous activity of the Dolomites (Southern Alps). Tectonophysics 113, 105–121. doi:10.1016/0040-1951(85)90112-X.

Bonadiman, C., Coltorti, M., Siena, F., 1994. Petrogenesis and T-fO_2 estimates of Mt. Monzoni complex (Central Dolomites, Soulhern Alps): a Triassic shoshonitic intrusion in a transcunent geodynamic setting. Eur J Mineral., 6, 943-966.

Bosellini, A., Castellarin, A., Doglioni, C., Guy, F., Lucchini, F., Perri, M.C., Rossi, P.M., Simboli, G., Sommavilla, E., 1982. Magmatismo e tettonica nel Trias delle Dolomiti, in: Guida Alla Geologia Del Sudalpino Centro-Orientale, pp. 189–210.

Bosellini, A., Gianolla, P., Stefani, M.M., 2003. Geology of the Dolomites. Episodes 26, 181–185.

Bouchez, J.L., Gleizes, G., Djouadi, T., & Rochette, P., 1990. Microstructure and magnetic susceptibility applied to emplacement kinematics of granites: the example of the Foix pluton (French Pyrenees). Tectonophysics 184, 157-171.

Brack, P., Mundil, R., Oberli, F., Meier, M., Rieber, H., 1996. Biostratigraphic and radiometric age data question the Milankovitch characteristics of the Latemar cycles (Southern Alps). Geology, 24, 371–375.

Brack, P., Mundil, R., Oberli, F., Meier, M., Rieber, H., 1997. Biostratigraphic and radiometric age data question the Milankovitch characteristics of the Latemar cycle (Southern Alps, Italy): Comment and Reply. Geology 25, 471-472.

Brack, P., Muttoni, G., 2000. High-resolution magnetostratigraphic and lithostratigraphic correlations in Middle Triassic pelagic carbonates from the Dolomites (northern Italy). Palaeogeogr. Palaeoclimatol. Palaeoecol. 161, 361–380. doi:10.1016/ S0031-0182(00)00081-X.

Brack, P., Rieber, H., 1993: Towards a better definition of the Anisian/Ladinian boundary: new biostratigraphic data and correlations of boundary sections from the Southern Alps. Ecl. geol. Helv., 86/2, 415-527.

Brack, P., Rieber, H., Mundil, R., Blendinger, W. Maurer, F., 2007. Geometry and chronology of growth and drowning of Middle Triassic carbonate platforms (Cernera and Bivera/Clapsavon) in the Southern Alps (northern Italy), Swiss Journal of Geosciences 100/3, 327– 348.

Brandner, R., 1984. Meeresspiegelschwankungen und Tektonik in der Trias der NW Tethys. Jb. Geol. B.-A., 126, 435-475.

Brandner, R., Keim, L., 2011. A 4-day geological field trip in the Western Dolomites. Geo.Alp 8, 76–118.

Brandner, R., Gruber, A., Morelli, C., Mair, V., 2016. Field trip 1. Pulses of Neotethys-Rifting in the Permomesozoic of the Dolomites. Geo.Alp 13, 7–70.

Brogger, W. C., 1895. Die Eruptivgesteine des Kristianiagebietes. II. Die Eruptionsfolge der triadischen Eruptivgesteine bei Predazzo in Siidtyrol: Skr. Norske Vid.-Akad. i Oslo, I., Mat. Nat. Kl, (7), 123-153.

Brusca, C., Gaetani, M., Jadoul, F., Viel, G., 1981. Paleogeografia ladino-carnica e metallogenesi del sudalpino. Mem. della Soc. Geol. Ital. 22, 65–82.

Büttner, S.H., 1999. The geometric evolution of structures in granite during continous deformation from magmatic to solid-state conditions: An example from the central European Variscan belt. Am. Mineral. 84, 1781–1792.

Callot, J.P., Geoffroy, L., Aubourg, C., Pozzi, J.P., Mege, D., 2001. Magma flow directions of shallow dykes from the East Greenland volcanic margin inferred from magnetic fabric studies. Tectonophysics 335, 313–329. doi:10.1016/S0040-1951(01)00060-9.

Carminati, E., Cavazza, D., Scrocca, D., Fantoni, R., Scotti, P., & Doglioni, C., 2010. Thermal and tectonic evolution of the southern Alps (northern Italy) rifting: Coupled organic matter maturity analysis and thermokinematic modeling. AAPG bulletin, 94(3), 369-397.

Carminati, E., Lustrino, M., Cuffaro, M., & Doglioni, C., 2010b. Tectonics, magmatism and geodynamics of Italy: what we know and what we imagine. Journal of the Virtual Explorer, 36(8).

Casetta, F., Coltorti, M., Marrocchino, E., 2017. Petrological evolution of the Middle Triassic Predazzo Intrusive Complex, Italian Alps. Int. Geol. Rev. 1–21. doi:10.1080/00206814.2017.1363676

Cashman, K.V., Sparks, R.S.J., 2013. How volcanoes work: A 25year perspective. Geol. Soc. Am. Bull. 125, 664-690.

Castellarin, A., Lucchini, F., Row, P.L., Simboli, G., Bosellini, A., Sommavilla, E. 1980. Middle Triassic magmatism in Southern Alps: a geodynamic model. Riv. Ital. Paleont. 85, 1111- 1124.

Castellarin, A., Lucchini, F., Row, P.L., Simboli, G., Bosellini, A., Sommavilla, E. 1980. Middle Triassic magmatism in Southern Alps: a geodynamic model. Riv. Ital. Paleont. 85, 1111- 1124.

Castellarin, A., Guy, F., Selli, L., 1982. Geologia dei dintorni del Passo di S. Nicolò e della Valle di Contrin (Dolomiti), in: Guida alla Geologia del Sudalpino Centro Orientale, pp. 231–242.

Castellarin, A., Lucchini, F., Rossi, P.L., Sartori, R., Simboli, G., Sommavilla, E., 1982b. Note geologiche sulle intrusioni di Predazzo e dei Monzoni, in: Guida Alla Geologia Del Sudalpino Centro-Orientale, pp. 211–220.

Castellarin, A., Lucchini, F., Rossi, P.L., Selli, L., Simboli, G., 1988. The Middle Triassic magmatic-tectonic arc development in the Southern Alps. Tectonophysics 146, 79–89.

Castellarin, A., Selli, L., Picotti, V., Cantelli, L., 1998. La tettonica delle Dolomiti nel quadro delle Alpi Meridionali orientali. Mem. della Soc. Geol. Ital. 53, 133–143.

Castellarin, A., Selli, L., Picotti, V., Cantelli, L., 1998b. Tettonismo e diapirismo Medio Triassico delle Dolomiti. Mem. Soc. Geol. Ital. 53, 145–169.

Castellarin, A., Cantelli, L., 2000. Neo-Alpine evolution of the Southern Eastern Alps. J. Geodyn. 30, 251–274. doi:10.1016/S0264-3707(99)00036-8.

Castellarin, A., Cantelli, L., Selli, L., 2004. Field Trip P54: Structure of the Italian Dolomites, partially along the southern sector of the transalp seismic profile, IGC Congress Field Trip Guidebook.

Castellarin, A., Nicolich, R., Fantoni, R., Cantelli, L., Sella, M., Selli, L., 2006. Structure of the lithosphere beneath the Eastern Alps (southern sector of the TRANSALP transect). Tectonophysics 414, 259–282. doi:10.1016/j.tecto.2005.10.013.

Castro, A., 1987. On granitoid emplacement and related structures. A review. Geol. Rundsch. 76, 101-124.

Cifelli, F., Minelli, L., Rossetti, F., Urru, G., Mattei, M., 2012. The emplacement of the Late Miocene Monte Capanne intrusion (Elba Island, Central Italy): constraints from magnetic fabric analyses. Int. J. Earth Sci. (Geol Rundsch) 101, 787-802.

Crisci, C. M., Ferrara, G., Mazzuoli, R., & Rossi, P. M., 1984. Geochemical and geochronological data on Triassic volcanism of the Southern Alps of Lombardy (Italy)-genetic implicaitons. Geol. Rundsch. 73, 279–292.

De Zanche, V., Gianolla, P., 1995: Litostratigrafia al limite Ladinico-Carnico (Sudalpino orientale). Ann. Univ. Ferrara, Sci. Terra, v. 5, 41-48.

De Zanche, V., Gianolla, P., Mietto, P., Siorpaes, C. Vail, P. 1993: Triassic sequence stratigraphy in the Dolomites (Italy). Memorie di Scienze Geologiche 45, 1–27.

Del Monte, M., Paganelli, L., & Simboli, G., 1967. The Monzoni intrusive rocks. A modal and chemical study. Mineral Petrogr Acta, 13, 75-118.

Djouadi, M.T., Gleizes, G., Ferré, E., Bouchez, J.L., Caby, R., Lesquer, A., 1997. Oblique magmatic structures of two epizonal granite plutons, Hoggar, Algeria: late-orogenic emplacement in a transcurrent orogen. Tectonophysics 279, 351–374. doi:10.1016/S0040-1951(97)00123-6.

Doglioni, C., 1982. Tettonica Triassica nella Valle di Livinallongo (Dolomiti centrali). Ann. Univ. Ferrara, Zsez.IX, Scienze Geol. Paleont. 8, 1-21.

Doglioni, C., 1983. Duomo medio-Triassico nelle Dolomiti. Rend. della Soc. Geol. Ital. 6, 13–16.

Doglioni, C., 1984a. Tettonica triassica transpressiva nelle Dolomiti. G. Di Geol. 46, 47–60.

Doglioni, C., 1984b. Triassic diapiric structures in the central Dolomites (northern Italy). Eclogae Geol. Helv. 77, 261–285.

Doglioni, C., 1985. The overthrusts in the Dolomites: ramp-flat systems. Eclogae Geol. Helv. 78, 335–350.

Doglioni C., 1987. Tectonics of the Dolomites (Southern Alps, Northern Italy). J. Struct. Geol. 9, 181-193.

Doglioni, C., 1988. Examples of strike-slip tectonics on platform-basin margins. Tectonophysics 156, 293–302. doi:10.1016/0040-1951(88)90066-2.

Doglioni, C., 2007. Tectonics of the Dolomites. Bull. Angew. Geol. 12, 11–15.

Doglioni, C., Carminati, E., 2008. Structural Styles and Dolomites Field Trip. Mem. Descr. della Cart. Geol. d'Italia 82, 301.

Emeleus, C.H., Troll, V.R., Chew, D.M., Meade, F.C., 2012. Lateral versus vertical emplacement in shallow-level intrusions? The Slieve Gullion Ring-complex revisited. J. Geol. Soc. London. 169, 157–171. doi:10.1144/0016-76492011-044.

Ernst, R.E., Baragar, W.R.A., 1992. Evidence from magnetic fabric for the flow pattern of magma in the Mackenzie giant radiating dyke swarm. Nature 356, 511–513. doi:10.1038/356511a0.

Ferry, J. M., Wing, B. A., Penniston-Dorland, S. C., & Rumble, D., 2002. The direction of fluid flow during contact metamorphism of siliceous carbonate rocks: new data for the Monzoni and Predazzo aureoles, northern Italy, and a global review. Contributions to Mineralogy and Petrology, 142(6), 679-699.

Gallien, F., Abart, R., & Wyhlidal, S., 2007. Contact metamorphism and selective metasomatism of the layered Bellerophon Formation in the eastern Monzoni contact aureole, northern Italy. Mineralogy and Petrology, 91(1-2), 25-53.

Garzanti, E., 1985. The sandstone memory of the evolution of a Triassic volcanic arc in the Southern Alps, Italy. Sedimentology 32, 423–433.

Gianolla, P., De Zanche, V., Mietto, P., 1998. Triassic sequence stratigraphy in the Southern Alps (Northern Italy): definition of sequences and basin evolution. In: de Graciansky, P.-C., Hardenbol, J., Jacquin, T. and P.R. Vail (Eds.). Mesozoic and Cenozoic Sequence Stratigraphy of European Basins. SEPM Special Publications 60, 719–747.

Gianolla, P., Avanzini, M., Breda, A., Kustatscher, E., Preto, N., Roghi, G., Furin, S., Massari, F., Picotti, V., Stefani, M., 2010. Field trip to the world heritage site of the Tethysian Triassic, September 5-10, 2010, Dolomites, Southern Alps, Italy. 122 pp.

Graham, J.W., 1954. Magnetic susceptibility anisotropy, an unexploited petrofabric element. Geol. Soc. Am. Bull. 65, 1257-1258.

Handy, M. R., Schmid, S. M., Bousquet, R., Kissling, E., & Bernoulli, D. (2010). Reconciling plate-tectonic reconstructions of Alpine Tethys with the geological–geophysical record of spreading and subduction in the Alps. *Earth-Science Reviews*, *102*(3-4), 121-158.

Hansel, V., 1878. Die petrographische Beschaffenheit des Monzonits von Predazzo. Jahrb. der Kais. Geol. Reichsanstalt 28, 449–466.

Hörnes, R., 1912. Zur Geologie von Predazzo. Sitzungsberichte der Akad. der Wissenschaften Math. Klasse 121, 3–31.

Hrouda, F., 1982. Magnetic anisotropy of rocks and its application in geology and geophysics. Geophys. Surv. 5, 37–82.

Hrouda, F., Jelínek, V., 1990. Resolution of ferromagnetic and paramagnetic anisotropies, using combined low-field and high-field measurements. Geophys. J. Int. 103, 75-84.

Hrouda, F., Jelínek, V., Zapletal, K., 1997. Refined technique for susceptibility resolution into ferromagnetic and paramagnetic components based on susceptibility temperature-variation measurement. Geophys. J. Int.129, 715-719.

Hutton, D.H.W., 1988. Granite emplacement mechanisms and tectonic controls: inferences from deformation studies. Trans. R. Soc. Edinb. Earth Sci. 79, 245–255. doi:10.1017/S0263593300014255.

Jelinek, V., 1977. The statistical theory of measuring anisotropy of magnetic susceptibility of rocks and its application. Geofyzika Brno, pp. 77.

Jelínek, V., 1981. Characterization of the magnetic fabric of rocks. Tectonophysics 79, 63-67.

Jelínek, V., Pokorný, J., 1997. Some new concepts in technology of transformer bridges for measuring susceptibility anisotropy of rocks. Physics and Chemistry of the Earth 22, 179-181.

Just, J., Kontny, A., De Wall, H., Hirt, A.M. & Martín-Hernandéz, F., 2004. Development of magnetic fabrics during hydrothermal alteration in the Soultz-sous-Forets granite from the EPS-1 borehole, Upper Rhine Graben. In: Martín-Hernández, F., Lunebrg, C.M., Aubourg, C. & Jackson, M. (eds) Magnetic Fabric: Methods and Applications. Geological Society, London, Special Publications 238, 509-526.

Kennedy, B.M., Mark Jellinek, A., Stix, J., 2008. Coupled caldera subsidence and stirring inferred from analogue models. Nat. Geosci. 1, 385–389. doi:10.1038/ngeo206.

Knight, M.D., Walker, G.P.L., 1988. Magma Flow Directions in Dikes of the Koolau Complex, Oahu, Determined From Magnetic Fabric Studies. J. Geophys. Res. 93, 4301-4319.

Leonardi, P., 1967. Le Dolomiti. Geologia dei monti tra Isarco e Piave. Consiglio Nazionale delle Ricerche. Rome, 1019 pp. (2 volumes).

Lucchini, F., Rossi, P.L., Simboli, G., 1982. Il magmatismo triassico dell’area di Predazzo (Alpi Meridionali, Italia). In A. CASTELLARIN e G.B. VAI (Eds.), Guida alla geologia del Sudalpino centro-orientale. Guide geol. reg. S.G.I., pp. 221-230, Bologna.

Maes, S.M., Tikoff, B., Ferré, E.C., Brown, P.E., Miller, J.D., 2007. The Sonju Lake layered intrusion, northeast Minnesota: Internal structure and emplacement history inferred from magnetic fabrics. Precambrian Res. 157, 269–288. doi:10.1016/j.precamres.2007.02.021.

Magee, C., O'Driscoll, B., Petronis, M.S., Stevenson, C.T.E., 2016. Three-dimensional magma flow dynamics within subvolcanic sheet intrusions. Geosphere 12, 842-866.

Marangon, A., Gattolin, G., Della Porta, G., Preto, N., 2011: The Latemar: a flat- topped, steep fronted platform dominated by microbialites and synsedimentary cements. Sedimentary Geology, doi: 10.1016/j.sedgeo.2011.09.001

Marinelli, M., Viel, G., Farabegoli, E., 1980. Il Permo-Trias delle Alpi Meridionali: evoluzione tardo-ercinica di un bacino marginale di retroarco sialico. L'Industria Mineraria 6, 1–14.

Marocchi, M., Morelli, C., Mair, V., Klötzli, U., & Bargossi, G. M., 2008. Evolution of large silicic magma systems: new U-Pb zircon data on the NW Permian Athesian Volcanic Group (Southern Alps, Italy). The Journal of Geology, 116(5), 480-498.

Marre, J., 1986. The Structural Analysis of Granitic Rocks. Elsevier, New York 123 pp.

Martin Hernandez, F., & Hirt, A.M., 2001. Separation of ferrimagnetic and paramagnetic anisotropies using a high- field torsion magnetometer. Tectonophysics 337, 209-221.

Masetti D., Trombetta G.L. 1998: L'eredità anisica nella nascita ed evoluzione delle piattaforme medio-triassiche delle Dolomiti occidentali, Mem. Sci. Geol., 50, 213-237.

Menegazzo Vitturi, L., Visonà, D., & Zantedeschi, C., 1995. Amphibole composition in rocks from Predazzo volcano-plutonic complex (Southern Alps, Italy). Memorie Di Scienze Geologiche, 47, 87-94.

Mietto, P., Manfrin, S., 1995. A high resolution Middle Triassic ammonoid standard scale in the Tethys Realm. A preliminary report. Bull. Soc. Géol. France 1995/5, 539-563.

Mietto, P., Manfrin, S., Preto, N., Rigo, M., Roghi, G., Furin, S., Gianolla, P., Posenato, R., Muttoni, G., Nicora, A., Buratti, N., Cirilli, S., Spötl, C., Ramezani, J., Bowring, S.A., 2012. The

Global Boundary Stratotype Section and Point (GSSP) of the Carnian Stage (Late Triassic) at Prati di Stuores/Stuores Wiesen Section (Southern Alps, NE Italy). Episodes 35, 414-430.

Mundil, R., 1996. High resolution U-Pb dating of Middle Triassic volcaniclastics: Verification of tuning parameters for carbonate sedimentation and time-scale calibration. [Ph.D. dissert.], Zurich, Swiss Federal Institute of Technology, No. 11767.

Nédélec, A., Trindade, R., Peschler, A., Archanjo, C., Macouin, M., Poitrasson, F., Bouchez, J.L., 2015. Hydrothermally-induced changes in mineralogy and magnetic properties of oxidized A-type granites. Lithos 212, 145-157.

O'Driscoll, B., Troll, V.R., Reavy, R.J., Turner, P., 2006. The Great Eucrite intrusion of Ardnamurchan, Scotland: Reevaluating the ring-dike concept. Geology 34, 189–192. doi:10.1130/G22294.1.

Ogilvie Gordon, M.M., 1902. Monzoni and Upper Fassa. Geol. Mag., dec. 10, vol. 9, p. 309, London.

Ogilvie Gordon, M.M., 1902-1903. The Geological Structure of Monzoni and Fassa. Transactions of the Edinburgh geological society. vol. VIII.

Paterson S.R., Fowler T.K., 1993. Re-examining pluton emplacement processes. J. Struct. Geol. 15, 191-206.

Paterson, S.R., Fowler, T.K., Schmidt, K.L., Yoshinobu, A.S., Yuan, E.S., Miller, R.B., 1998. Interpreting magmatic fabric patterns in plutons. Lithos 44, 53–82. doi:10.1016/S0024-4937(98)00022-X.

Penck, W., 1911. Der geologische Bau des Gebirges von Predazzo. Neues Jahrb. f. Min., Geol. u. Paläont. 32, 239—382.

Petronis, M.S., Hacker, D.B., Holm, D.K., Geissman, J.W., Harlen, S.S., 2005. Magnetic flow paths and paleomagnetism of the Miocene Stoddard Mountain laccolith, Iron Axis region, southwest Utah, USA. In: Martın-Hernandez, F., Luneburg, C.M., Aubourg, C., Jackson, M. (Eds.), Magnetic Fabric: Methods and Applications. Geol. Soc. Spec. Publ. 238, 251–283.

Petronis, M.S., O'Driscoll, B., Lindline, J., 2011. Late stage oxide growth associated with hydrothermal alteration of the Western Granite, Isle of Rum, NW Scotland. Geochemistry, Geophysics, Geosystems 12, 1.

Petronis, M.S., Delcamp, A., van Wyk de Vries, B., 2013. Magma emplacement into the Lemptégy scoria cone (Chaîne Des Puys, France) explored with structural, anisotropy of magnetic susceptibility, and paleomagnetic data. Bulletin of Volcanology 75, 753.

Petrovský, E.D., Kapička, A., 2006. On determination of the Curie point from thermomagnetic curves. J. Geophys. Res. Solid Earth 111, 1–10.

Pisa, G., Castellarin A., Lucchini, F., Rossi, P.L., Simboli, G., Bosellini, A., Sommavilla, E. 1980. Middle Triassic magmatism in Southern Alps. I: a review of general data in the Dolomites. Riv. It. Paleont. Strat. 85, 1093-1110.

Polteau, S., Ferré, E.C., Planke, S., Neumann, E.R., and Chevallier, L., 2008. How are saucer-shaped sills emplaced? Constraints from the Golden Valley Sill, South Africa. J. Geophys. Res. 113, B12104.

Raposo, M.I.B., Gastal, P.M.P., 2009. Emplacement mechanism of the main granite pluton of the Lavras do Sul intrusive complex, South Brazil, determined by magnetic anisotropies. Tectonophysics 466, 18-31.

Raposo, M.I.B., Pressi, L.F., de Assis Janasi, V., 2012. Magnetic fabrics and their relationship with the emplacement of the Piracaia pluton, SE Brazil. Int. J. Earth Sci. 101, 773–786. doi:10.1007/s00531-011-0696-5.

Roche, O., Druitt, T.H., Merle, O., 2000. Experimental study of caldera formation. J. Geophys. Res. 105, 395-416.

Rochette, P., Fillion, G., Mollard, P., Vergne, R., 1983. Utilisation d'un magnétomètre à effet Josephson pour l'analyse de l'anisotropie magnétique des roches. CR Acad. Sci. Paris 296, 557-559.

Rochette, P., Jackson, M., Aubourg, C., 1992. Rock magnetism and interpretation of anisotropy of magnetic susceptibility. Review of Geophysics 30, 209-226.

Román-Berdiel, T., Gapais, D., Brun, J.P., 1997. Granite intrusion along strike-slip zones in experiment and nature. Am. J. Sci. 297, 651–678. doi:10.2475/ajs.297.6.651.

Rosenberg, C.L., 2004. Shear zones and magma ascent: A model based on a review of the Tertiary magmatism in the Alps. Tectonics 23, 21. doi:10.1029/2003TC001526.

Sarti, M., Ardizzoni F. 1984. Tettonica triassica nel Gruppo di cima Pape-Pale di Sanson (Dolomiti Bellunesi). Mem. Sc. Geol. Padova, 36, 353-370.

Schaltegger, U., Brack, P., 2007. Crustal-scale magmatic systems during intracontinental strike-slip tectonics: U, Pb and Hf isotopic constraints from Permian magmatic rocks of the Southern Alps. Int. J. Earth Sci. 96, 1131–1151. doi:10.1007/s00531-006-0165-8.

Sloman, L., 1989. Triassic shoshonites from the Dolomites, northern Italy: alkaline arc rocks in a strike-slip setting. J. Geophys. Res. 94, 4655–4666.

Sparks, R.S.J., 2003. Forecasting volcanic eruptions. Earth and Planet. Sci. Lett. 210, 1-15.

Staehle, V., Frenzel, G., Hess, J. C., Saup, F., Schmidt, S. T. & Schneider, W., 2001. Permian metabasalt and Triassic alkaline dykes in the northern Ivrea zone: clues to the post-Variscan geodynamic evolution of the Southern Alps. Schweizerische Mineralogische und Petrographische Mitteilungen 81, 1–21.

Stefani, M., Furin, S., Gianolla, P., 2010. The changing climate framework and depositional dynamics of Triassic carbonate platforms from the Dolomites, Pal. Pal. Pal., 290, 43–57.

Talbot, J.Y., Chen, Y., Faure, M., 2005. A magnetic fabric study of the Aigoual-Saint Guiral-Liron granite pluton (French Massif Central) and relationships with its associated dikes. J. Geophys. Res. Solid Earth. 110, 1–14. doi:10.1029/2005JB003699.

Tarling, D.H., Hrouda, F., 1993. The Magnetic Anisotropy of Rocks. Chapman & Hall, London, pp. 217.

Tibaldi, A., Pasquarè, F.A., 2008. A new mode of inner volcano growth: The "flower intrusive structure". Earth and Planet. Sci. Lett. 271, 202-208.

Tikoff, B., Teyssier, C., 1992. Crustal-scale, en echelon "P-shear' tensional bridges: a possible solution to the batholithic room problem. Geology 20, 927–930. doi:10.1130/0091-7613(1992)020<0927:CSEEPS>2.3.CO;2.

Tomek, F., Žák, J., Chadima, M., 2014. Magma flow paths and strain patterns in magma chambers growing by floor subsidence: a model based on magnetic fabric study of shallow-level plutons in the Štiavnica volcano-plutonic complex, Western Carpathians. Bull. Volcanol. 76. doi:10.1007/s00445-014-0873-z.

Tomek, F., Žák, J., Verner, K., Holub, F. V., Sláma, J., Paterson, S. R., Memeti, V., 2017. Mineral fabrics in high-level intrusions recording crustal strain and volcano–tectonic interactions: the Shellenbarger pluton, Sierra Nevada, California. J. Geol. Soc. 174, 193-208.

Van der Voo, R., Klootwijk, C.T., 1972. Paleomagnetic reconnaissance study of the Flamanville granite with a special reference to the anisotropy of its susceptibility. Geol. Mijnbouw 51, 609-617.

Vardabasso, S., 1929. Rapporti tra attività magmatica e vicende tettoniche nella provincia petrografica di Predazzo: Studi Trentini Di Scienze Naturali, 11, 49–64.

Vardabasso, S., 1930. Carta geologica del territorio eruttivo di Predazzo e Monzoni: Ufficio Idrografico del Magistrato alle Acque di Venezia. scale 1:25000, 2 sheet.

Viel G., 1979. Litostratigrafia ladinica: una revisione. Ricostruzione paleogeografica e paleostrutturale dell'area Dolomitica-Cadorina (Alpi Meridionali). Riv. It. Paleont. Strat. 85(1), 85–125, 85(2), 297–352.

Viel, G., 1982. Polarità tettonica e vulcanismo ladino-carnici del Sudalpino. Rend. Soc. Geol. Ital. v. 4 (1981), pp.261-262, Roma.

Visonà, D., 1997. The Predazzo multipulse intrusive body (Western Dolomites, Italy). Field and mineralogical studies. Mem. Sci. Geol. 49, 117– 125.

Visonà, D., Fioretti, A.M., Poli, M.E., Zanferrari, A., Fanning, M., 2007. U-Pb SHRIMP zircon dating of andesite from the Dolomite area (NE Italy): geochronological evidence for the early onset of Permian Volcanism in the eastern part of the southern Alps. Swiss J. Geosci. 100, 313–324. doi:10.1007/s00015-007-1219-z.

Von Richthofen, F.F., 1860. Geognostische Beschreibung der Umgebung von Predazzo, Sanct Cassian und der Seiser Alpe in Süd-Tyrol. Verlag von Justus Perthes, Gotha.

Zanetti, A., Mazzucchelli, M., Sinigoi, S., Giovanardi, T., Peressini, G., Fanning, M., 2013. SHRIMP U-Pb ZirconTriassic Intrusion Age of the Finero Mafic Complex (Ivrea-Verbano Zone, Western Alps) and its Geodynamic Implications. J. Petrol. 54, 2235–2265. doi:10.1093/petrology/egt046.

Wotzlaw, J. F., Brack, P., & Storck, J. C., 2018. High-resolution stratigraphy and zircon U–Pb geochronology of the Middle Triassic Buchenstein Formation (Dolomites, northern Italy): precession-forcing of hemipelagic carbonate sedimentation and calibration of the Anisian–Ladinian boundary interval. Journal of the Geological Society, 175(1), 71-85.

Figures

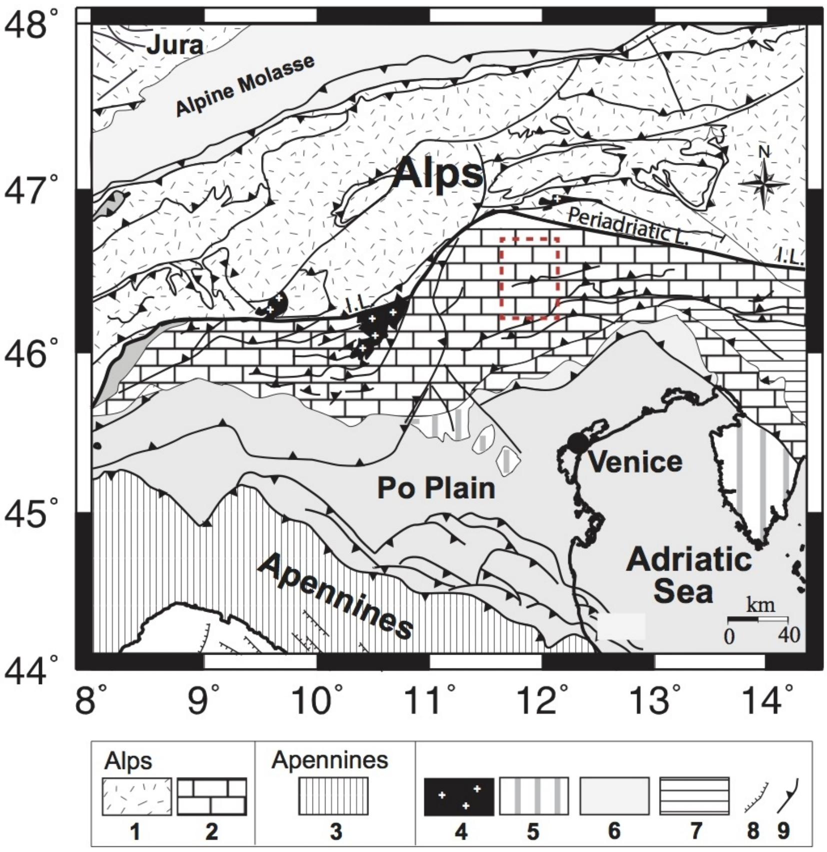

Figure 1: Simplified geological map of the Southern Alps. Alps: 1) Australpine, Penninic and Helvetic units; 2) Southern Alps units. Apennines: 3) Apenninic units; 4) Cenozoic volcanic and plutonic bodies; 5) foreland units; 6) foreland basin units; 7) Dinaric units; 8) normal faults; 9) thrust faults. Redrawn and simplified from Bigi et al. (1990). The dashed rectangle shows the location of the map of Figure 2. I.L.: Insubric line.

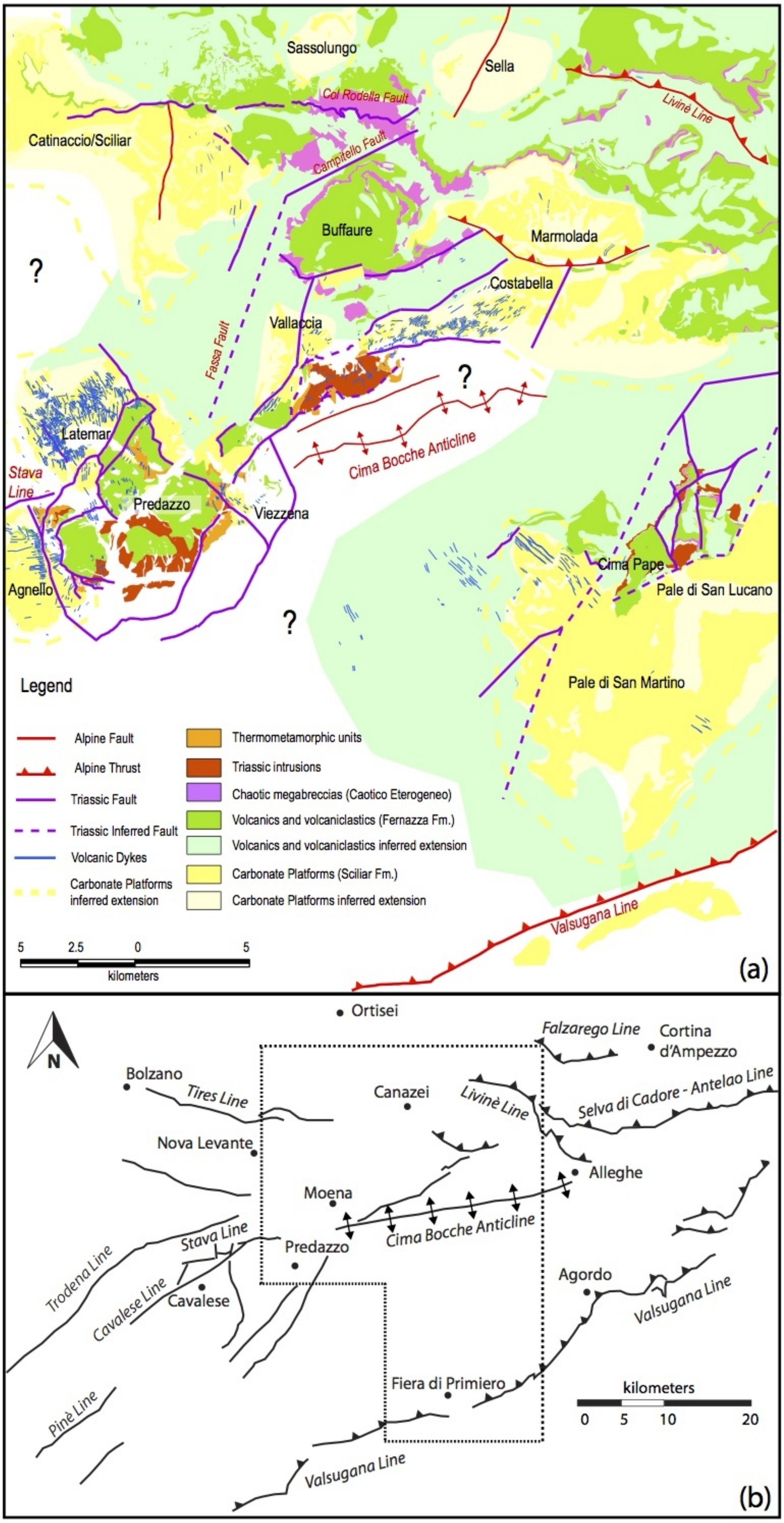

Sassolungo
Sella
Col Rodella Fault
Livinè Line
Catinaccio/Sciliar
Campitello Fault
Buffaure
Marmolada
?
Costabella
Fassa Fault
Vallaccia
?
Latemar
Cima Bocche Anticline
Stava Line
Predazzo
Viezzena
Cima Pape
Agnello
Pale di San Lucano
?
Pale di San Martino
Legend
Alpine Fault
Alpine Thrust
Triassic Fault
Triassic Inferred Fault
Volcanic Dykes
Carbonate Platforms inferred extension
Thermometamorphic units
Triassic intrusions
Chaotic megabreccias (Caotico Eterogeneo)
Volcanics and volcaniclastics (Fernazza Fm.)
Volcanics and volcaniclastics inferred extension
Carbonate Platforms (Sciliar Fm.)
Carbonate Platforms inferred extension
Valsugana Line
5 2.5 0 5
kilometers
(a)
Ortisei
N
Falzarego Line
Cortina d'Ampezzo
Bolzano
Tires Line
Canazei
Livinè Line
Selva di Cadore - Antelao Line
Nova Levante
Alleghe
Moena
Cima Bocche Anticline
Stava Line
Predazzo
Trodena Line
Cavalese Line
Cavalese
Agordo
Valsugana Line
Fiera di Primiero
kilometers
0 5 10 20
Pinè Line
Valsugana Line
(b)

1125

Figure 2: a) Unrestored paleogeographic map at Ladinian times of the central-western region of the Dolomites. Notice the regional extent of volcanics and the continuity of plutonic bodies and associated thermo-metamorphic rocks for more than 20 km in a SW-NE direction, i.e., parallel to major Triassic faults. Cenozoic faults and structures are shown for reference. The location of the map is shown in Fig. 1. b) Simplified tectonic map of the Dolomites, showing only major faults, not differentiated by their age. The dashed area represents the location of panel a.

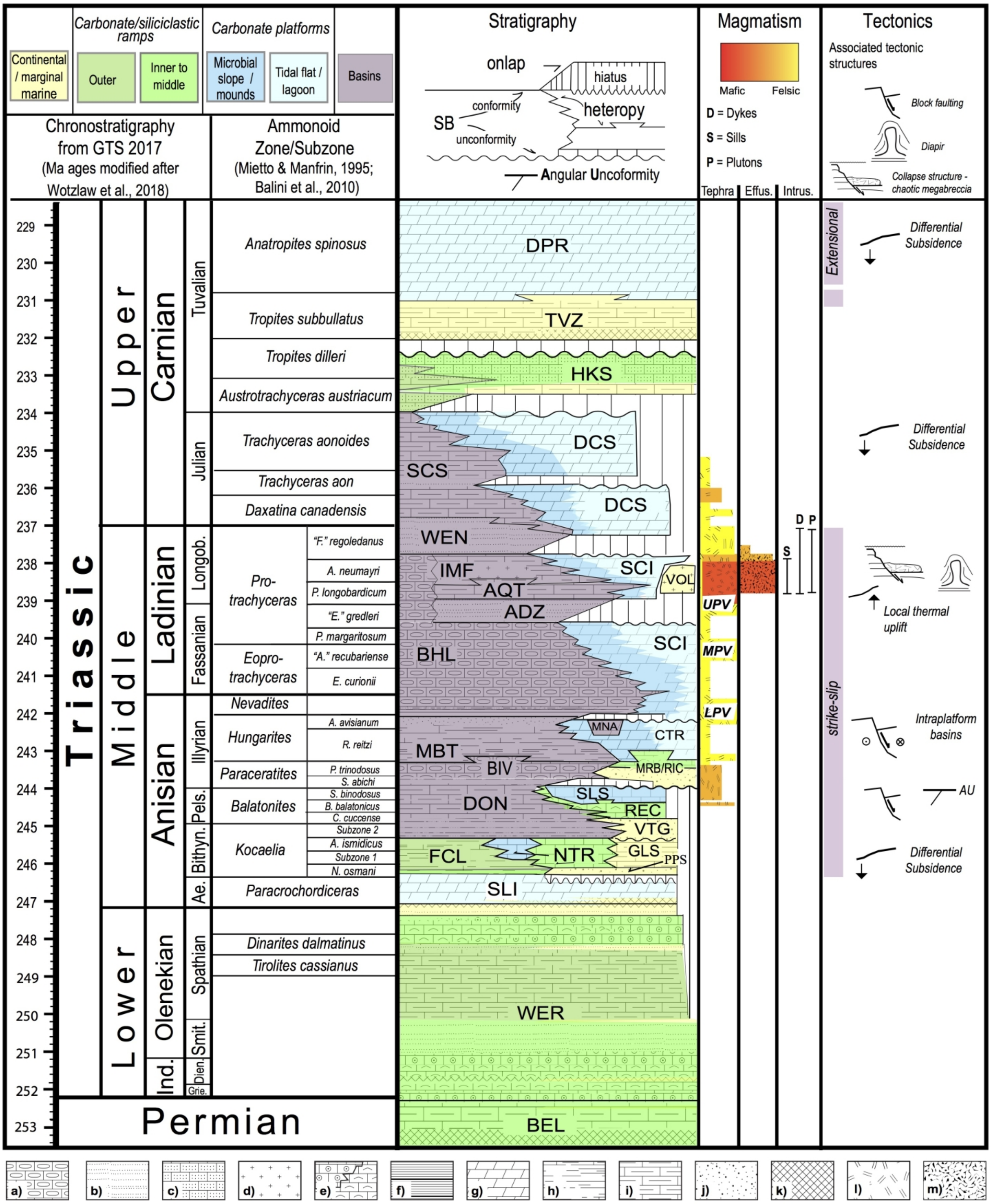

Figure 3: Schematic bio-chrono-stratigraphic scheme of the Middle-Upper Triassic succession of the Dolomites with the most important magmatic pulse recorded as ash falls, tefhras or effusives. The position of the known possible source volcanic areas from the Southern Alps is indicated. In the subsurface of Venetian Plain, a significant number of volcanic products (mainly effusve and

intrusive) is known (e.g., Brusca et al., 1981) Lithostratigraphic abbreviations: BEL: Bellerophon Formation; WER: Werfen Formation; SLI: Lower Serla Dolomite; PPS: Piz da Peres Conglomerate; FCL: Coll'Alto dark Limestones; NTR: Monte Rite Formation; GLS: Gracilis Formation; VTG: Voltago Conglomerate; DON: Dont Formation; REC: Recoaro Limestone; SLS Upper Serla Dolomite/Formation; MRB/RIC: Richthofen Conglomerate and Morbiac dark Limestone; BIV: Bivera Formation; MBT: Ambata Formation; MNA: Moena Formation; CTR: Contrin Formation; BHL: Livinallongo Formation; SCI: Sciliar Formation; ADZ: Zoppè Sandstone; AQT: Aquatona Formation; IMF: Fernazza Volcanic Complex (Fernazza Formation); WEN: Wengen Formation; SCS: San Cassiano Formation; DCS: Cassian Dolomite; HKS: Heiligkreuz Formation; TVZ: Travenanzes Formation; DPR: Dolomia Principale. Lithologies: a) cherty limestone; b) sandstone; c) sandy limestone; d) volcanics and volcaniclastics; e) oolitic-bioclastic limestone; f) black platy limestone or dolostone, black shale; g) dolostone; h) marlstone, claystone and shale; i) marly limestone; j) conglomerate; k) evaporates; l) tuffs, pyroclastics; m) lava, pillow-lava-pillow breccia; m) volcanos with mainly effusive eruptions. LPV, MPV, UPV= Lower -Middle - Upper Pietra Verde.

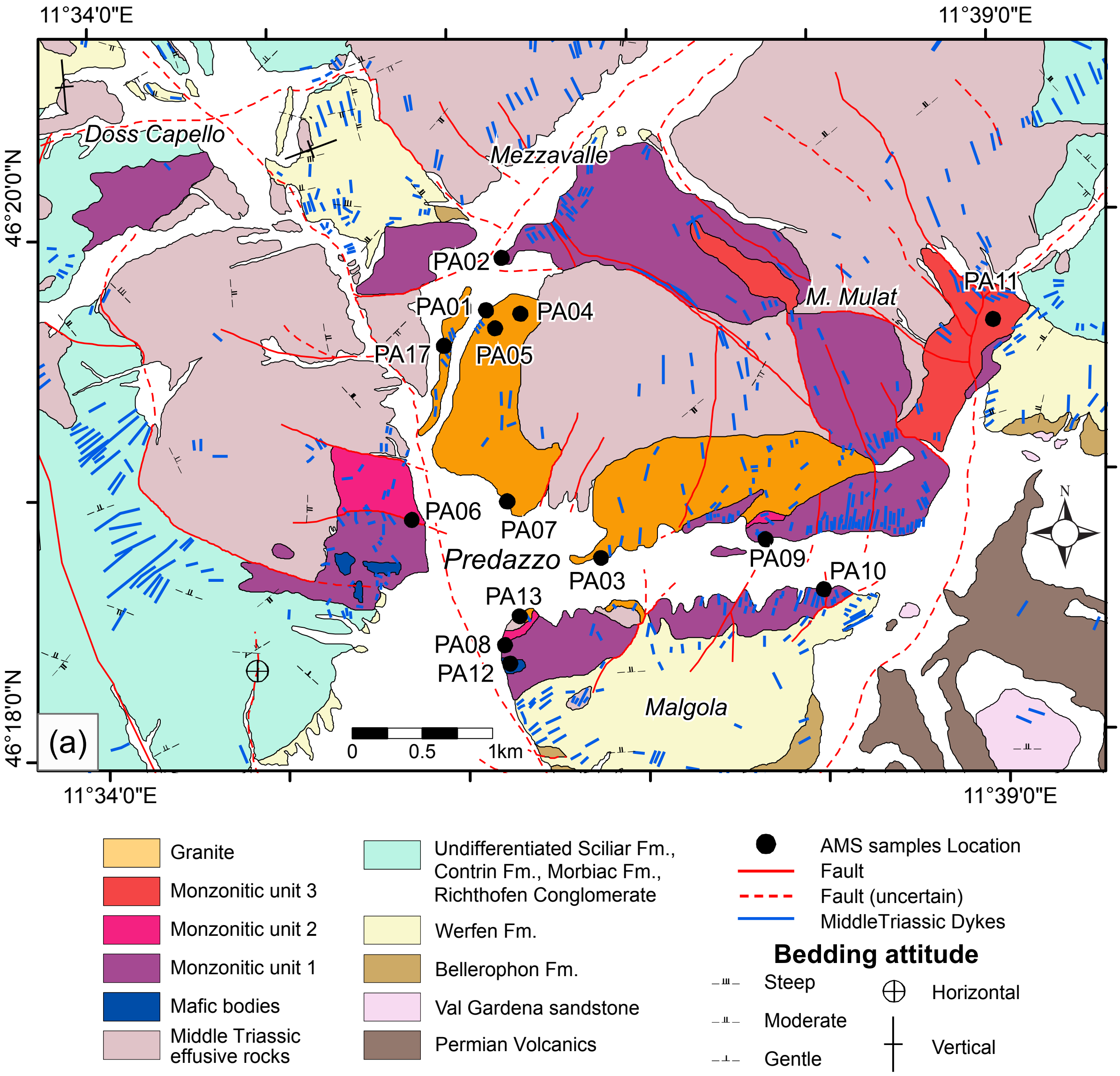
11°34'0"E
11°39'0"E
46°20'0"N
46°18'0"N
Doss Capello
Mezzavalle
M. Mulat
Predazzo
Malgola
PA01
PA02
PA03
PA04
PA05
PA06
PA07
PA08
PA09
PA10
PA11
PA12
PA13
PA17
0
0.5
1km
N
(a)
Granite
Monzonitic unit 3
Monzonitic unit 2
Monzonitic unit 1
Mafic bodies
Middle Triassic effusive rocks
Undifferentiated Sciliar Fm., Contrin Fm., Morbiac Fm., Richthofen Conglomerate
Werfen Fm.
Bellerophon Fm.
Val Gardena sandstone
Permian Volcanics
AMS samples Location
Fault
Fault (uncertain)
MiddleTriassic Dykes
Bedding attitude
Steep
Moderate
Gentle
Horizontal
Vertical

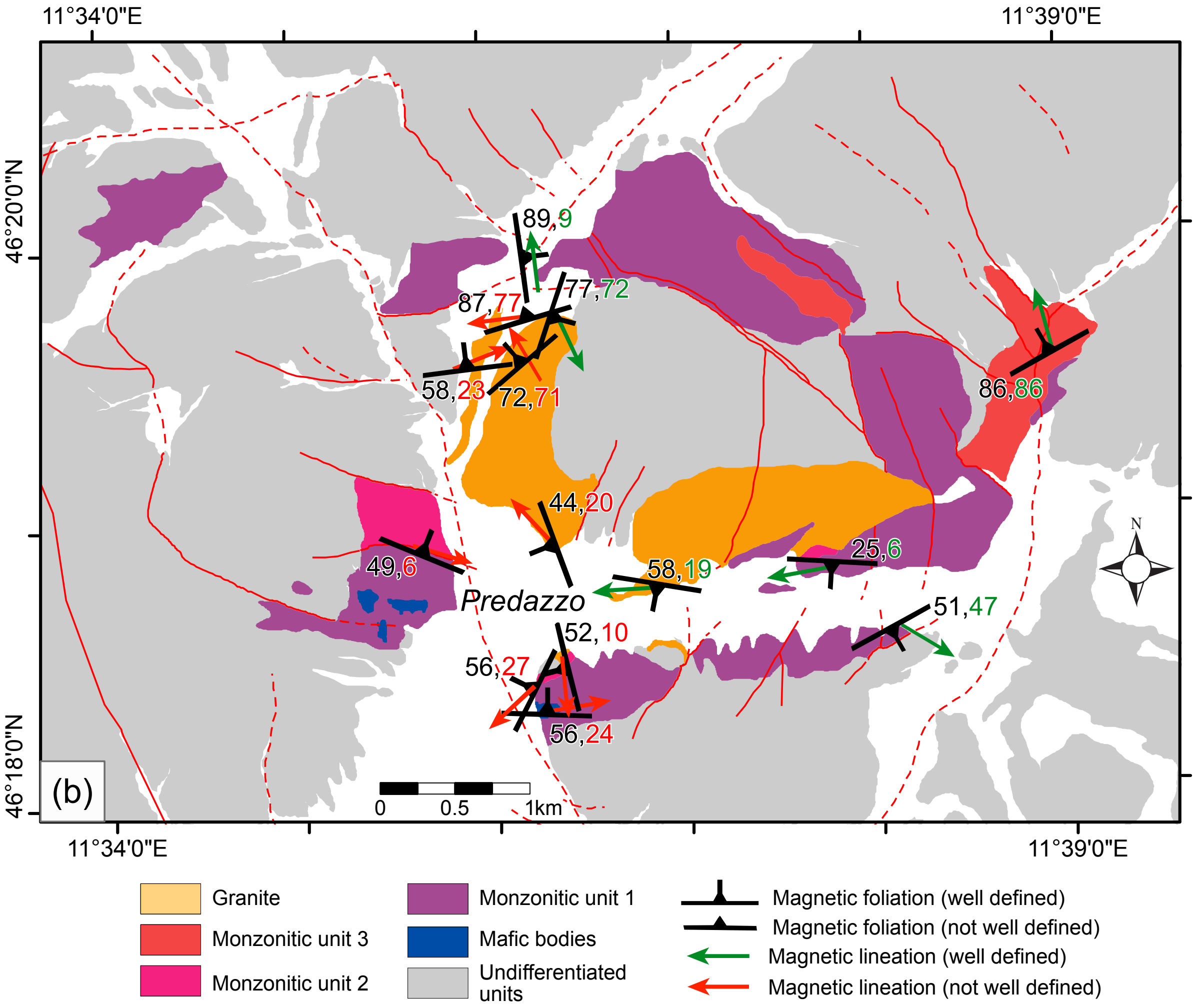

Figure 4: Geological map of the pre-Quaternary units of the Predazzo area (from Visonà, 1997), showing the location of the sampling sites (a) and measured magnetic foliations and lineations (b). The two numbers besides each site indicate the magnetic foliation and lineation dips, respectively.

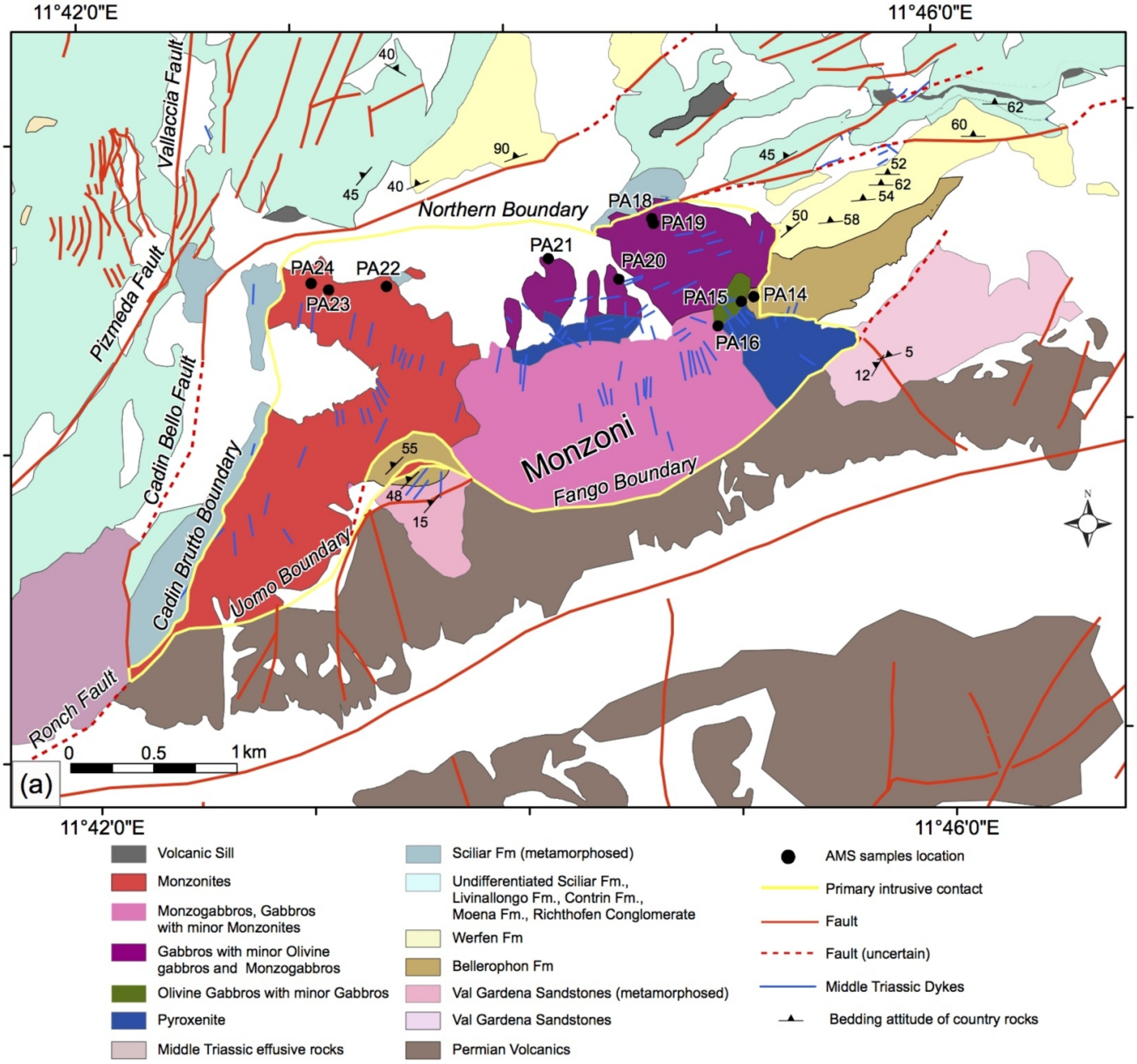

11°42'0"E
11°46'0"E
46°24'0"N
46°22'0"N
Vallaccia Fault
Pizmeda Fault
Cadin Bello Fault
Cadin Brutto Boundary
Uomo Boundary
Northern Boundary
Fango Boundary
Ronch Fault
Monzoni
PA14
PA15
PA16
PA18
PA19
PA20
PA21
PA22
PA23
PA24
0
0.5
1 km
(a)
Volcanic Sill
Monzonites
Monzogabbros, Gabbros with minor Monzonites
Gabbros with minor Olivine gabbros and Monzogabbros
Olivine Gabbros with minor Gabbros
Pyroxenite
Middle Triassic effusive rocks
Sciliar Fm (metamorphosed)
Undifferentiated Sciliar Fm., Livinallongo Fm., Contrin Fm., Moena Fm., Richthofen Conglomerate
Werfen Fm
Bellerophon Fm
Val Gardena Sandstones (metamorphosed)
Val Gardena Sandstones
Permian Volcanics
AMS samples location
Primary intrusive contact
Fault
Fault (uncertain)
Middle Triassic Dykes
Bedding attitude of country rocks

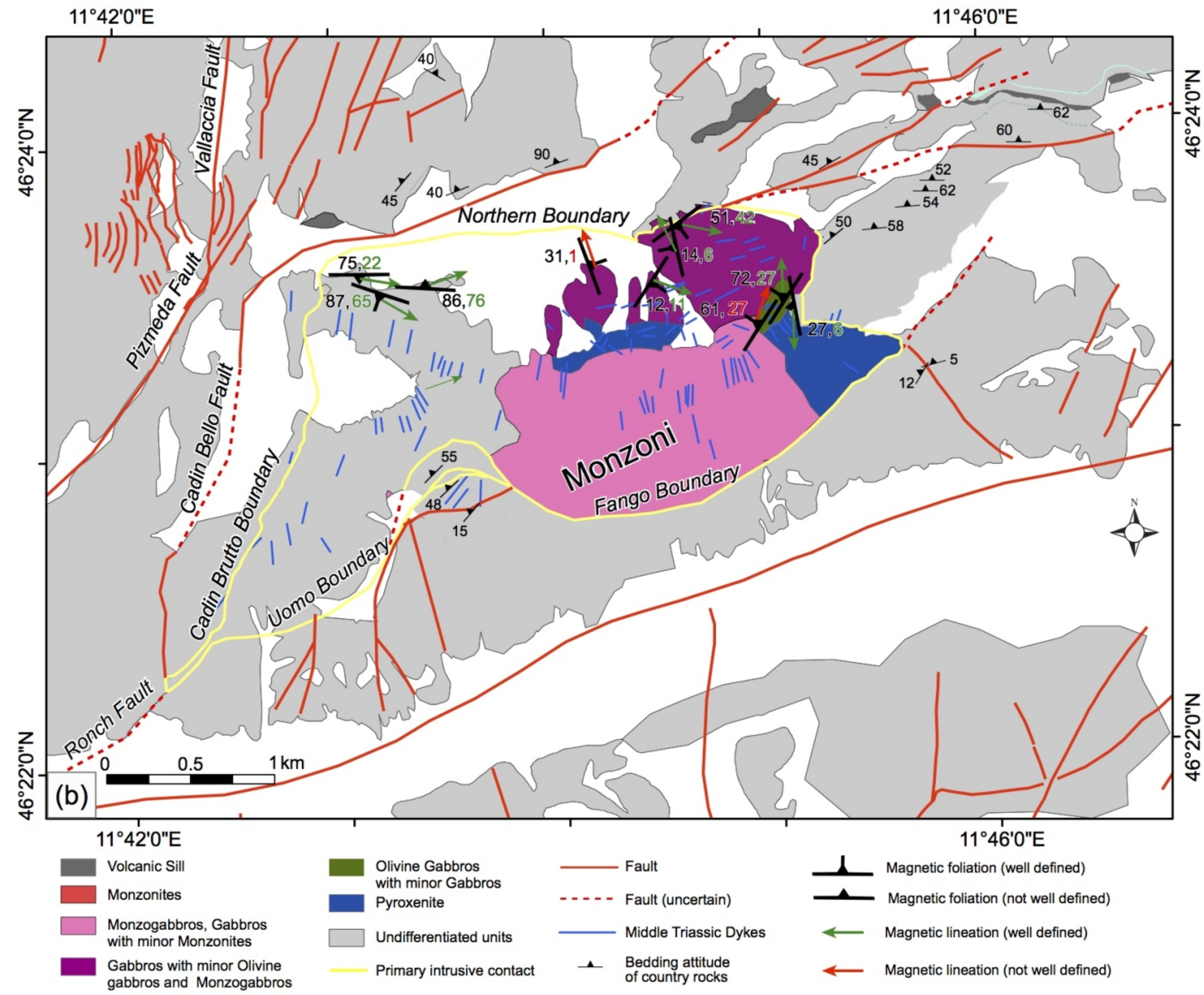

Figure 5: Geological map of the pre-Quaternary units of the Monzoni area, showing the location of the sampling sites (a) and measured magnetic foliations and lineations (b). The two numbers at each site indicate the magnetic foliation and lineation dips, respectively.

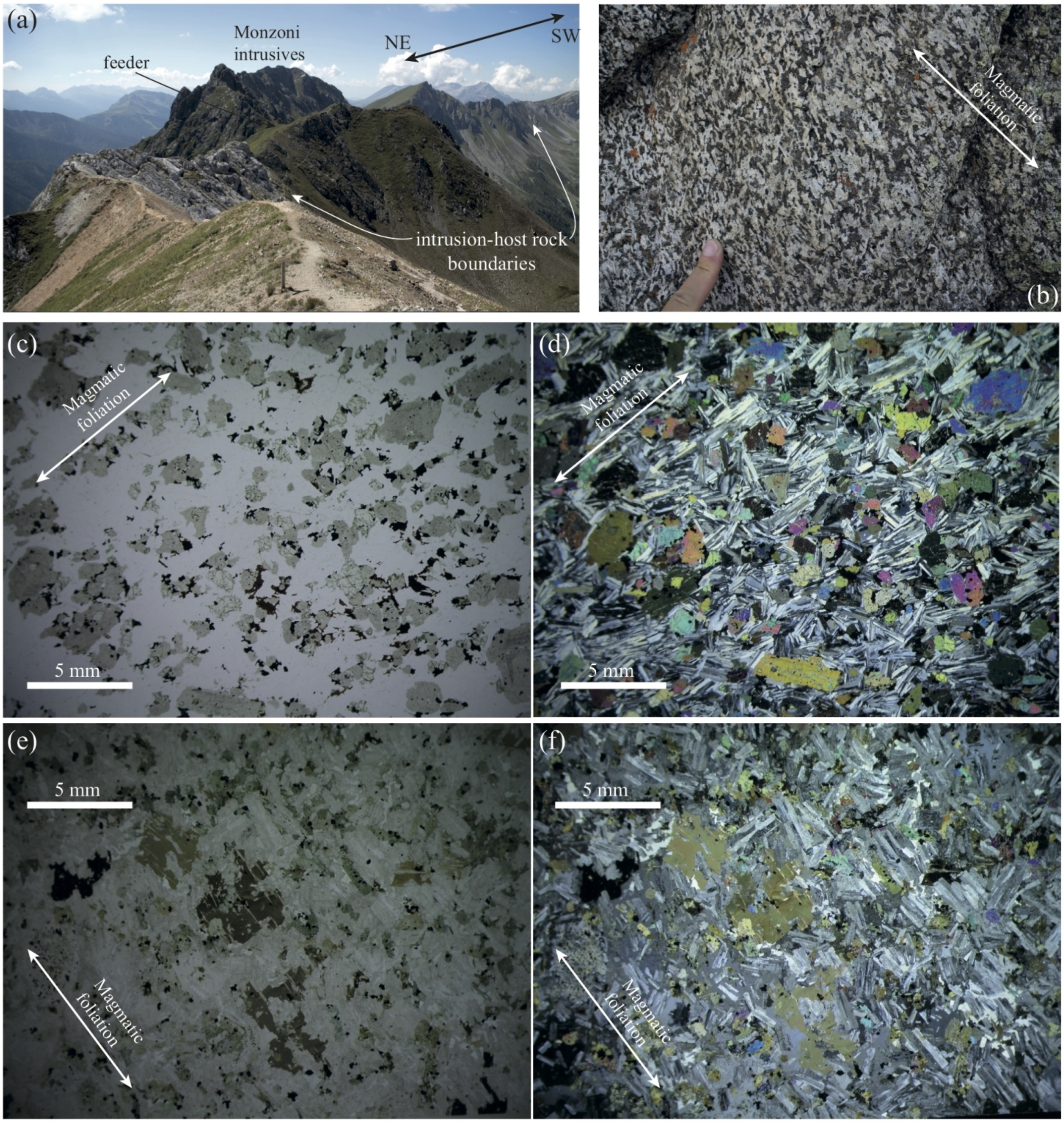

Figure 6: a) Monte Monzoni crest, showing the contacts between intrusive and host rocks. The location of the feeder area is also shown. b) Granite from the Predazzo body showing a well defined magmatic foliation; c) Olivine gabbro showing preferred orientation of plagioclase and pyroxene crystals (sample PA20); c) Monzonite showing preferred orientation of plagioclase and biotite crystals (sample PA22A, same location of sample 22).

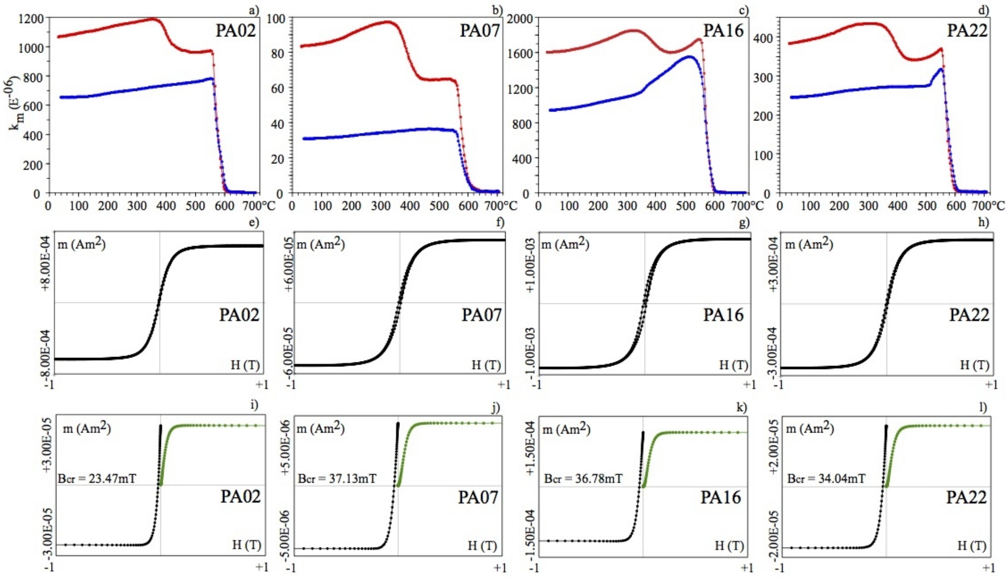

Figure 7: Magnetic mineralogy results for selected samples from Predazzo and Monzoni plutons. a-d) Thermomagnetic curves; red and blue lines represent the heating □-cooling cycle respectively. e-h) Hysteresis loops, corrected for the paramagnetic linear trend. i-l) IRM acquisition curves (green lines) and backfield applications (black lines).

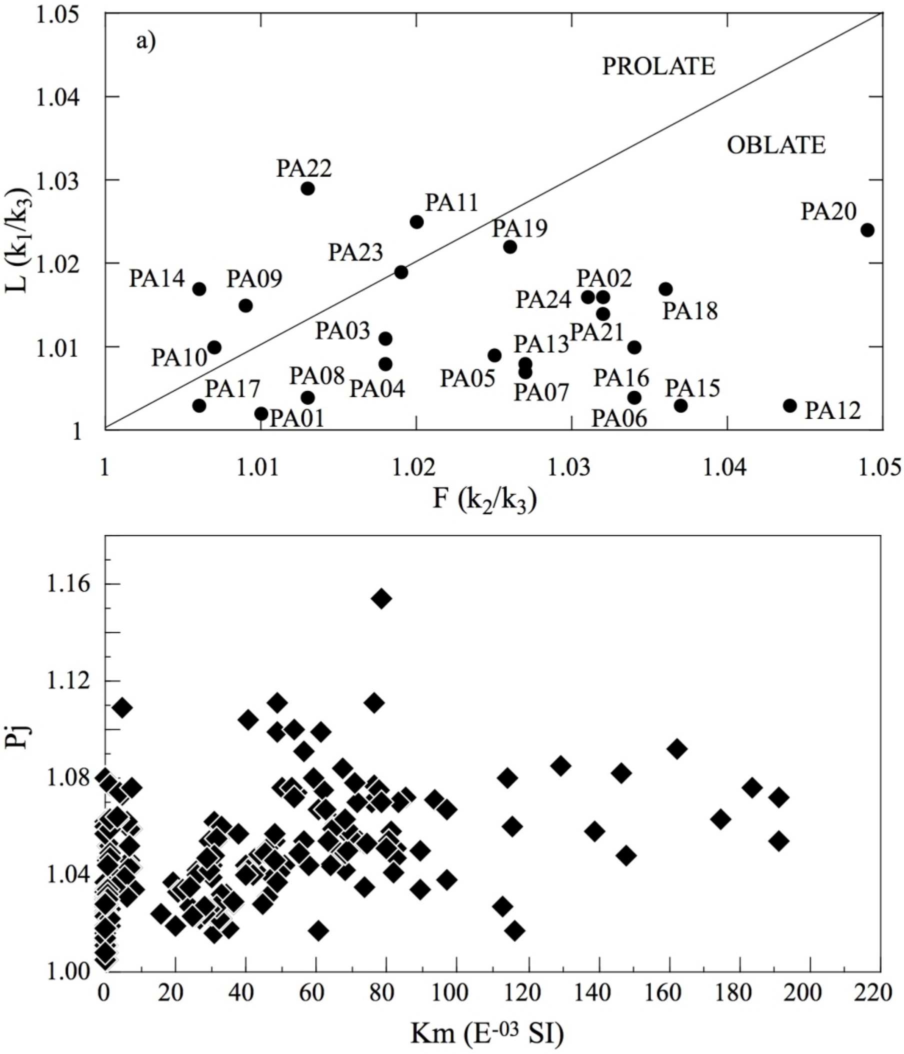

Figure 8: Shape parameters for the analysed sites: a) F-L diagram; b) K-Pj diagram.

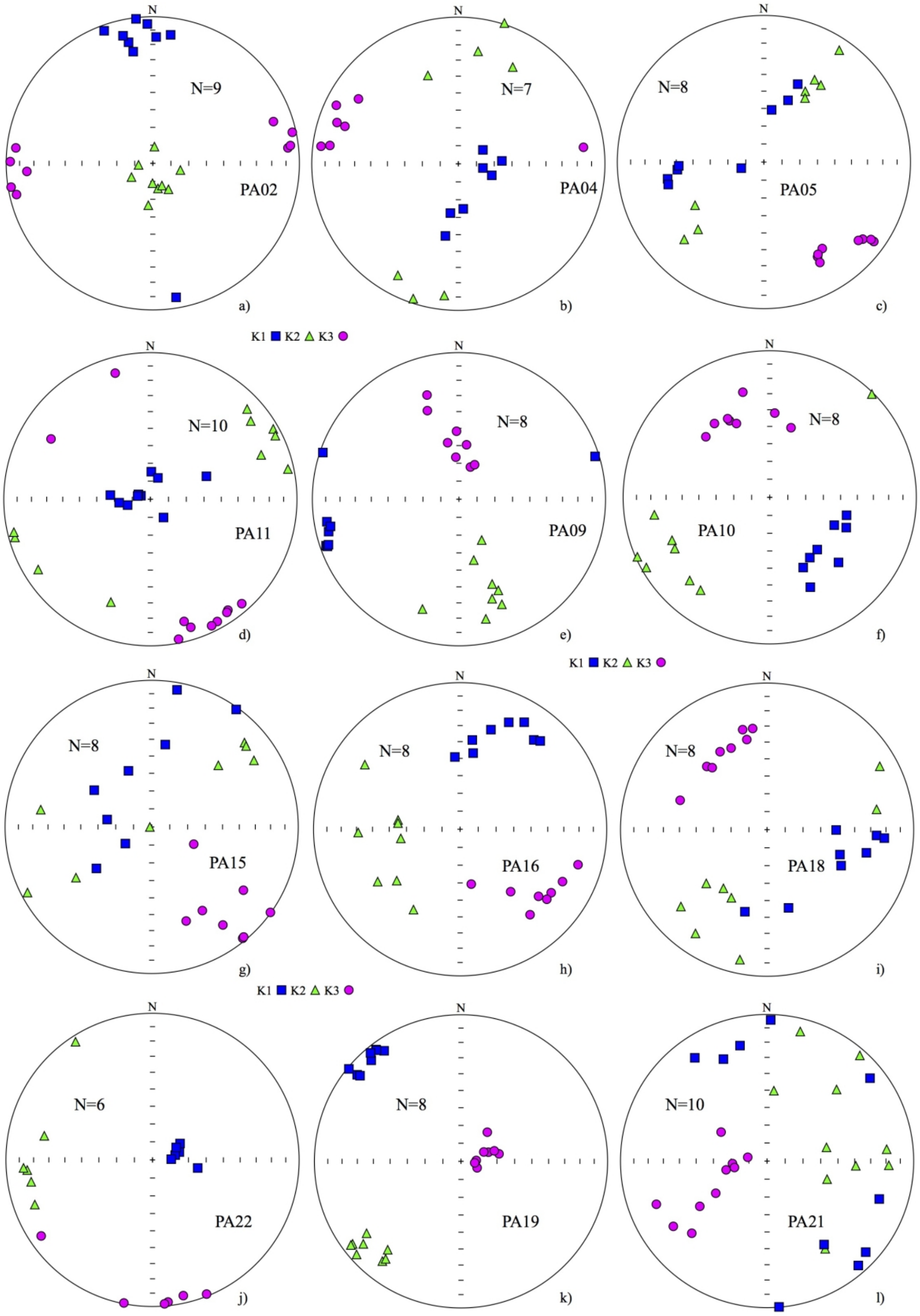

Figure 9: Low-field AMS plots for representative sites in the Predazzo (a-f) and Monzoni (g-l) intrusive bodies. Data are plotted on lower hemisphere, equal area projections. Squares, triangles and circles represent maximum, intermediate and minimum axes, respectively, plotted relative to paleo-geographic coordinates.

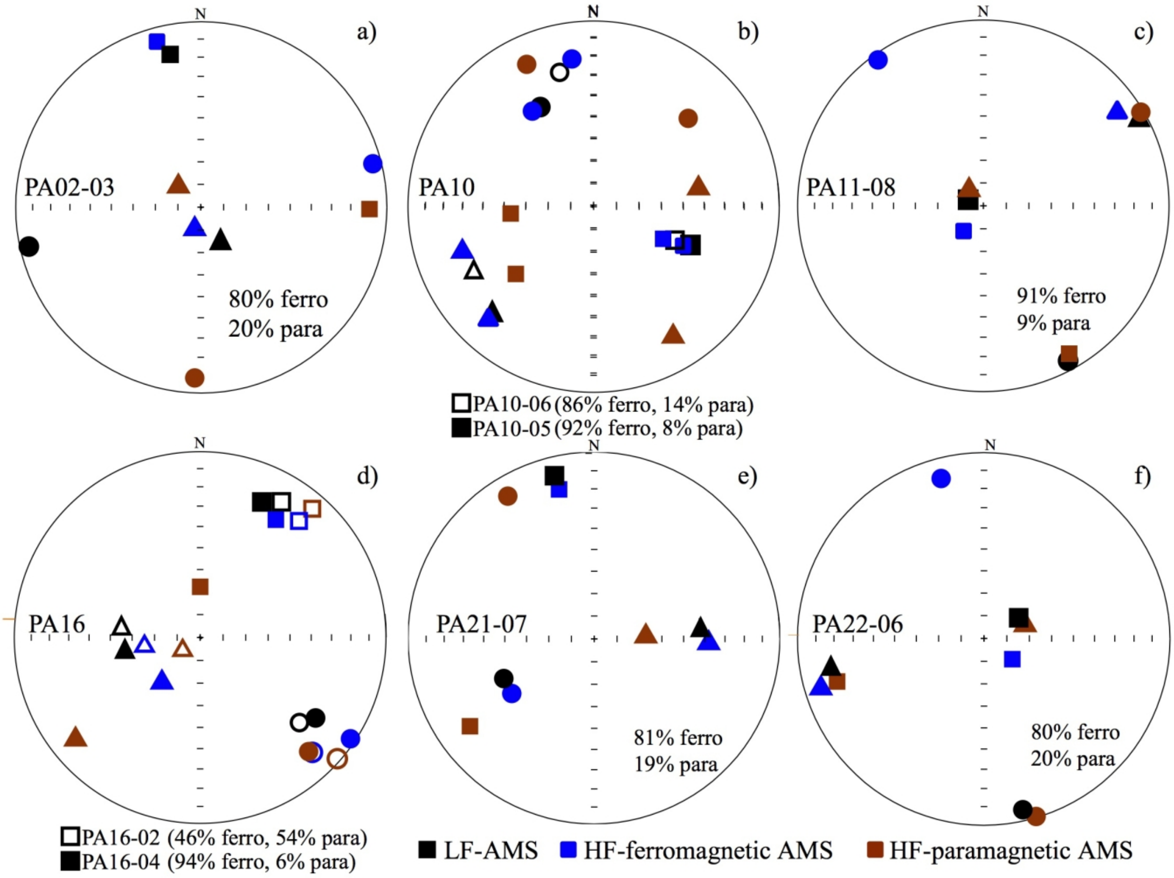

Figure 10: Lower hemisphere equal area projections of the principal axes of the low-field/room temperature (black symbols), high-field paramagnetic (red symbols) and high-field ferromagnetic (blu symbols) susceptibility ellipsoids. Percentages of the relative contribution of ferromagnetic and paramagnetic susceptibility to the magnetic fabric is also reported for each specimen.

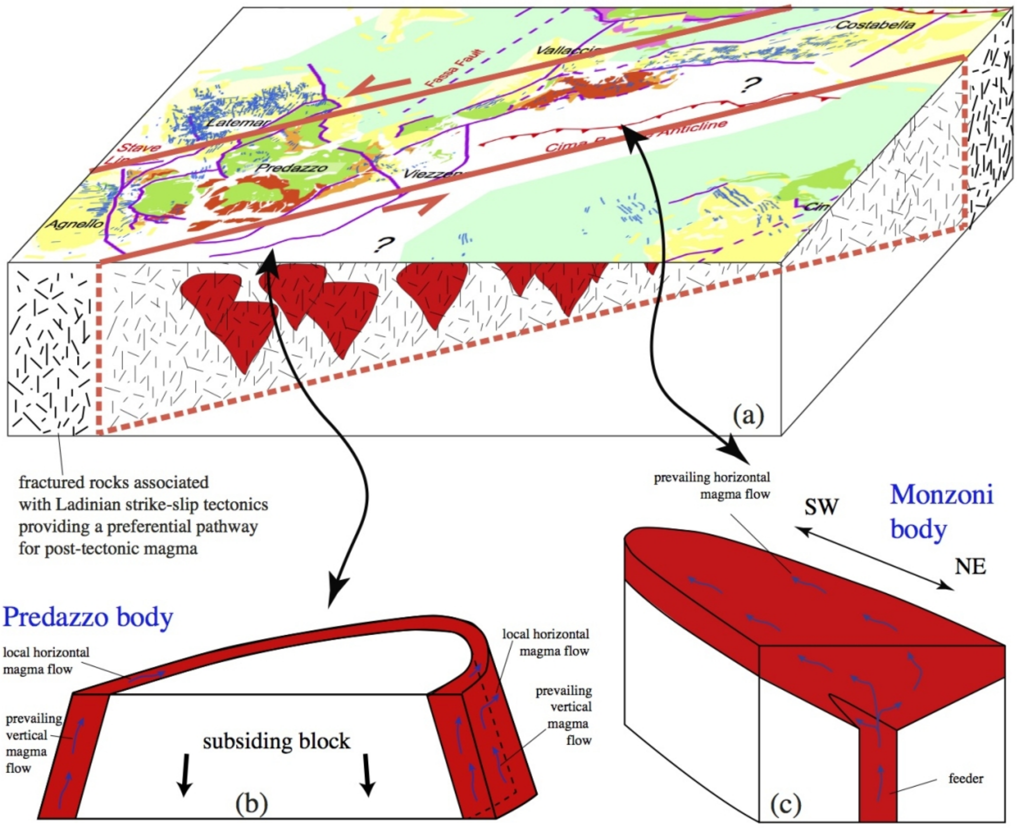

Figure 11: a) Sketch showing the emplacement of Ladinian intrusive bodies along a wide fractured zone associated with previous strike-slip tectonics. b) Sketch of the emplacement mode for the Predazzo body; c) Sketch of the emplacement mode for the Monzoni body.

TABLES

Site	Lithology	Lat	Long	N	Km	std	L	std	F	std	Pj	std	T	std	D,I (k_1)	E_{2-3}	D,I (k_3)	E_{1-2}
PA01	Albitized granite	46°19'41"N	11°36'09"E	10	4.04E^{-04}	3.75 E^{-04}	1.002	0.01	1.010	0.011	1.013	0.018	0.667	0.461	263,77	74.7/36.4	162,3	40.9/21.3
PA02	Monzonites	46°19'53"N	11°36'15"E	8	6.90E^{-02}	2.70E^{-03}	1.016	0.006	1.032	0.006	1.049	0.006	0.318	0.217	353,9	11.3/7.8	262,1	9.4/5.4
PA03	Biotite granite	46°18'42"N	11°36'45"E	8	4.48E^{-03}	3.3E^{-03}	1.011	0.009	1.018	0.013	1.030	0.01	0.256	0.443	266,19	23.7/20.5	9,32	24.1/18.5
PA04	Albitized granite	46°19'39"N	11°36'21"E	6	1.03E^{-04}	1.01 E^{-05}	1.008	0.002	1.018	0.005	1.026	0.006	0.394	0.188	154,72	23.5/3.6	288,13	11.2/5.6
PA05	Albitized granite	46°19'36"N	11°36'13"E	7	8.43E^{-05}	3.88 E^{-05}	1.009	0.01	1.025	0.015	1.035	0.02	0.483	0.329	329,71	35.9/8.2	139,18	18.1/5.9
PA06	Diorite	46°18'52"N	11°35'44"E	9	4.41E^{-02}	8.80 E^{-03}	1.004	0.006	1.034	0.008	1.042	0.008	0.809	0.284	107,6	37.2/4.7	202,41	6.3/4.1
PA07	Biotite granite	46°18'56"N	11°36'14"E	5	6.37E^{-03}	3.99 E^{-04}	1.007	0.008	1.027	0.006	1.036	0.012	0.577	0.184	317,20	45.8/13.3	70,46	16.1/9.3
PA08	Monzodiorite	46°18'23"N	11°36'09"E	8	3.72E^{-02}	3.13 E^{-03}	1.004	0.003	1.013	0.006	1.018	0.006	0.496	0.286	227,27	39.4/7.7	116,34	10.2/8.1
PA09	Monzodiorite	46°18'46"N	11°37'40"E	8	3.11E^{-02}	1.47 E^{-03}	1.015	0.003	1.009	0.004	1.024	0.003	-0.244	0.283	260,6	12.6/4.1	3,65	12.3/3.7
PA10	Monzonites	46°18'38"N	11°37'59"E	8	7.39E^{-03}	9.51 E^{-03}	1.01	0.007	1.007	0.005	1.017	0.012	-0.204	0.262	121,47	13.1/4	331,39	9.2/5.2
PA11	Monzonites to Syenite	46°18'52"N	11°39'26"E	9	2.91E^{-02}	2.00 E^{-02}	1.025	0.01	1.02	0.09	1.046	0.012	-0.099	0.265	344,86	18.9/7.4	151,4	16.6/7.1
PA12	Clinopyroxenite	46°18'16"N	11°36'11"E	8	1.63E^{-01}	2.33 E^{-02}	1.003	0.01	1.044	0.015	1.052	0.015	0.858	0.318	79,24	68.5/18.3	182,26	18.4/12.6
PA13	Biotite granite	46°18'29"N	11°36'17"E	4	1.63E^{-03}	7.49 E^{-04}	1.008	0.007	1.027	0.017	1.037	0.015	0.542	0.423	174,10	37.2/11.8	76,38	17.6/9.4
PA14	Monzodiorite	46°19'33"N	11°35'54"E	9	2.57E^{-02}	3.13 E^{-03}	1.017	0.004	1.006	0.009	1.024	0.006	-0.495	0.409	177,6	13.9/6.9	75,63	40.1/9.6
PA15	Gabbros	46°23'25"N	11°45'07"E	9	7.34E^{-02}	2.53 E^{-02}	1.003	0.013	1.037	0.039	1.045	0.046	0.850	0.55	357,67	70.6/14.9	137,18	24.5/15.0
PA16	Gabbros (cumulate)	46°23'25"N	11°45'04"E	9	1.63E^{-03}	1.64 E^{-03}	1.01	0.012	1.034	0.025	1.047	0.028	0.532	0.36	26,27	25.4/6.5	132,29	12.0/4.8
PA17	Albitized granite	46°23'20"N	11°44'57"E	9	1.02E^{-04}	1.32 E^{-05}	1.003	0.004	1.006	0.004	1.010	0.007	0.334	0.413	68,23	35.2/15.9	173,32	24.7/17.8
PA18	Olivine gabbros	46°23'41"N	11°44'39"E	8	7.68E^{-02}	1.12 E^{-02}	1.017	0.009	1.036	0.01	1.055	0.011	0.351	0.272	107,42	18.4/6.3	331,39	16.4/3.8
PA19	Olivine gabbros	46°23'40"N	11°44'40"E	8	3.07E^{-02}	1.30 E^{-03}	1.022	0.005	1.026	0.003	1.049	0.006	0.084	0.12	317,6	7.3/3.2	73,76	6.4/3.8
PA20	Olivine gabbros	46°23'30"N	11°44'30"E	9	5.26E^{-02}	6.07 E^{-03}	1.024	0.01	1.049	0.017	1.075	0.015	0.344	0.239	108,11	17.8/11.0	310,78	18.6/7.6
PA21	Monzogabbros	46°23'34"N	11°44'10"E	9	6.22E^{-02}	2.19 E^{-02}	1.014	0.014	1.032	0.018	1.048	0.01	0.383	0.481	336,1	19.1/11.9	244,59	25.0/10.1

Site	Lithology	Lat	Long	N	Km	std	L	std	F	std	Pj	std	T	std	D,I (k_1)	E_{2-3}	D,I (k_3)	E_{1-2}
PA22	Monzonites	46°23'30"N	11°43'24"E	6	$3.73E^{-02}$	$1.54\ E^{-02}$	1.029	0.007	1.013	0.011	1.043	0.016	-0.364	0.185	76,76	5.7/4.4	184,4	37.6/2.8
PA23	Monzonites	46°23'30"N	11°43'08"E	8	$7.36E^{-02}$	$2.79\ E^{-02}$	1.019	0.007	1.019	0.015	1.038	0.013	-0.02	0.47	121,65	10.8/7.1	25,3	14.8/7.8
PA24	Monzonites	46°23'31"N	11°43'03"E	9	$8.14E^{-02}$	$2.10\ E^{-02}$	1.016	0.007	1.031	0.014	1.049	0.021	0.325	0.149	97,22	22.4/11.7	0,15	17.3/11.0

Table I: Location of sampling sites in the Predazzo and Monzoni plutons and measured magnetic parameters. N = number of specimens; $K_m = (k_{max} + k_{int} + k_{min}) / 3$ (mean susceptibility, in SI units); $L=k_1/k_2$; $F=k_3/k_1$ $Pj = \exp \{2[(\eta_1 - \eta)^2 + (\eta_2 - \eta)^2 + (\eta_3 - \eta)^2]\}^{1/2}$ (corrected anisotropy degree; Jelinek, 1981); $T = 2(\eta_2 - \eta_3) / (\eta_1 - \eta_3) - 1$ (shape factor; Jelinek, 1981); $\eta_1 = \ln k_1$; $\eta_2 = \ln k_2$; $\eta_3 = \ln k_3$; $\eta = (\eta_1 + \eta_2 + \eta_3) / 3$; D, I ($k_1$) = declination and inclination of the maximum susceptibility axis (paleo-geographic coordinates); D,I (k_3) = declination and inclination of the minimum susceptibility axis (paleo-geographic coordinates); α_{95}: confidence angles; std: standard deviation.

Emplacement modes of the Ladinian plutonic rocks of the Dolomites: insights from Anisotropy of Magnetic Susceptibility

Hassan Abbas [1], Maria Michail [2], Francesca Cifelli [3], Massimo Mattei [3], Piero Gianolla [2], Michele Lustrino [1,4], Eugenio Carminati [1]

1) Dipartimento di Scienze della Terra, Sapienza Università di RomaP.le A. Moro 5, 00185, Roma, Italy
2) Dipartimento di Fisica e Scienze della Terra, Università degli studi di Ferrara, Via Saragat 1, 44122, Ferrara, Italy
3) Dipartimento di Scienze, Università di Roma Tre, Largo San Leonardo Murialdo 1, 00146, Roma, Italy
4) CNR - Istituto di Geologia Ambientale e Geoingegneria, P.le A. Moro, 5, 00185 Roma, Italy

Corresponding author:
Prof. Dr Eugenio Carminati
Dipartimento di Scienze della Terra
Università degli Studi di Roma "La Sapienza"
P.le Aldo Moro 5
I-00185 Roma
Italia

Tel.: ++39-06-49914950
Fax: ++39-06-4454729
Email: eugenio.carminati@uniroma1.it

Abstract

In the Dolomites (Eastenr Southern Alps, Italy), a diffuse Middle Triassic igneous activity is now present mostly as lava flow and pyroclastic successions, with rare shallow-depth intrusive bodies cropping out at Predazzo, Monzoni and Cima Pape areas. In this work, the emplacement modes of the Predazzo and Monzoni bodies were investigated by means of petrographic and anisotropy of magnetic susceptibility (AMS) data coupled with a field geological study. The presence of intrusive rocks in between these two bodies and the continuity of the metamorphic aureola from west of the Predazzo to east of the Monzoni body suggest that they are parts of a ~20 km wide SW-NE oriented continuous pluton, sub-parallel to Ladinian strike-slip faults.

AMS and petrographic data from the Predazzo body are consistent with a multistage ring-dyke emplacement mode, with areas of upward flow of the magma located in the NE and SW part of the intrusion, whereas in the southern sector of the pluton our data suggest prevalently horizontal flows. In general, the Predazzo sheets indicate either ~~updip (~~upward~~?)~~ magma flow or along-strike lateral magma transport, and the round shape suggests no influence of Ladinian tectonic structures.

On the contrary, the ENE-WSW elongated shape of the Monzoni body was controlled by the occurrence of strike-slip faults associated with Ladinian-tectonics, the feeder being likely located at the NE edge of the body. However, the absence of deformation at the field- and micro-scale is consistent with a post Ladinian-tectonics timing of emplacement, as for the Predazzo pluton.

Keywords: Dolomites, anisotropy of magnetic susceptibility, pluton, Predazzo, Monzoni, mode of emplacement

1. Introduction

The Middle Triassic igneous activity in the Dolomites (eastern Southern Alps, Italy; Figs. 1 and 2) is well known from nearly two centuries (e.g., von Richthofen, 1860; Hansel, 1878). The Dolomites represent a worldwide reference area for the relationships between magmatism, sedimentation and tectonics (e.g., Ogilvie-Gordon, 1902, 1903; Hörnes, 1912; Penck, 1911; Vardabasso, 1929, 1930; Leonardi, 1967; Castellarin et al., 1982, 1982b; Visonà, 1997). The igneous activity of the Dolomites is ~~a~~ part of a more widespread magmatism developed during Middle and early Late Triassic in the western Tethys comprising the Southern Alps ~~(Adriatic foreland; Brescian Alps, Vicentinian Alps, Carnia and Julian Alps)~~, Dinarids, Transdanubian Range and Austroalpine (Lucchini et al., 1982). In the Dolomites area, Middle Triassic igneous rocks are mostly pyroclastic, but abundant submarine and subaerial lava and dyke swarms also occur, with magma chambers eroded to shallow-depth intrusive body levels, cropping out ~~only~~ at Predazzo, Monzoni and Cima Pape (Fig. 2).

Several contrasting geodynamic/tectonic models were proposed to explain Middle Triassic igneous activity in the Southern Alps: 1) An aborted continental rifting, based on the association of extensional structures and volcanism (Bechstädt et al., 1977); 2) Northward subduction and delamination of lower continental crust in the upper mantle, based on the calcalkaline and shoshonitic magmatic association and on local compressional structures of Middle Triassic age (Castellarin et al., 1980, 1988; Casetta et al., 2017); 3) Sinistral strike-slip tectonics associated with local compressional and extensional structures (“rhomb-horsts” and “pull-apart basins”) generating magma extrusion and ~~a~~ subsidence as result of the collapse of magma chamber roofs (Blendinger, 1985; Doglioni, 1987, 1988); 4) Marginal back-arc basin associated with the post-Variscan evolution of the Alpine sector (Marinelli et al. 1980; Viel, 1982); 5) Partial melting of a mantle source modified during the preceding Variscan orogeny and contaminated by the incorporation of large portions of crustal material (Crisci et al., 1984; Sloman, 1989; Bonadiman et al., 1994); 6) Intra-Pangea dextral megashear system with lithosphere-scale extension enabling hybridization between mantle melts and lower crust lithologies (Brandner and Keim, 2011); 7) Rifting related with the opening of the Neotethys (Beltran-Trivinõ et al., 2016; Brandner et al., 2016); 8) Active upwelling of hot asthenospheric mantle due to the insulating thermal effect of the huge Pangea landmass (Stahle et al., 2001); 9) Subduction of a small Permian back-arc oceanic (Garzanti 1985; Zanetti et al. 2013). The models involving subduction (2,4,9) are not coherent with the geological context of the Southern Alps that shows no evidence of volcanic arcs or oceanic subduction. The other models are consistent with geodynamic scenarios involving extensional tectonics, either controlled by rifting or strike-slip tectonics. The recognition of Middle Triassic NE-SW strike-slip faults in the Dolomites (e.g., Doglioni 1984a) testifies for the importance of wrench tectonics in this period.

The Predazzo, Monzoni and Cima Pape Middle Triassic intrusive bodies in the Dolomites crop out close to ~~the~~ Middle Triassic NE-SW strike-slip faults (e.g. Stava line; Fig. 2), suggesting a potential role for strike-slip tectonics in the emplacement of these plutons. The generation, ascent and emplacement of magma through the crust and its relation to strike-slip faulting ~~is~~ are still matter of debate (Castro 1987; Tikoff and Teyssier 1992; Paterson and Fowler 1993; Romá~~a~~n-Berdiel et al. 1997; Rosenberg 2004). The emplacement of intrusive bodies can be considered either as controlled by regional tectonics (syntectonic) if the magmatic fabric is consistent with the regional strain field, or caused by the internal dynamics of the magma chamber if the magmatic fabric patterns are independent from the regional tectonic structures (Hutton, 1988; Paterson et al., 1998; Rosenberg, 2004).

In the past years, several structural studies on intrusive bodies have been carried out using the anisotropy of magnetic susceptibility (AMS) technique (e.g., Van der Voo and Klootwijk 1972; Bouchez et al. 1990; Raposo and Gastal 2009, Cifelli et al., 2012). The magnetic fabric in a pluton is affected by several factors, such as the flow of the magma, the changes in its effective viscosity and the finite deformation it undergoes before complete crystallization. Assuming a direct relationship between mineral and magnetic fabrics (e.g., Graham 1954), the analysis of the AMS in igneous bodies can be used to define the relationship between magma emplacement and tectonics. This is particularly crucial for rocks that often appear isotropic and where magmatic foliation and lineation are difficult to observe and measure at the outcrop scale, such as granites (e.g., Knight and Walker, 1988, Tarling and Hrouda 1993).

In this study, we investigate the space and time relationship between the Ladinian Predazzo and Monzoni plutons and Middle Triassic strike-slip faulting in the Dolomites using AMS techniques, coupled with petrographic and field studies. In addition to this regional significance, our work can contribute to the understanding of magma migration and emplacement in the upper crust. A few exposed subvolcanic and caldera-related plutons have been reported and magma-plumbing systems of active volcanic areas cannot be directly studied. Therefore, developing and testing models for the emplacement mechanisms of the ancient exposed sheet intrusions can contribute to the assessment of volcanic hazard and risk in active volcanic areas (Sparks, 2003; Tibaldi and Pasquarè, 2008; Cashman and Sparks, 2013).

2. Geological setting

The Dolomites (Figs. 1 and 2) are located in the central-eastern portion of the Southern Alps, a south-verging fold-and-thrust belt that belongs to the much larger Alpine Orogeny (Carminati et al., 2010b; Handy et al., 2010). The Southern Alps (Fig. 1) are located south of the dextral Neogene Periadriatic Line (also known as Insubric Line) and represent the retro-wedge of the double-vergent Alpine Chain (Doglioni, 1987; Castellarin et al., 1998; Castellarin and Cantelli, 2000; Bosellini et al., 2003; Doglioni and Carminati, 2008). The Southern Alps consist of a well-preserved Mesozoic passive continental margin inverted during the Alpine orogeny (Doglioni, 1987, 2007; Handy et al., 2010).

The area of the Dolomites testify several tectonic and magmatic events recorded in the stratigraphic succession ~~(Fig. 3)~~, including: 1) Permian extensional tectonics and massive acid magmatism (Barth et al., 1993; Schaltegger and Brack, 2007; Visonà et al., 2007; Brandner et al.,

2016) that induced a lithospheric anisotropy that significantly influenced the Triassic and Alpine evolution; 2) Middle Triassic tectonics, associated with differential subsidence and uplift and diffuse magmatic events during the late Ladinian (Fig. 3); 3) A magmatic rifting, started in the Late Triassic (Fig. 3), evolved into the western Tethys spreading during Early Jurassic times (Carminati et al., 2010); 4) Several superimposed phases of compressional Alpine deformation including the Eo-Alpine, Mesoalpine and Neoalpine phases (Castellarin et al., 2004, 2006).

The dolomitic area was a wide shallow sea during Late Permian and Early Triassic times, but started to differentiate at the beginning of early-middle Anisian (Bosellini et al., 2003), probably as consequence of strike-slip tectonics development (Fig. 3; Brandner, 1984; Doglioni, 1984a, 1987; Masetti and Trombetta, 1998; Bosellini et al., 2003). Later, a sudden increase in subsidence combined with a strong sea level rise (Gianolla et al., 1998) drove to a general deepening, associated with the formation of high-relief carbonate buildups and retreat of the siliciclastic shoreline (De Zanche et al., 1993; Brack et al., 2007; Stefani et al., 2010; Marangon et al., 2011). Subsidence rates reached a climax during late Anisian, when the paleogeography of the Dolomites featured numerous small isolated microbial carbonate platforms (Sciliar Formation) surrounded by a deep basin (Buchenstein Formation). During Middle Triassic (Ladinian) the Dolomites witnessed a short-lived massive magmatic event, associated with a strong and localized tectonic activity (Assereto et al., 1977; Viel, 1979; Bosellini et al., 1982; Castellarin et al. 1988). Magmatic edifices such as Predazzo, Monzoni and Cima Pape (Fig. 2; Castellarin et al., 1982b; Sarti and Ardizzoni, 1984), now eroded to subvolcanic to epi-pluton levels, developed during significant tectonic displacement and huge accumulation of megabreccia and chaothic mass-flow deposits (Caotico Eterogeneo, Fernazza Formation). The volcanic sequence (both submarine pillow lava and pillow breccias and subaerial lava flows) is composed of alkali olivine basalt to latite association (Castellarin et al., 1982b; Visona, 1997) and huge volumes of tuffs and volcaniclastics (Fernazza Formation). The rRare quartz syenitic and the much more common shoshonitic dyke swarms cut the sedimentary cover and intrude the magmatic edifices (Vardabasso, 1930; Castellarin et al, 1982b;

Doglioni, 1983). Volcanic activity is also associated with the formation of evaporitic diapirs (sourced in the Upper Permian evaporitic Bellerophon Formation) that deform sedimentary covers in areas adjacent to volcanic centers. The syn-volcanic age of these structures is documented by the fact that they are often cut by the magmatic dykes (Castellarin et al., 1998b). The volcanic activity ceased in upper Ladinian time and large volumes of volcanic material were dismantled and deposited as delta and turbiditic sequences in the surrounding basins (Wengen Formation). From late Ladinian to early Carnian, the subsidence rate decreased, resulting in the progradation of the southern shoreline and a general shallowing of the basins. This regressive trend culminated in the late Carnian, with a strong north-eastward shift of the coastline and complete flattening of the palaeotopography restoring a relative homogeneity in sedimentary palaeoenvironments, as documented by the Heiligkreuz and Travenanzes Formations (~~Gianolla~~ Stefani et al., 2010). A new transgression in the latest Carnian allowed the deposition of the thick peritidal succession of the Dolomia Principale (~~Gianolla~~ Stefani et al., 2010), which records a huge regional platform that extended for hundreds of kilometres from north to south and east to west. Widespread carbonate platforms then characterised the Southern Alps for several million years, from the late Carnian to (at least) the late Norian.

2.1 Age and duration of the Ladinian magmatic event.

The age of the igneous activity is well constrained by biostratigraphy and geochronology. The first tephra horizon (Fig. 3) with a mafic mineral association (clinopyroxene, plagioclase and olivine) is recorded in the Acquatona Fm. (~~Longobardicum~~ *longobardicum* ~~Subzone~~ammonoid subzone; ~~Viel.,~~ Viel., 1979; De Zanche and Gianolla, 1995; Gianolla et al., 1998 ~~Fig. 3~~) and in the coeval Buchenstein Fm. (*sensu* Brack amd Rieber, 1993) ~~Viel., 1979; De Zanche and Gianolla, 1995~~). The main phase of volcanic activity is recorded by the Fernazza Fm. (~~Neumayri~~ *neumayri* and early ~~Regoledanus~~ *regoledanus* ~~Subzones~~ammonoid subzones) while the often unconformably overlaid post volcanic unit (Wengen Fm.) is assigned to the ~~Regoledanus~~ *regoledanus* ~~Zone~~ ammonoid zone (Stefani et al., 2010; Mietto et al., 2012). Absolute ages from ash layers of the Seceda section (Brack et al., 1996, 1997; Brack and Muttoni, 2000; Wotzlaw et al., 2018) suggest that the first evidence of mafic activity (tuffs, lava flows or submarine debris flow with lava blocks) is younger than 239.04 ± 0.04 Ma (U-Pb geochronology, Wotzlaw et al., 2018) and possibly coeval with the Upper Pietra Verde volcaniclastics, where an ash layer (close to the *l~~L~~ongobardicum/n~~N~~eumayri* subzones boundary) showed an age of 238.0 ± 0.05 Ma (Mundil et al. 1996). The age of the ~~upper limit, or the~~ termination of the paroxysmal effusive phase, is given by a tuff from the area of Alpe di Siusi (Mietto et al., 2012), where an ash layer, few meters above the top of the pillow-lava, gives an age of 237.77 ± 0.05 Ma (U-Pb geochronology).

These ages confine the duration of the paroxysmal phase of Ladinian volcanism in the Dolomites to a time interval no more than 0.7 ~~Ma~~ Myrs long (considering all analytical errors) and are in agreement with the absolute age from the Predazzo intrusion, where zircons from the granitic phase were dated to 237.3 ± 1.0 Ma (Mundil, 1996; Brack et al., 1997) and thus confirming a short-lived Upper Ladinian magmatic Event.

2.2 Ladinian tectonics in the Dolomites

During Middle Triassic time, the Dolomites were affected by N 70°-90°E trending strike-slip faulting (along the Stava, Trodena and Cavalase Lines), which locally was associated with transtensional and transpressional structures. These faults cut basement and sedimentary succession up to lower-middle Ladinian rocks (Doglioni, 1984b; Doglioni, 1987; Doglioni and Carminati, 2008). These structures are concentrated along the alignment of the Stava Line – northern limb of the Cima Bocche Anticline – where flower structures suggest a sinistral kinematics.

Middle Triassic compressional structures were locally documented in the Dolomites and consist of folds and reverse faults (Bechstadt et al., 1977, Pisa et al., 1980, Bosellini et al., 1982; Castellarin et al., 1982; Doglioni 1982, 1984a, 1984b, 1985, 1987; Doglioni and Carminati, 2008). In addition, diapiric structures (originating from the Upper Permian evaporitic Bellerophon Fm.) elongated along N70E axis and dated to the Middle Triassic crop out in the central Dolomites (Doglioni, 1984a). These Middle Triassic compressional structures were interpreted as related to N70E sinistral transpressional tectonics (Doglioni 1984a, 1984b, 1987, 2007), resulting from the sinistral relative movement between Africa and Europe (Doglioni 1984b). According to Doglioni (1983) Ladinian mafic volcanic dykes in Dolomites show a radial pattern, which was interpreted as related to a domal uplift induced by coeval magmatism, possibly inheriting previous structures~~ (Doglioni, 1983)~~.

2.3 The Predazzo intrusive complex

The Predazzo intrusive complex (Fig. 4) is ring-shaped, ~4 km in diameter and covers an area of ~13 km^2. It has been subdivided into four intrusive units on the basis of magma chemistry, geometry and relative geochronology (Menegazzo et al. 1995; Visonà 1997). Monzonitic unit M1 represents the first intruded unit and forms the outer part of the ring with mainly monzonitic composition associated with ultramafic rock types (pyroxenites). These ultramafic bodies are generally small, tabular and vertical with sinuous sharp contacts. Monzonitic unit M2 is intruded into the Middle Triassic volcanic rocks~~s~~ and into the M~~m~~onzonitic unit M1 and cut them with short dykes. This unit crops out in the western part of the igneous complex and is mainly composed of quartz monzonite with subordinate leuco-quartz monzonite and quartz monzodiorite. In more recent studies, M1 and M2 units were merged into a single shoshonitic silica-saturated (SS) series (Casetta et al., 2017). Monzonitic unit M3 is mainly located in the eastern part of the pluton and intrudes both volcanic rocks~~s~~ and M~~m~~onzonitic unit M1. It consists of monzodiorite to syenite, both quartz- or foid-bearing. The granite unit is located in the central part of the pluton and cuts both volcanic rocks~~s~~ and Monzonitic units M~~1~~1 and M2. It consists of two separate lithotypes: a) biotite granite, b) tourmaline leuco-granite (Visonà, 1997). In Fig. 4 we observe v~~V~~ariably (mainly NNW-SSE~~radially~~) oriented systems of basaltic to trachytic ~~composition~~ dykes that cut the entire intrusive complex together with the surrounding volcanic products, ~~that~~ which in total cover an area of ~25 km^2 (Casetta et al., 2017).

2.4 The Monzoni intrusive complex

The Monzoni intrusive complex (Fig. 5and 6), located 8 km to the NE of the Predazzo complex (2) is a NE-SW elongated pluton with a length of <5 km covering an area of ~8 km^2. The Monzoni pluton played a central role not only for the study of the Middle Triassic magmatism but also in the development of petrography, being the type locality for monzonitic rocks (Brogger, 1895). The intrusion comprises a series of basic to intermediate plutonic rocks, which consist of gabbroic rocks (gabbro, olivine gabbro, monzogabbro), cropping out in the north-eastern part of the complex together with clinopyroxenite, while monzonites and monzodiorites constitute the western part of the intrusion (Del Monte et al., 1967; Bonadiman et al., 1994; Gallien et al., 2007) (Fig. 5). The Monzoni complex and its thermo-metamorphosed Permian to Triassic host-rocks are cut by quartz syenitic and shoshonitic dyke swarms (Bonadiman et al., 1994).

2.5 Intrusions' host rocks

The country rocks of the Ladinian plutons include (Castellarin et al, 1982b~~Gianolla et al., 2010~~) lower Permian acidic volcanic rocks of the Athesian Volcanic Group (mostly rhyolites; Marocchi et al., 2008), a ~~widespread~~ succession of volcanites up to >2 km thick, the Upper Permian fluvial red beds of Val Gardena Sandstones (~100 m thick; Figs. 4, 5), the Upper Permian ~~dolomitic limestones~~marls and evaporites of the Bellerophon Fm. (~300 m; Fig. 4), the Lower Triassic clastic-carbonate Werfen Fm. (~280-500 m; Figs. 3, 4), the middle Anisian ~~low relief unit~~mixed carbonate-siliciclastics units (from Richthofen to Contrin Fm.; ~150-200 m; Figs. 3, 5), the ~~high relief~~ Sciliar carbonate platform (~800 m) and the ~~basinal deposits~~mainly cherty limestones of Buchenstein Fm (max 80 m).

The sedimentary cover is overprinted by the local effects of contact metamorphism around the plutons (Vardabasso, 1929,1930; Ferry, et al., 2002, Gallien, et al., 2007), and exhibit strong evidence of regional tectonic deformation. The area around the intrusions is characterized also by significant collapses of the sedimentary cover (Vardabasso, 1930; Castellarin et al., 1982b) with vertical displacements of several hundred meters (e.g., Monte Agnello area) and platform-block tilting (e.g., Vallaccia area).

3. Sampling and Methods

3.1 Sampling

In this study, sSampling for petrographic and AMS analyses was carried out both in the Predazzo and Monzoni plutons (Table 1). In the Predazzo intrusive body, 14 sites were sampled and 107 cylindrical cores were collected for AMS analysis (Fig. 4a). In the Monzoni intrusive body, 10 sites were sampled for a total of 84 cylindrical cores (Fig. 5a). At each site, cores were drilled using an ASC 280E petrol-powered portable drill and oriented *in situ* by a magnetic compass, corrected to account for a local ~2° magnetic declination according to the NOAA National Geophysical data center. The geographic distribution of the sampling was influenced by the difficulty to find accessible outcrops in many areas, preventing the possibility to make a homogeneously distributed sampling throughout the two intrusive bodies.

3.2 Petrographic analysis

The collected samples were cut with a diamond-disc saw to obtain 29 thin sections for petrographic study and the reminder parts were grounded in a steel mill to about mm-scale fragments. Then, the fragments were washed with distilled water and then dried in an oven at 110 °C for 10 hours and eventually pulverized in a low-blank agate mortar. The petrographic description of the thin sections was accomplished using an optical polarizing microscope.

3.3 Magnetic mineralogy

The AMS technique provides a quick and accurate determination of igneous rock fabric. The magnetic fabric (lineation and foliation) data obtained from AMS measurement can record the primary magma flow in magmatic sheet intrusions (Polteau et al., 2008; Petronis et al., 2013, Andersson et al., 2016; Magee et al., 2016), although magnetic fabric data are sometimes complex and in some cases subject of controversy.

The precise knowledge of the magnetic mineralogy is an important aspect to use AMS for tectonic purposes because the preferred orientation of different magnetic minerals reflects the deformation history of the rock (e.g., Rochette et al. 1992; Hrouda et al. 1997). Magnetic mineralogy analyses were carried out in order to characterize which are the main magnetic minerals in the sampled sites. The variation of magnetic susceptibility with temperature was measured on powders from 24 representative samples, one for each site, by means of the same Agico KLY-3 Kappabridge used for LF-AMS measurements, equipped with a CS-2 furnace, at the paleomagnetic laboratory of the Department of Sciences of Roma Tre University. Samples were heated up to 700 °C and cooled back to 40 °C to estimate the Curie/Néel range of temperatures, according to the inverse susceptibility method proposed by Petrovský and Kapička (2006), and to examine any possible mineralogical changes associated to the heating process in air. Moreover, the hysteresis properties of powders from 21 representative samples were measured on a Princeton Measurements Corporation 3900 vibrating sample magnetometer (VSM), in field up to 1 T. The powders have been placed in pharmaceutical gel caps suitable for vibrating in the VSM, in order to determine, after subtracting the high field linear trend, the coercive force (Bc), the saturation remanent magnetization (Mrs), as well as the saturation magnetization (Ms). The coercivity of remanence (Bcr) values have been extrapolated from backfield remagnetization curves up to -1 T, following forward magnetization in a +1 T field. These measurements were carried out in the Istituto Nazionale di Geofisica e Vulcanologia (INGV, Rome).

3.4 Anisotropy of low-field magnetic susceptibility (LF-AMS)

AMS is defined by a second rank tensor and represented geometrically by an ellipsoid in which the greatest intensity of magnetization is induced along the long axis k_1 and the weakest intensity along the short axis k_3 (with the principal axes $k_1 > k_2 > k_3$). Since the pioneering work of Graham (1954), a close correlation between the directions of the main axes of AMS ellipsoid (k_1,k_2,k_3) and the petrofabric strain axes (λ_1,λ_2,λ_3) has been widely demonstrated. Several parameters have been defined both for the quantification of the magnitude of anisotropy and for defining the shape of the ellipsoid (Table; Jelinek, 1981; Hrouda, 1982). The mean susceptibility values k_m have been computed as $k_m = (k_1+k_2+k_3)/3$. The magnetic lineation is computed by L (k_1/k_3) and has an orientation defined by the orientation of k_1, while the magnetic foliation is computed by F (k_2/k_3) and it is defined as the plane perpendicular to k_3. T is the shape parameter and range from -1 (perfectly prolate ellipsoid with $L >> F$) to +1 (perfectly oblate ellipsoid with $F >> L$) with zero values corresponding to a triaxial shape ($F \sim L$). The anisotropy degree is computed by the parameter Pj (Jelinek, 1981), which is obtained considering all the three principal susceptibility values.

Measurement of the anisotropy of low-field magnetic susceptibility (LF-AMS) represents a rapid and non-destructive technique for the characterisation of the mineral fabric in rocks (Hrouda, 1982). In this study, the LF-AMS was measured on about 200 specimens, with an Agico KLY-3S susceptibility bridge (Jelínek and Pokorný, 1997) in the paleomagnetic laboratory of the Department of Sciences of Roma Tre University. The anisotropy measurements at both the specimen and the site scale were evaluated using Jelínek's statistics (Jelinek, 1977).

3.5 Anisotropy of high-field magnetic susceptibility (HF-AMS)

As the LF-AMS is the sum of the contribution from all minerals, which include ferromagnetic, paramagnetic and diamagnetic phases (Rochette et al., 1983), we measured high-field AMS (HF-AMS) on 13 selected samples in order to discriminate the relative contribution of ferromagnetic and paramagnetic minerals to the magnetic anisotropy (e.g., Martin Hernandez and Hirt, 2001). HF-AMS measurements were carried out, using magnetic fields up to 1500 mT. These fields are strong enough to saturate all ferromagnetic minerals except hematite (not present in the analyzed samples), and allow the separation of paramagnetic and ferromagnetic contribution to the magnetic anisotropy (e.g., Hrouda and Jelínek, 1990). Measurements were made with a high-field torque magnetometer (Bergmüller et al., 1994) in the Laboratory of Natural Magnetism of the Institute of Geophysics ETH in Zürich.

4. Results

4.1. Petrographic description

A complete petrographic description of the samples (Table 1) is provided in Appendix A. Here a summary is presented.

In the Predazzo pluton, lithologies vary from cumulitic clinopyroxenite (samples PA12, PA11a, b, c) to cumulitic gabbro (PA~~R-~~10), diorites (PA06), monzonite (PA02, PA10), monzodiorite (PA08, PA14c, PA09), monzogabbro (PA12) albitized granite (PA01, PA04, PA05, PA17) and biotite granite (PA07, PA03, PA13). We found evidence of hydrothermal alteration in samples from the northern part of granite body of the Predazzo pluton (PA01, PA04, PA05, and PA17).

The samples from Monzoni pluton are classified into two main groups: gabbroic rocks and monzonites. Gabbroic rocks are mainly located in the north-eastern sector of the pluton and consist of monzogabbros (PA21), non-cumulitic gabbros (PA16) cumulitic gabbros (PA15) and olivine gabbros (PA20, PA18). Monzonites (PA22, PA22a, PA23, PA24) are mainly located in the south-western sector of the pluton and represent the most widespread rock type.

As ~~widely~~accurately described in the appendix, t~~T~~he samples from both plutons show purely magmatic structures (for most of lithologies hypidiomorphic inequigranular medium- to coarse-grained textures with anhedral, to euhedral crystals) with undeformed feldspar, clinopyroxene, and amphibole~~ devoid of any deformation~~. In few cases, kinked biotite occurs. Quartz does not show any or very limited undulatory extinction, and no or rare sub-grains.

4.2 Magnetic fabric results

The magnetic susceptibility and main anisotropy parameters of the analyzed sites are listed in Table 1. The orientation of the magnetic foliation and magnetic lineation has been reported in pre-tilting coordinates, on the base of the regional structural evolution and geological mapping, which show a 10° of tilting toward NE in the Predazzo area and 15° toward N in the Monzoni area. In the Predazzo pluton, a bimodal distribution of k_m values is observed, which reflects the lithological differences of the analyzed samples (Tab~~.~~le 1). Samples taken from granites show low values, in the range of E^{-03}-E^{-05} SI, whereas samples from clinopyroxenites, gabbros and diorites show higher values (up to 1.63 E^{-01} SI), qualitatively suggesting a major contribution of ferromagnetic minerals to the magnetic susceptibility in these latter lithologies. These data are consistent with the occurrence of magmatic foliation (Fig. 6b) both at meso- and micro-scale. In the Monzoni pluton, monzonites and gabbroic rocks show similar values of k_m, in the range of E^{-02} SI, suggesting a strong contribution of ferromagnetic minerals (Tab~~.~~le 1) consistent with preferred orientation of minerals observed in thin sections (Fig. 6c,d,e,f). ~~-~~The susceptibility *vs.* temperature heating-cooling curves indicate that low-Ti content titanomagnetite and magnetite are the main ferromagnetic minerals both in the Pradazzo and Monzoni intrusive bodies. A slight to moderate step around 350 °C is attributed to the presence of a small amount of maghemite which converted to hematite as confirmed by the slightly lower susceptibilities recorded along the cooling curves (Fig. 7~~6~~ a-d). Also, a well-defined Hopkinson peak has been recorded in few samples, before a sudden drop in susceptibility which might correspond to a partially oxidized titanomagnetite (Fig. 7~~6~~ ~~-~~c and d). Hysteresis loops (Fig. 7~~6~~ e-h), isothermal remanent magnetization (IRM) acquisition curves and backfield applications are well defined, due to the relatively high values of the concentration dependent magnetic parameters. The results are mainly consistent with a prevailing low-coercivity component, as evidenced by Bcr values, which is are lower than 40 mT (Fig. 76 i-l).

In most of the sites, the magnetic foliation is well developed and its values (F) are greater than those of the magnetic lineation (L; Table Tab. 1 and Fig. 87). Magnetic shape factors (T) in most of the samples show a dominant oblate shape, and for few samples, it shows prolate and triaxial shape (Table. 1 and Fig. 7). The degree of anisotropy (Pj) values do not show significant difference between monzonite and granites and vary between 1.01 and 1.15 (Fig. 8b Table 1).

In the Predazzo intrusives, the Monzonitic Unit M1 has been sampled in different sites along the southern (PA08, PA09, PA10), the south-western (PA06) and north-western (PA02) borders of the plutonic body (Fig. 4a). In all these sites AMS shows a well-defined magnetic foliation, which ranges from moderately dipping (235°) to vertical (898°) and strikes almost parallel to the intrusive borders. In particular the magnetic foliation is oriented WSW-ENE at sites PA08, PA09, and PA10, WNW-ESEENE-WSW at site PA06, and N-S at site PA02 (Figs. 4b and 98a, e, f). Furthermore, we sampled a site (PA12) in one of the mafic bodies that outcrop along the western part of the intrusive. The magnetic foliation dips outward the intrusive body at sites PA02, PA09 and PA10 and toward the boundary within Monzoniticce Unit M2 at sites PA06, PA08 and in the mafic body site PA12. The magnetic lineation shows gentle to sub-horizontal dipping, and is variably oriented respect to the intrusive body, ranging from sub parallel to the boundary (PA02, PA06, PA08, PA09) to orthogonal to it (PA10) to disperse around a great circle (PA12). The Monzonitic Unit M3 has been sampled at one site (PA11), located in the eastern part of the intrusive. In this site, magnetic foliation is very well defined and is sub-vertical with a WSW-ENE direction, parallel to the elongation of this unit. Magnetic lineation is also well defined and sub-vertical (Figs. 4b and 98d)..

The granite intrusion has been sampled in 7 sites, located in the north-western (PA01, PA04, PA05 and PA17), in the south and south-western (PA03, PA07 and PA08) boundaries of the body (Fig. 4a). The magnetic foliation is well defined in all the sites, but in site PA01 where it shows a significant dispersion around an E-W direction. In the north-western part of the intrusion magnetic foliation is oriented NNE-SSW at sites PA04 and PA05, where it is sub-vertical and dips toward the internal and the external border of the intrusive body, respectively (Figs. 4b and 98b, c), whereas at site PA17 the magnetic foliation is E-W oriented and dips toward the north. In the south-western part of the granitic body, the magnetic foliation is also parallel to the border of the intrusion, being W-E oriented at site PA03 and NW-SE at site PA07. In both sites, the foliation is dipping toward the external part of the intrusion. The magnetic lineation is very poorly defined at sites PA01 and PA07, whereas is sub-vertical at sites PA04 and PA057. At sites PA03 and PA17 the magnetic lineation is poorly grouped with a sub-horizontal E-W orientation (Figsg. 4 and 98a-f).

In the Monzoni pluton we sampled mafic rocks in the eastern part of the intrusive, and monzonite units in the western part of the body (Fig. 5a). In the monzonite sites (PA22, PA23, and PA24), the magnetic foliation is well defined, with a W-E orientation and a sub-vertical attitude. In these sites, the magnetic lineation is well defined and mostly shows sub-vertical dip (Figs. 5b and 98j). In the mafic units, the magnetic foliation is well defined and varies from gently dipping toward the SE (PA18) to a sub-horizontal attitude (PA19, PA20, PA21). In all these sites, the magnetic lineation is well defined with a WNW-ESE orientation (Figs 5b and 98i, k, l). At sites located in the eastern part of the pluton, the magnetic foliation is well defined at sites PA15 and PA16, where it shows a NE-SW orientation and a step dipping to NW. At site PA14 the magnetic foliation is poorly defined, being dispersed in a E-W direction. Magnetic lineation is well defined at sites PA14 and PA16, where it is sub-horizontal and N-S oriented respectively, whereas it is poorly defined at site PA15. (Figsg. 5b and 98g-hi).

HF-AMS measurements indicate that, for most of the samples, the observed magnetic fabric is dominated by the ferromagnetic component (Fig. 109) in most of the sites and a very good correspondence between the orientation of the principal axes of the ellipsoid at low-field and those of the ferromagnetic ellipsoid in high-filel d exists. This suggests that the magnetic fabric can be described in terms of the orientation of the ferromagnetic minerals. In samples where the HF-paramagnetic fraction is significant (>50%), there is a good correlation between low-field and high-field (ferromagnetic and paramagnetic) magnetic ellipsoids, whereas when the paramagnetic fraction is very low its orientation cannot be determined with the necessary accuracy (Fig. 10~~9~~d).

5. Discussion

~~The AMS technique provides a quick and accurate determination of igneous rock fabric. The magnetic fabric (lineation and foliation) data obtained from AMS measurement can record the primary magma flow in magmatic sheet intrusions (Polteau et al., 2008; Petronis et al., 2013, Andersson et al., 2016; Magee et al., 2016), although magnetic fabric data are sometimes complex and in some cases subject of controversy. In particular,~~ M~~m~~agnetic fabric in intrusions can be purely magmatic (related to internal magma chamber processes, such as convection, magma surges, and dyke injection) or it can be the result of regional deformation (syn- to post-tectonic strain) or a combination of these two processes (Paterson et al., 1998). In the Predazzo and Monzoni ~~samples~~bodies, thin section analyses show that the microstructures are purely magmatic (i.e., just after the complete crystallization of magma). The absence of evident solid-state deformation suggests that the magnetic fabric is not related to tectonic deformation after cooling, but it rather developed during magma emplacement and cooling (Büttner, 1999). Hydrothermal fluids can also modify the magnetic fabric orientation and parameters acquired during magma emplacement and cooling, thus complicating the interpretation of magnetic fabric data (e.g. Just et al. 2004; Petronis et al. 2011; Nédélec et al. 2015; Tomek et al., 2017). Although some samples from the northern part of the Predazzo granite body (PA01, PA04, PA05, and PA17) showed evidence of hydrothermal alteration, ~~We found evidences of hydrothermal alteration in sites from the northern part of granite body of the Predazzo pluton (PA01, PA04, PA05, and PA17). However,~~ in most of these sites magnetic foliations are generally tangent to the ring shape of the pluton. This suggests that hydrothermal alteration had no or minor effect on the magnetic fabric, with the exception of sample PA17, that is strongly hydrothermally altered and fractured and show a distinctive magnetic fabric. Therefore, site PA17 will be no longer considered in the discussion of the emplacement mode of the

Predazzo pluton. ~~Concerning~~ S~~the Monzoni pluton, sample~~amples from site PA11, belonging to Monzontic Unit M3 of the Predazzo body, ~~is~~ are highly altered and transformed as a result of hydrothermal solutions. However, the magnetic fabric orientation is concordant with NE-SW elongation shape of Monzontic Unit M3 and shows well-clustered magnetic fabric. The compatibility of the magnetic fabric with the elongation shape of this unit could be explained as the hydrothermal fluid was likely coeval with the emplacement as a single event (e.g. Nédélec et al., 2015). Moreover, the NE-SW orientation of the magnetic fabric and elongation of the Monzonitic Unit M3 suggests that the emplacement of this unit was controlled by NE-SW Middle Triassic (Ladinian) tectonic structures.

In the following, the Predazzo and Monzoni plutons will be discussed separately. However, Figure 2 shows that these intrusive bodies may be parts of a single large and rather continuous body, as suggested by the outcrop of a small volume of intrusive rocks between the plutons and by the continuity of a metamorphic aureola from west of the Predazzo body to the Monzoni body. The emplacement of Ladinian intrusive bodies likely occurred along a fractured zone associated with previous strike-slip tectonics (Fig. 11a), as suggested by the parallelism between Ladinian intrusives and Middle Triassic faults (e.g., Stava-Trodena line, Fig. 2b).

The Predazzo and Monzoni plutonic rocks show distinct shapes, the first being roughly round shaped and characterized by ring type successive intrusions, the second being markedly NE-SW elongated, sub-parallel to the Middle Triassic Stava-Trodena line. Similarly, the AMS analyses show markedly different results for the two intrusive bodies, suggesting different emplacement modes. Both the Predazzo and Monzoni bodies are the result of multiple intrusions, as indicated by the variety of lithologies described above (see also appendix A).

5.1 Emplacement mode of the Predazzo pluton

In the Predazzo body, AMS has been measured in the different intrusive bodies that form the pluton, showing distinctive pattern of magnetic fabric. The Monzonitic Units M1 and M2~~The Monzonite intrusion (M1+M2)~~, that represent~~s~~ the older portion of the pluton, ~~is~~ are characterized by an annular ellipsoidal shape, gently elongated in a ENE-WSW direction. In this body, the magnetic foliation is generally oriented parallel to the borders of the intrusion (i.e., parallel to its perimeter). In sites that are located along the external rim, the foliations are predominantly steeply or shallowly radially dipping away from the pluton. On the contrary, in sites located along the internal rim of the annular intrusion the foliations radially dip towards the cent~~e~~re of the pluton. The magnetic lineation is generally gently dipping to sub-horizontal and parallel to the border of the intrusion. In the granite body the magnetic foliation is almost parallel to the rims of the pluton and dips away from the intrusion, whereas the magnetic lineation varies from sub-vertical to sub-horizontal. The rough ring shape of the Predazzo multistage intrusive complex and the presence of volcanic rocks at the centre of the ring (suggesting a caldera collapse of this area), led Castellarin et al. (1982b) to suggest a ring dyke emplacement mode. Ring dykes are cylindrical sheet intrusions occurring at subvolcanic level characterized by outward-dipping walls on all sides. They are due to magma ascent along steep outward-dipping ring fractures, induced by the collapse of the central block subsidence (e.g., O'Driscoll et al., 2006). The development of caldera ring-faults and the related subsidence of a central block are the main structural processes that permit the intrusion of ring-dikes (Roche et al., 2000).

Our AMS data are consistent with the ring dyke emplacement mode. In particular magnetic foliation in the Monzonitic units is dominantly oblate and consistently parallel to the boundaries of the intrusion and prevalently dips away from the intrusion. Only in places, where sites have been sampled close to the internal boundary of the Monzonitic units, the foliation is very steep and dipping toward the internal rim, describing a symmetrical pattern of the magnetic foliation respect to the dike rims. This geometry has been widely recognized in volcanic dykes, where it has been interpreted as related to imbrication of the magnetic foliation along the dyke margins, related to upward flow of the magma (Aubourg et al., 2002). In this mechanism, the horizontal magnetic lineation can be interpreted as an intersection lineation between differently oriented foliation planes , which is oriented orthogonal to the magma flow. In sites far from the pluton margins (e.g. PA11), the steep lineations associated with steeply dipping foliations are likely related to ascent paths of magma, in particular with laminar flow and wall friction during injection (Andersson et al., 2016). On the other hand, in sites far from the intrusive rims (e.g. PA02) the occurrence of sub-horizontal lineations (tangential to the shape of the pluton) could be related to lateral flow of magma induced by "roll-over" at propagating sheet tips (Emeleus et al., 2012; Andersson et al., 2016) or to semi-chaotic particle movement during ring fissure flow, as observed in analogue models (Kennedy et al., 2008). The occurrence in some samples of magmatic layering steeply dipping inward and magnetic lineations plunging toward the centre of the intrusion suggests that the shape of the walls was not as regular (i.e., constantly outward dipping) as assumed in ring dyke models (complex flow due to complex sheet geometry of Andersson et al., 2016). The steep attitude of inward dipping foliations is not consistent with a lopolithic geometry of the Predazzo intrusion.

The degree of anisotropy (Pj’) varies between 1.01 and 1.150~~07~~ and is not controlled by lithology (i.e., low and high values are found both in monzonites and granites). More remarkably, the values do not show a pattern (e.g., high values aligned along WSW-ENE directions, typical of Ladinian tectonics) but are rather randomly distributed. This confirms a primary (i.e., emplacement-related) nature of magnetic anisotropy. Moreover, the nonlinear relationship between Km and Pj’ s ~~s~~upports that the obtained low Pj~~P~~ values indicate the existence of low strain during the emplacement.

Finally, also the orientation of dykes (mainly trending NNW-SSE) crosscutting intrusive rocks is at odds with sinistral strike slip tectonics along WSW-ENE structures, that would be rather associated with NE-SW trending dilational (extensional) structure. NE-SW trending dykes are rather found in the host rocks of the pluton, suggesting that they utilized previous extensional structures associated with sinistral strike-slip faulting. Thus, their emplacement and the emplacement of the pluton were post-tectonics.

In summary, field petrographic and AMS data are consistent with a multistage ring dyke emplacement mode, similar to the piston floor subsidence mechanism (Tomek et al., 2014), likely post-tectonics. ~~In particular, AMS data suggest that areas of upward flow of the magma are located in the NE and SW part of the Monzonitic intrusion, whereas in the southern part of the pluton data suggests prevalently horizontal flows.~~ T~~Generally, t~~he Predazzo sheets were emplaced via ~~either~~ prevalent updip magma flow ~~or~~ associated with local along-strike lateral magma transport (Fig. 11b).

~~NON SI CAPISCE TOGLIEREI~~

5.1 Emplacement mode of the Monzoni pluton

The shape of the Monzoni pluton was clearly controlled by Middle Triassic tectonics, being it elongated WSW-ENE, parallel to the Stava-Trodena strike-slip fault. It remains to be discussed whether this control was direct (syn-tectonic emplacement of the pluton) or indirect (emplacement along pre-existing tectonic structures). The host rocks of the Monzoni pluton are affected on all sides by contact metamorphism. This suggests that the host rock-pluton contacts are primary, thus no or very poorly affected by post-emplacement tectonics.

Comparing magnetic and deformation fabrics in the pluton with strain markers in the country rocks one can determine whether the magnetic fabric in pluton is primary or reflects regional tectonic strain (Benn et al., 1998, 2001; Talbot et al., 2005; Raposo et al., 2012). Three different areas, with distinct magnetic fabric can be recognized in the Monzoni body. In the NW side, the magnetic foliation is well defined, sub-vertical, and parallel to the E-W oriented boundaries of the igneous body in this area, with a very steep magnetic lineation. Along the NE side of the intrusive body the magnetic foliation and magnetic lineation vary from very gently dipping to sub-horizontal. Along the SE side the magnetic foliation is almost parallel to the boundary of the intrusive and gently to strongly dipping toward the internal part of the pluton, whereas the magnetic lineation is prevalently gently plunging~~sub-horizontal~~.

Our AMS results suggest that the magnetic fabric in Monzoni pluton was not directly controlled by Middle Triassic or post-tectonic deformation. This conclusion is supported by the absence of solid state deformation, by the general steeply magnetic fabric on the two sides of the pluton with absence of the NE-SW horizontal magnetic lineation and by the low degree of anisotropy (P_j), suggesting that magnetic fabric developed during magma emplacement and cooling and was likely controlled by the shape of the magma chamber.

The magnetic fabric can be read in terms of direction of flow and can help to infer the location and geometry of the feeding or root zones for magmatic bodies (e.g., Marre, 1986; Djouadi et al., 1997; Callot et al., 2001; Petronis et al., 2005; O'Driscoll et al., 2006; Maes et al., 2007). Magma originating from a planar dyke generates a parallel flow pattern with lineations pointing to opposing, but consistent directions, on either side of the dyke (Knight and Walker, 1988; Ernst and Baragar, 1992; Maes et al., 2007). Generally, the magnetic lineation, which represents the magma flow, plunges toward the magma source (Knight and Walker, 1988; Ernst and Baragar, 1992; Maes et al., 2007). In case of magma fed from a sub-vertical conduit, radial magma flow pattern is expected. Multiple feeders can produce more complex patterns of magma flow (Maes et al., 2007). In the Monzoni pluton, the magnetic lineations ~~on the two sides of pluton trajectories~~ converge towards the north-eastern part of the pluton (PA15, PA16, PA18, PA22, PA23, and PA24), suggesting that the root zone was not located at the cent~~er~~e of the pluton but rather towards NE. This interpretation is also consistent with the magmatic evolution of the pluton. Indeed, the most evolved rocks are located at the south-western edge of the pluton, while the less evolved rocks are located at the north-eastern part of the pluton.

In the Monzoni pluton, steep to moderate foliations and lineations at the western and eastern borders of the pluton leave space to shallowly dipping fabric in its intermediate parts. This fabric may have been induced by shear of magma along the host-rocks at the top of the pluton. This inference is in agreement with field host-rocks above the pluton, in agreement with geological observations that allow to infer that the top boundary of the pluton was located just above the mountain peaks in the central part of the pluton (Castellarin et al., 1982b).

In summary, field, petrographic and AMS data and the ENE-WSW elongated shape indicate that the site and shape of the Monzoni pluton was controlled by strike-slip faults associated with Ladinian-tectonics. However, the absence of deformation at the field- and micro- scale is consistent with a post Ladinian-tectonics timing of emplacement, as for the Predazzo body.

6. Conclusions

Petrographic and AMS data, coupled with field geological data allowed us to investigate the emplacement modes of the Predazzo and Monzoni bodies. Although these plutons are considered in the literature as separated bodies, the outcrop of a small volume of intrusive rocks between the bodies and the continuity of metamorphic aureola from west of the Predazzo body to east of the Monzoni body suggest that they are parts of a ~20 km long SW-NE oriented continuous pluton, sub-parallel to Ladinian strike-slip faults. However, our results suggest a variable control of Ladinian tectonic structures on the emplacement modes of the two bodies.

AMS and petrographic data from the Predazzo body are consistent with a multistage ring dyke emplacement mode, with areas of upward flow of the magma located in the NE and SW part of the intrusion, whereas in the southern part of the pluton our data suggest prevalently horizontal flows. Generally, the Predazzo sheets were emplaced via either updip magma flow or along-strike lateral magma transport, and the round shape suggests no influence of Ladinian tectonic structures.

On the contrary, the ENE-WSW elongated shape of the Monzoni body was controlled by the occurrence of strike-slip faults associated with Ladinian-tectonics, the feeder being likely located at the NE edge of the body. However, the absence of deformation at the field- and micro- scale is consistent with a post Ladinian-tectonics timing of emplacement, as for the Predazzo pluton.

Acknowledgements

The Editor (Ian Alsop) and two reviewers (Teresa Román-Berdiel and an anonymous referee) are warmely thanked for their constructive criticisms. Financial support from PRIN2015-Project 2015EC9PJ5_001 and Progetti di Ateneo Sapienza 2017 (E. Carminati) is acknowledged. Marcello Caggiati and Massimo Coltorti provided invaluable help in the field. Aldo Winkler and Ann Marie Hirt are warmly thanked for doing hysteresis and HF-AMS measurements, respectively. The Trento province is thanked for providing permissions for sampling in the Dolomites, that are an UNESCO protected site. Erasmus Mundus European Commission is acknowledged for providing financial support the PhD program project of Hassan Abbas in the framework of EU METALIC II project (Erasmus Mundus Action 2).

Appendix A

Petrographic description

Predazzo pluton

Clinopyroxenite (PA12, PR11a, b, c)

Clinopyroxenites show a typical hypidiomorphic inequigranular medium- to coarse grained cumulitic texture. Cumulitic phase (clinopyroxene) accounts for more than ~65% of the rock with usually subhedral, fresh and rarely twinned crystals. Clinopyroxene is mainly medium grained (~3 mm) but a few reach larger dimensions, up to ~6 mm. The intercumulus phases consist of subhedral fine- to medium-grained opaques (~0.3-1.3 mm; ~15%), sometimes included in larger biotite crystals, anhedral to subhedral biotite (~13%) with an average size of ~4 mm and anhedral to subhedral small (~1 mm) plagioclase (~7%). In few cases biotites are partly chloritized, while plagioclases are usually partially sericitized. Fine-grained opaques, biotite and plagioclase are also found included in the clinopyroxene oikocrysts (poikilitic). Apatite and zircon are the common accessory minerals usually found as tiny grains included in clinopyroxene and biotite.

Cumulitic gabbro (PA~~R~~ 10)

The cumulitic gabbro is medium-grained with hypidiomorphic inequigranular texture. The cumulitic phases are plagioclase (~50%), clinopyroxene (~36%) and opaques (~10%). Subhedral to euhedral medium-grained (~3 mm) plagioclase is highly altered to sericite with cores more altered than rims. Clinopyroxene is subhedral medium grained (~2 mm), highly fractured, slightly altered and usually twinned. Opaques occurs as subhedral to anhedral fine grained (<1 mm) and usually found in clusters with clinopyroxene or included in clinopyroxene and biotite. The intercumulus phases (~4%) consist of anhedral to subhedral fine grained (<1 mm) biotite and plagioclase. Biotite and plagioclase also occur as anhedral small grains included in the clinopyroxenes. Apatite is a common accessory mineral occurring as minute inclusion in clinopyroxene and biotite.

Diorite (PA06)

The diorite is characterized by hypidiomorphic inequigranular with medium- to fine-grained texture. The rock is composed of plagioclase (~60%), amphibole (~15%), biotite (~10%), clinopyroxene (~10%), plus smaller amounts of K-feldspar, opaques, quartz and accessory minerals. Plagioclase occurs as slightly sericitized tabular to equant subhedral crystals with an average size of ~1.5 mm. Anhedral to subhedral amphibole, biotite and clinopyroxene occur as small (~1 mm) interstitial clusters, together with subhedral fine-grained opaques, usually found as inclusion in these minerals. Clinopyroxene is generally replaced to different degrees to amphibole. Most of the biotite crystals are slightly to moderately altered to chlorite. K-feldspar and quartz (<1 mm) occur as anhedral intergranular crystals in between plagioclase laths. Apatite and rare zircon are present as small inclusions mainly within plagioclase and clinopyroxene.

Monzonites (PA02, PA10), monzodiorites (PA08, PR14c, PA09) and monzogabbro (PR12)

These three types of rocks generally share the same petrographic features, being different only for the relative K-feldspar/plagioclase ratio. The amount of mafic minerals increases from monzonites to monzodiorites and monzogabbros. This rock group shows hypidiomorphic inequigranular texture. Monzonite and monzogabbros are medium-grained, while monzodiorites are medium- to fine-grained. The rocks are poikilitic, with big anhedral K-feldspars including other minerals.

The rocks are generally composed, in order of abundance, of plagioclase, K-feldspar, clinopyroxene, amphibole, biotite, quartz, opaques, orthopyroxene and accessory minerals. Plagioclase is usually euhedral with variable grain size (~0.5-3 mm) and sometimes zoned, with cores always more altered than the rims (i.e. sericitized and saussuritized). Few crystals show combined pericline and albite twining. Alkali feldspar (~1-4 mm) occurs as anhedral irregular grains characterized by perthitic exsolution. Clinopyroxene is subhedral with medium size (~1-2 mm), sometimes twined and in most cases found in clusters. The clinopyroxene crystals are partially to completely altered to amphibole (uralitization). Amphibole is anhedral to subhedral (~0.5-1.5 mm) and mostly found along the margin of clinopyroxene. Biotite occurs as subhedral to anhedral crystals with different grain size (~2-0.5mm) and often found in clusters. In some cases large biotite crystals are poikilitic for the presence of opaque mineral inclusions. The biotite state generally is good, but in some case it is partly altered into chlorite. Anhedral quartz is fine- to medium-grained (~1.5-0.3 mm) and occurs as interstitial phase. Orthopyroxene is subhedral to anhedral and are usually found in few percent and recorded not in all the thin sections. Also orthopyroxenes show alteration to amphibole with various degrees. Opaques are small subhedral grains usually included in the other mafic minerals or occupying interstitial areas. The accessory minerals are apatite, zircon and sphene, observed as inclusions or along mineral boundaries.

Granite group (PA01, PA03, PA04, PA05, PA07, PA13, PA17)

The samples exhibit hypidiomorphic inequigranular texture. In a few cases, granophyric texture is also recorded. The granite rocks are classified into two main groups: albitized granite (affected by hydrothermal alteration) and biotite granite.

In the first group biotite is completely transformed mainly to sericite and minor chlorite (PA01, PA04, PA05, PA17), while in the second group biotite is generally found in a good state of preservation (PA07, PA03, PA13). The biotite granite group is characterized by the presence of microgranular quartz usually forming aggregates around feldspar crystals.

The rocks are made up, in order of abundance, of K-feldspar, quartz and plagioclase with minor biotite, muscovite, chlorite and rare amphibole.

K-feldspar occurs as subhedral medium grained (~2-4 mm) crystals characterized by perthitic exsolution lamellae. Carlsbad twining is common and the crystals usually shows minor alteration.

Quartz mainly occurs in anhedral grains (~1-3 mm) but is also sometimes found in the interstitial areas (<0.5 mm) or forming aggregates around feldspar crystals. Quartz crystal shows no or incipient undulatory extinction. Plagioclase is subhedral medium grained (~1-3 mm), sometimes zoned and usually show albite twinning. In biotite granite, Most of the plagioclase crystals are slightly to moderately altered (sericitized and saussuritized), with the cores more altered than the rims. On the other hand, in albitized granite plagioclase is completely transformed having lost completely its anorthite component. Biotite is present as subhedral platy crystals (~0.5-2 mm) and usually forms clusters of numerous crystals. Biotite is partially to completely altered to chlorite and sericite. Sericite occurs as anhedral to subhedral (~1-2 mm) pseudomorphs after biotite and is commonly associated with chlorite. Chlorite is subhedral to anhedral (~0.5-2 mm) pseudomorphs after biotite. Rare amphibole crystals have been recorded in the second group. Accessory minerals are zircon, apatite, fluorite, iron oxide and monazite.

Monzonite to Syenite? (PA11)

This sample is strongly affected by hydrothermal alteration and a precise classification cannot be conducted.

Monzoni pluton

The samples from Monzoni pluton have been classified into two main groups: Gabbroic Rock (olivine-gabbros, gabbros, monzogabbros), mainly located at the northeastern part of Monzoni pluton, and monzogabbros (PA21).

These rocks are medium- to coarse-grained with hypidiomorphic inequigranular texture. The rocks are composed, in order of abundance, of plagioclase, clinopyroxene, K-feldspar, opaques, olivine, biotite and accessory minerals.

Plagioclase is the most abundant phase. It is euhedral to subhedral medium-grained (~1-4 mm), always twinned, rarely zoned and mostly unaltered. Clinopyroxene is represented by subhedral medium- to coarse-grained (~1-5 mm) unaltered crystals. K-feldspar is anhedral to subhedral medium- to fine-grained (~0.5-4 mm), unaltered, untwined, usually occupying the interstitial areas and in some cases as oikocryst, including the other minerals (poikilitic texture). Opaques are subhedral fine- to medium-grained (~0.2-1.3 mm), mainly included within other minerals (biotite, clinopyroxene and olivine) or occupying interstitial areas. Olivine is subhedral medium-grained (~1-5 mm), usually unaltered and fractured. Biotite is anhedral to subhedral fine- to medium-grained and unaltered, occupying the interstitial areas between the early crystallized minerals.

Gabbro (non-cumulitic) PA 16. This rock exhibits coarse-grained with hypidiomorphic inequigranular texture. It is made up with plagioclase, clinopyroxene, opaque, biotite and accessory minerals (in order of occurrence). Plagioclase is euhedral medium- to coarse-grained (~2-5 mm), usually found in good state or showing slight alteration to sericite and is usually twinned. Clinopyroxene is subhedral medium- to coarse-grained (~2-6 mm), unaltered, rarely twinned, with ophitic and subopthic texture (plagioclase partially or completely enclosed by clinopyroxene). Opaques are subhedral fine- to medium-grained (~0.3-1.3 mm), occupying the interstitial areas or included within the biotite and clinopyroxene. Biotite is anhedral to subhedral, fine- to medium-grained (~0.5-2.5 mm), unaltered, and interstitial.

Gabbro (cumulitic) PA15. This rock is coarse-grained with cumulitic texture. Cumulus phases are mainly clinopyroxene with minor olivine. Intercumulus phases are primarily plagioclase and biotite with minor opaque oxides. Clinopyroxene is euhedral to subhedral coarse- to medium-grained (~2-8 mm), rarely twinned and sometimes slightly zoned. Olivine is subhedral medium-grained (~1-3 mm) and usually found in good state with fracture. It is slightly altered to iddingsite particularly along the fractures. Plagioclase is euhedral to subhedral medium-grained (~1-2 mm), slightly altered to sericite and always twinned. Biotite is subhedral to anhedral medium- to fine-grained (~0.5-2 mm) and in a few cases is slightly chloritized. Opaques are subhedral fine- to medium-grained (~0.1-1.5 mm). They occur both as interstitial phases or included within clinopyroxene and biotite.

Olivine gabbro (PA20, PA18). These rocks are medium- to coarse-grained. Cumulus phases are represented by clinopyroxene, plagioclase, and olivine. Clinopyroxenes occurs as subhedral medium- to coarse-grained (~ 2-6 mm), unaltered and usually untwined. Clinopyroxene oikocrysts usually include small crystals from opaques, plagioclase, olivine and biotite. Olivine crystals are subhedral medium-grained (~ 1-2.5 mm). Olivine in sample PA20 is fresh and fractured, whereas in sample PA18, it is completely altered to secondary minerals (iddingsite, bowlingite and celadonite). Plagioclase is euhedral to subhedral medium-grained (~ 1-2.5 mm), rarely zoned, and always showing twining. Plagioclase is fresh in sample PA20 and slightly altered in PA18. Intercumulus phases are composed of plagioclase, biotite, opaques, and K-feldspar. Plagioclase occurs as fresh subhedral fine-grained (~ 1 mm). Biotite is fresh medium-grained (~ 1-3 mm), subhedral or sometimes anhedral, when occupying interstitial positions. Opaques occur as subhedral fine- to medium-grained (~ 0.5-1.3 mm), and commonly are interstitial phases or are included in clinopyroxene, biotite and olivine. K-feldspar is clear anhedral fine- to medium-grained (~ 0.5-1.5 mm) and is usually found as interstitial crystals between the early crystallized minerals.

Monzonite (PA22, 22A, 23, 24). These rocks are mainly located in the south-western sector of Monzoni pluton and represent the most widespread rock type. These rocks are medium- to fine-grained and exhibit hypidiomorphic inequigranular texture. The rocks are composed, in order of abundance, of plagioclase, K-feldspar, biotite, clinopyroxene, amphibole, opaques, quartz and accessory minerals.

Plagioclase represents the most abundant phase with euhedral to subhedral tabular laths with variable grain size (up to 4 mm), usually twinned. Plagioclase crystals generally show slight to moderate degrees of alteration (sericitization). K-feldspar occurs as anhedral to subhedral, rarely perthitic, untwined with variable size (up to 5 mm) and is usually found in a good state or in some cases slightly sericitized. K-feldspar oikocrysts usually include other minerals in a poikilitic relation. Clinopyroxene is subhedral to anhedral fine- to medium-grained (up to 2 mm), usually showing different degrees of alteration to amphibole (uralitization). Biotite is subhedral to anhedral fine- to medium-grained (up to 3 mm), generally found in good state or sometimes showing slight to moderate alteration to chlorite. Quartz occurs as fine interstitial grains between the early crystallized minerals. Opaques are subhedral to anhedral fine-grained (~0.2-1 mm), and occupy the irregular interstices in between the other minerals or are included within K-feldspar. Orthopyroxene is rarely found with anhedral to subhedral medium-grained. Sample PA24 is highly altered compared to the other Monzonite samples.

References

Andersson, M., Almqvist, B.S.G., Burchardt, S., Troll, V.R., Malehmir, A., Snowball, I., Kübler, L., 2016. Magma transport in sheet intrusions of the Alnö carbonatite complex, central Sweden. Sci. Rep. 6, 1–13. doi:10.1038/srep27635.

Assereto, R.L., Brusca, C., Gaetani, M., Jadoul, F., 1977. The Pb-Zn mineralization in the Triassic of the Dolomites Geological history and genetic interpretations. L'Industria Mineraria 28, 1–34.

Aubourg, C., Giordano, G., Mattei M., Speranza, F., 2002. Magma flow in rhyolitic dikes inferred from magnetic fabric analysis (Ponza Island, W Italy). Physics and Chemistry of the Earth, 27, 1263-1272.

Balini, M., Lucas, S.G., Jenks, J.F., Spielmann, J.A., 2010. Triassic ammonoid biostratigraphy: an overview. Geol. Soc. (Lond.) Spec. Publ. 334, 221–262.

Barth, S., Oberli, F., Meier, M., Blattner, P., Bargossi, G.M., Di Battistini, G., 1993. The evolution of a calc-alkaline basic to silicic magma system: Geochemical and Rb-Sr, Sm-Nd, and $^{18}O/^{16}O$ isotopic evidence from the Late Hercynian Atesina-Cima d'Asta volcano-plutonic complex, northern Italy. Geochim. Cosmochim. Acta 57, 4285–4300.

Bechstadt, T., Brandner, R., Mostler, H., Schmidt, K., 1977. Aborted rifting in the Triassic of the Eastern and Southern Alps. N. Jb. Geol. Palaont. Abh. 156, 157-178.

Beltrán-Triviño, A., Winkler, W., von Quadt, A., Gallhofer, D., 2016. Triassic magmatism on the transition from Variscan to Alpine cycles: evidence from U–Pb, Hf, and geochemistry of detrital minerals. Swiss J. Geosci. 109, 309–328. doi:10.1007/s00015-016-0234-3.

Benn, K., Ham, N.M., Pignotta, G.S., Bleeker, W., 1998. Emplacement and deformation of granites during transpression: Magnetic fabrics of the Archean Sparrow pluton, Slave Province, Canada. J. Struct. Geol. 20, 1247–1259. doi:10.1016/S0191-8141(98)00065-0.

Benn, K., Paterson, S.R., Lund, S.P., Pignotta, G.S., Kruse, S., 2001. Magmatic fabrics in batholiths as markers of regional strains and plate kinematics: Example of cretaceous Mt. Stuart batholith.

Phys. Chem. Earth, Part A Solid Earth Geod. 26, 343–354. doi:10.1016/S1464-1895(01)00064-3.

Bergmüller, F., Bärlocher, C., Geyer, B., Grieder, M., Heller, F., & Zweifel, P., 1994. A torque magnetometer for measurements of the high-field anisotropy of rocks and crystals. Measurement Science and Technology. 5, 1466-1470.

Bigi, G., Cosentino, D., Parrotto, M., Sartori, R., Scandone, P., 1990. Structural model of Italy, Scale 1:500.000, C.N.R. Progetto Finalizzato Geodinamica.

Blendinger, W., 1985. Middle Triassic strike-slip tectonics and igneous activity of the Dolomites (Southern Alps). Tectonophysics 113, 105–121. doi:10.1016/0040-1951(85)90112-X.

Bonadiman, C., Coltorti, M., Siena, F., 1994. Petrogenesis and T-fO_2 estimates of Mt. Monzoni complex (Central Dolomites, Soulhern Alps): a Triassic shoshonitic intrusion in a transcunent geodynamic setting. Eur J Mineral., 6, 943-966.

Bosellini, A., Castellarin, A., Doglioni, C., Guy, F., Lucchini, F., Perri, M.C., Rossi, P.M., Simboli, G., Sommavilla, E., 1982. Magmatismo e tettonica nel Trias delle Dolomiti, in: Guida Alla Geologia Del Sudalpino Centro-Orientale, pp. 189–210.

Bosellini, A., Gianolla, P., Stefani, M.M., 2003. Geology of the Dolomites. Episodes 26, 181–185.

Bouchez, J.L., Gleizes, G., Djouadi, T., & Rochette, P., 1990. Microstructure and magnetic susceptibility applied to emplacement kinematics of granites: the example of the Foix pluton (French Pyrenees). Tectonophysics 184, 157-171.

Brack, P., Mundil, R., Oberli, F., Meier, M., Rieber, H., 1996. Biostratigraphic and radiometric age data question the Milankovitch characteristics of the Latemar cycles (Southern Alps). Geology, 24, 371–375.

Brack, P., Mundil, R., Oberli, F., Meier, M., Rieber, H., 1997. Biostratigraphic and radiometric age data question the Milankovitch characteristics of the Latemar cycle (Southern Alps, Italy): Comment and Reply. Geology 25, 471-472.

Brack, P., Muttoni, G., 2000. High-resolution magnetostratigraphic and lithostratigraphic correlations in Middle Triassic pelagic carbonates from the Dolomites (northern Italy). Palaeogeogr. Palaeoclimatol. Palaeoecol. 161, 361–380. doi:10.1016/ S0031-0182(00)00081-X.

Brack, P., Rieber, H., 1993: Towards a better definition of the Anisian/Ladinian boundary: new biostratigraphic data and correlations of boundary sections from the Southern Alps. Ecl. geol. Helv., 86/2, 415-527.

Brack, P., Rieber, H., Mundil, R., Blendinger, W. Maurer, F., 2007. Geometry and chronology of growth and drowning of Middle Triassic carbonate platforms (Cernera and Bivera/Clapsavon) in the Southern Alps (northern Italy), Swiss Journal of Geosciences 100/3, 327– 348.

Brandner, R., 1984. Meeresspiegelschwankungen und Tektonik in der Trias der NW Tethys. Jb. Geol. B.-A., 126, 435-475.

Brandner, R., Keim, L., 2011. A 4-day geological field trip in the Western Dolomites. Geo.Alp 8, 76–118.

Brandner, R., Gruber, A., Morelli, C., Mair, V., 2016. Field trip 1. Pulses of Neotethys-Rifting in the Permomesozoic of the Dolomites. Geo.Alp 13, 7–70.

Brogger, W. C., 1895. Die Eruptivgesteine des Kristianiagebietes. II. Die Eruptionsfolge der triadischen Eruptivgesteine bei Predazzo in Siidtyrol: Skr. Norske Vid.-Akad. i Oslo, I., Mat. Nat. Kl, (7), 123-153.

Brusca, C., Gaetani, M., Jadoul, F., Viel, G., 1981. Paleogeografia ladino-carnica e metallogenesi del sudalpino. Mem. della Soc. Geol. Ital. 22, 65–82.

Büttner, S.H., 1999. The geometric evolution of structures in granite during continous deformation from magmatic to solid-state conditions: An example from the central European Variscan belt. Am. Mineral. 84, 1781–1792.

Callot, J.P., Geoffroy, L., Aubourg, C., Pozzi, J.P., Mege, D., 2001. Magma flow directions of shallow dykes from the East Greenland volcanic margin inferred from magnetic fabric studies. Tectonophysics 335, 313–329. doi:10.1016/S0040-1951(01)00060-9.

Carminati, E., Cavazza, D., Scrocca, D., Fantoni, R., Scotti, P., & Doglioni, C., 2010. Thermal and tectonic evolution of the southern Alps (northern Italy) rifting: Coupled organic matter maturity analysis and thermokinematic modeling. AAPG bulletin, 94(3), 369-397.

Carminati, E., Lustrino, M., Cuffaro, M., & Doglioni, C., 2010b. Tectonics, magmatism and geodynamics of Italy: what we know and what we imagine. Journal of the Virtual Explorer, 36(8).

Casetta, F., Coltorti, M., Marrocchino, E., 2017. Petrological evolution of the Middle Triassic Predazzo Intrusive Complex, Italian Alps. Int. Geol. Rev. 1–21. doi:10.1080/00206814.2017.1363676

Cashman, K.V., Sparks, R.S.J., 2013. How volcanoes work: A 25year perspective. Geol. Soc. Am. Bull. 125, 664-690.

Castellarin, A., Lucchini, F., Row, P.L., Simboli, G., Bosellini, A., Sommavilla, E. 1980. Middle Triassic magmatism in Southern Alps: a geodynamic model. Riv. Ital. Paleont. 85, 1111- 1124.

Castellarin, A., Lucchini, F., Row, P.L., Simboli, G., Bosellini, A., Sommavilla, E. 1980. Middle Triassic magmatism in Southern Alps: a geodynamic model. Riv. Ital. Paleont. 85, 1111- 1124.

Castellarin, A., Guy, F., Selli, L., 1982. Geologia dei dintorni del Passo di S. Nicolò e della Valle di Contrin (Dolomiti), in: Guida alla Geologia del Sudalpino Centro Orientale, pp. 231–242.

Castellarin, A., Lucchini, F., Rossi, P.L., Sartori, R., Simboli, G., Sommavilla, E., 1982b. Note geologiche sulle intrusioni di Predazzo e dei Monzoni, in: Guida Alla Geologia Del Sudalpino Centro-Orientale, pp. 211–220.

Castellarin, A., Lucchini, F., Rossi, P.L., Selli, L., Simboli, G., 1988. The Middle Triassic magmatic-tectonic arc development in the Southern Alps. Tectonophysics 146, 79–89.

Castellarin, A., Selli, L., Picotti, V., Cantelli, L., 1998. La tettonica delle Dolomiti nel quadro delle Alpi Meridionali orientali. Mem. della Soc. Geol. Ital. 53, 133–143.

Castellarin, A., Selli, L., Picotti, V., Cantelli, L., 1998b. Tettonismo e diapirismo Medio Triassico delle Dolomiti. Mem. Soc. Geol. Ital. 53, 145–169.

Castellarin, A., Cantelli, L., 2000. Neo-Alpine evolution of the Southern Eastern Alps. J. Geodyn. 30, 251–274. doi:10.1016/S0264-3707(99)00036-8.

Castellarin, A., Cantelli, L., Selli, L., 2004. Field Trip P54: Structure of the Italian Dolomites, partially along the southern sector of the transalp seismic profile, IGC Congress Field Trip Guidebook.

Castellarin, A., Nicolich, R., Fantoni, R., Cantelli, L., Sella, M., Selli, L., 2006. Structure of the lithosphere beneath the Eastern Alps (southern sector of the TRANSALP transect). Tectonophysics 414, 259–282. doi:10.1016/j.tecto.2005.10.013.

Castro, A., 1987. On granitoid emplacement and related structures. A review. Geol. Rundsch. 76, 101-124.

Cifelli, F., Minelli, L., Rossetti, F., Urru, G., Mattei, M., 2012. The emplacement of the Late Miocene Monte Capanne intrusion (Elba Island, Central Italy): constraints from magnetic fabric analyses. Int. J. Earth Sci. (Geol Rundsch) 101, 787-802.

Crisci, C. M., Ferrara, G., Mazzuoli, R., & Rossi, P. M., 1984. Geochemical and geochronological data on Triassic volcanism of the Southern Alps of Lombardy (Italy)-genetic implicaitons. Geol. Rundsch. 73, 279–292.

De Zanche, V., Gianolla, P., 1995: Litostratigrafia al limite Ladinico-Carnico (Sudalpino orientale). Ann. Univ. Ferrara, Sci. Terra, v. 5, 41-48.

De Zanche, V., Gianolla, P., Mietto, P., Siorpaes, C. Vail, P. 1993: Triassic sequence stratigraphy in the Dolomites (Italy). Memorie di Scienze Geologiche 45, 1–27.

Del Monte, M., Paganelli, L., & Simboli, G., 1967. The Monzoni intrusive rocks. A modal and chemical study. Mineral Petrogr Acta, 13, 75-118.

Djouadi, M.T., Gleizes, G., Ferré, E., Bouchez, J.L., Caby, R., Lesquer, A., 1997. Oblique magmatic structures of two epizonal granite plutons, Hoggar, Algeria: late-orogenic emplacement in a transcurrent orogen. Tectonophysics 279, 351–374. doi:10.1016/S0040-1951(97)00123-6.

Doglioni, C., 1982. Tettonica Triassica nella Valle di Livinallongo (Dolomiti centrali). Ann. Univ. Ferrara, Zsez.IX, Scienze Geol. Paleont. 8, 1-21.

Doglioni, C., 1983. Duomo medio-Triassico nelle Dolomiti. Rend. della Soc. Geol. Ital. 6, 13–16.

Doglioni, C., 1984a. Tettonica triassica transpressiva nelle Dolomiti. G. Di Geol. 46, 47–60.

Doglioni, C., 1984b. Triassic diapiric structures in the central Dolomites (northern Italy). Eclogae Geol. Helv. 77, 261–285.

Doglioni, C., 1985. The overthrusts in the Dolomites: ramp-flat systems. Eclogae Geol. Helv. 78, 335–350.

Doglioni C., 1987. Tectonics of the Dolomites (Southern Alps, Northern Italy). J. Struct. Geol. 9, 181-193.

Doglioni, C., 1988. Examples of strike-slip tectonics on platform-basin margins. Tectonophysics 156, 293–302. doi:10.1016/0040-1951(88)90066-2.

Doglioni, C., 2007. Tectonics of the Dolomites. Bull. Angew. Geol. 12, 11–15.

Doglioni, C., Carminati, E., 2008. Structural Styles and Dolomites Field Trip. Mem. Descr. della Cart. Geol. d'Italia 82, 301.

Emeleus, C.H., Troll, V.R., Chew, D.M., Meade, F.C., 2012. Lateral versus vertical emplacement in shallow-level intrusions? The Slieve Gullion Ring-complex revisited. J. Geol. Soc. London. 169, 157–171. doi:10.1144/0016-76492011-044.

Ernst, R.E., Baragar, W.R.A., 1992. Evidence from magnetic fabric for the flow pattern of magma in the Mackenzie giant radiating dyke swarm. Nature 356, 511–513. doi:10.1038/356511a0.

Ferry, J. M., Wing, B. A., Penniston-Dorland, S. C., & Rumble, D., 2002. The direction of fluid flow during contact metamorphism of siliceous carbonate rocks: new data for the Monzoni and Predazzo aureoles, northern Italy, and a global review. Contributions to Mineralogy and Petrology, 142(6), 679-699.

Gallien, F., Abart, R., & Wyhlidal, S., 2007. Contact metamorphism and selective metasomatism of the layered Bellerophon Formation in the eastern Monzoni contact aureole, northern Italy. Mineralogy and Petrology, 91(1-2), 25-53.

Garzanti, E., 1985. The sandstone memory of the evolution of a Triassic volcanic arc in the Southern Alps, Italy. Sedimentology 32, 423–433.

Gianolla, P., De Zanche, V., Mietto, P., 1998. Triassic sequence stratigraphy in the Southern Alps (Northern Italy): definition of sequences and basin evolution. In: de Graciansky, P.-C., Hardenbol, J., Jacquin, T. and P.R. Vail (Eds.). Mesozoic and Cenozoic Sequence Stratigraphy of European Basins. SEPM Special Publications 60, 719–747.

Gianolla, P., Avanzini, M., Breda, A., Kustatscher, E., Preto, N., Roghi, G., Furin, S., Massari, F., Picotti, V., Stefani, M., 2010. Field trip to the world heritage site of the Tethysian Triassic, September 5-10, 2010, Dolomites, Southern Alps, Italy. 122 pp.

Graham, J.W., 1954. Magnetic susceptibility anisotropy, an unexploited petrofabric element. Geol. Soc. Am. Bull. 65, 1257-1258.

Handy, M. R., Schmid, S. M., Bousquet, R., Kissling, E., & Bernoulli, D. (2010). Reconciling plate-tectonic reconstructions of Alpine Tethys with the geological–geophysical record of spreading and subduction in the Alps. *Earth-Science Reviews*, *102*(3-4), 121-158.

Hansel, V., 1878. Die petrographische Beschaffenheit des Monzonits von Predazzo. Jahrb. der Kais. Geol. Reichsanstalt 28, 449–466.

Hörnes, R., 1912. Zur Geologie von Predazzo. Sitzungsberichte der Akad. der Wissenschaften Math. Klasse 121, 3–31.

Hrouda, F., 1982. Magnetic anisotropy of rocks and its application in geology and geophysics. Geophys. Surv. 5, 37–82.

Hrouda, F., Jelínek, V., 1990. Resolution of ferromagnetic and paramagnetic anisotropies, using combined low-field and high-field measurements. Geophys. J. Int. 103, 75-84.

Hrouda, F., Jelínek, V., Zapletal, K., 1997. Refined technique for susceptibility resolution into ferromagnetic and paramagnetic components based on susceptibility temperature-variation measurement. Geophys. J. Int.129, 715-719.

Hutton, D.H.W., 1988. Granite emplacement mechanisms and tectonic controls: inferences from deformation studies. Trans. R. Soc. Edinb. Earth Sci. 79, 245–255. doi:10.1017/S0263593300014255.

Jelinek, V., 1977. The statistical theory of measuring anisotropy of magnetic susceptibility of rocks and its application. Geofyzika Brno, pp. 77.

Jelínek, V., 1981. Characterization of the magnetic fabric of rocks. Tectonophysics 79, 63-67.

Jelínek, V., Pokorný, J., 1997. Some new concepts in technology of transformer bridges for measuring susceptibility anisotropy of rocks. Physics and Chemistry of the Earth 22, 179-181.

Just, J., Kontny, A., De Wall, H., Hirt, A.M. & Martín-Hernandéz, F., 2004. Development of magnetic fabrics during hydrothermal alteration in the Soultz-sous-Forets granite from the EPS-1 borehole, Upper Rhine Graben. In: Martín-Hernández, F., Lunebrg, C.M., Aubourg, C. & Jackson, M. (eds) Magnetic Fabric: Methods and Applications. Geological Society, London, Special Publications 238, 509-526.

Kennedy, B.M., Mark Jellinek, A., Stix, J., 2008. Coupled caldera subsidence and stirring inferred from analogue models. Nat. Geosci. 1, 385–389. doi:10.1038/ngeo206.

Knight, M.D., Walker, G.P.L., 1988. Magma Flow Directions in Dikes of the Koolau Complex, Oahu, Determined From Magnetic Fabric Studies. J. Geophys. Res. 93, 4301-4319.

Leonardi, P., 1967. Le Dolomiti. Geologia dei monti tra Isarco e Piave. Consiglio Nazionale delle Ricerche. Rome, 1019 pp. (2 volumes).

Lucchini, F., Rossi, P.L., Simboli, G., 1982. Il magmatismo triassico dell’area di Predazzo (Alpi Meridionali, Italia). In A. CASTELLARIN e G.B. VAI (Eds.), Guida alla geologia del Sudalpino centro-orientale. Guide geol. reg. S.G.I., pp. 221-230, Bologna.

Maes, S.M., Tikoff, B., Ferré, E.C., Brown, P.E., Miller, J.D., 2007. The Sonju Lake layered intrusion, northeast Minnesota: Internal structure and emplacement history inferred from magnetic fabrics. Precambrian Res. 157, 269–288. doi:10.1016/j.precamres.2007.02.021.

Magee, C., O'Driscoll, B., Petronis, M.S., Stevenson, C.T.E., 2016. Three-dimensional magma flow dynamics within subvolcanic sheet intrusions. Geosphere 12, 842-866.

Marangon, A., Gattolin, G., Della Porta, G., Preto, N., 2011: The Latemar: a flat- topped, steep fronted platform dominated by microbialites and synsedimentary cements. Sedimentary Geology, doi: 10.1016/j.sedgeo.2011.09.001

Marinelli, M., Viel, G., Farabegoli, E., 1980. Il Permo-Trias delle Alpi Meridionali: evoluzione tardo-ercinica di un bacino marginale di retroarco sialico. L'Industria Mineraria 6, 1–14.

Marocchi, M., Morelli, C., Mair, V., Klötzli, U., & Bargossi, G. M., 2008. Evolution of large silicic magma systems: new U-Pb zircon data on the NW Permian Athesian Volcanic Group (Southern Alps, Italy). The Journal of Geology, 116(5), 480-498.

Marre, J., 1986. The Structural Analysis of Granitic Rocks. Elsevier, New York 123 pp.

Martin Hernandez, F., & Hirt, A.M., 2001. Separation of ferrimagnetic and paramagnetic anisotropies using a high- field torsion magnetometer. Tectonophysics 337, 209-221.

Masetti D., Trombetta G.L. 1998: L'eredità anisica nella nascita ed evoluzione delle piattaforme medio-triassiche delle Dolomiti occidentali, Mem. Sci. Geol., 50, 213-237.

Menegazzo Vitturi, L., Visonà, D., & Zantedeschi, C., 1995. Amphibole composition in rocks from Predazzo volcano-plutonic complex (Southern Alps, Italy). Memorie Di Scienze Geologiche, 47, 87-94.

Mietto, P., Manfrin, S., 1995. A high resolution Middle Triassic ammonoid standard scale in the Tethys Realm. A preliminary report. Bull. Soc. Géol. France 1995/5, 539-563.

Mietto, P., Manfrin, S., Preto, N., Rigo, M., Roghi, G., Furin, S., Gianolla, P., Posenato, R., Muttoni, G., Nicora, A., Buratti, N., Cirilli, S., Spötl, C., Ramezani, J., Bowring, S.A., 2012. The

Global Boundary Stratotype Section and Point (GSSP) of the Carnian Stage (Late Triassic) at Prati di Stuores/Stuores Wiesen Section (Southern Alps, NE Italy). Episodes 35, 414-430.

Mundil, R., 1996. High resolution U-Pb dating of Middle Triassic volcaniclastics: Verification of tuning parameters for carbonate sedimentation and time-scale calibration. [Ph.D. dissert.], Zurich, Swiss Federal Institute of Technology, No. 11767.

Nédélec, A., Trindade, R., Peschler, A., Archanjo, C., Macouin, M., Poitrasson, F., Bouchez, J.L., 2015. Hydrothermally-induced changes in mineralogy and magnetic properties of oxidized A-type granites. Lithos 212, 145-157.

O'Driscoll, B., Troll, V.R., Reavy, R.J., Turner, P., 2006. The Great Eucrite intrusion of Ardnamurchan, Scotland: Reevaluating the ring-dike concept. Geology 34, 189–192. doi:10.1130/G22294.1.

Ogilvie Gordon, M.M., 1902. Monzoni and Upper Fassa. Geol. Mag., dec. 10, vol. 9, p. 309, London.

Ogilvie Gordon, M.M., 1902-1903. The Geological Structure of Monzoni and Fassa. Transactions of the Edinburgh geological society. vol. VIII.

Paterson S.R., Fowler T.K., 1993. Re-examining pluton emplacement processes. J. Struct. Geol. 15, 191-206.

Paterson, S.R., Fowler, T.K., Schmidt, K.L., Yoshinobu, A.S., Yuan, E.S., Miller, R.B., 1998. Interpreting magmatic fabric patterns in plutons. Lithos 44, 53–82. doi:10.1016/S0024-4937(98)00022-X.

Penck, W., 1911. Der geologische Bau des Gebirges von Predazzo. Neues Jahrb. f. Min., Geol. u. Paläont. 32, 239—382.

Petronis, M.S., Hacker, D.B., Holm, D.K., Geissman, J.W., Harlen, S.S., 2005. Magnetic flow paths and paleomagnetism of the Miocene Stoddard Mountain laccolith, Iron Axis region, southwest Utah, USA. In: Martın-Hernandez, F., Luneburg, C.M., Aubourg, C., Jackson, M. (Eds.), Magnetic Fabric: Methods and Applications. Geol. Soc. Spec. Publ. 238, 251–283.

Petronis, M.S., O'Driscoll, B., Lindline, J., 2011. Late stage oxide growth associated with hydrothermal alteration of the Western Granite, Isle of Rum, NW Scotland. Geochemistry, Geophysics, Geosystems 12, 1.

Petronis, M.S., Delcamp, A., van Wyk de Vries, B., 2013. Magma emplacement into the Lemptégy scoria cone (Chaîne Des Puys, France) explored with structural, anisotropy of magnetic susceptibility, and paleomagnetic data. Bulletin of Volcanology 75, 753.

Petrovský, E.D., Kapička, A., 2006. On determination of the Curie point from thermomagnetic curves. J. Geophys. Res. Solid Earth 111, 1–10.

Pisa, G., Castellarin A., Lucchini, F., Rossi, P.L., Simboli, G., Bosellini, A., Sommavilla, E. 1980. Middle Triassic magmatism in Southern Alps. I: a review of general data in the Dolomites. Riv. It. Paleont. Strat. 85, 1093-1110.

Polteau, S., Ferré, E.C., Planke, S., Neumann, E.R., and Chevallier, L., 2008. How are saucer-shaped sills emplaced? Constraints from the Golden Valley Sill, South Africa. J. Geophys. Res. 113, B12104.

Raposo, M.I.B., Gastal, P.M.P., 2009. Emplacement mechanism of the main granite pluton of the Lavras do Sul intrusive complex, South Brazil, determined by magnetic anisotropies. Tectonophysics 466, 18-31.

Raposo, M.I.B., Pressi, L.F., de Assis Janasi, V., 2012. Magnetic fabrics and their relationship with the emplacement of the Piracaia pluton, SE Brazil. Int. J. Earth Sci. 101, 773–786. doi:10.1007/s00531-011-0696-5.

Roche, O., Druitt, T.H., Merle, O., 2000. Experimental study of caldera formation. J. Geophys. Res. 105, 395-416.

Rochette, P., Fillion, G., Mollard, P., Vergne, R., 1983. Utilisation d'un magnétomètre à effet Josephson pour l'analyse de l'anisotropie magnétique des roches. CR Acad. Sci. Paris 296, 557-559.

Rochette, P., Jackson, M., Aubourg, C., 1992. Rock magnetism and interpretation of anisotropy of magnetic susceptibility. Review of Geophysics 30, 209-226.

Román-Berdiel, T., Gapais, D., Brun, J.P., 1997. Granite intrusion along strike-slip zones in experiment and nature. Am. J. Sci. 297, 651–678. doi:10.2475/ajs.297.6.651.

Rosenberg, C.L., 2004. Shear zones and magma ascent: A model based on a review of the Tertiary magmatism in the Alps. Tectonics 23, 21. doi:10.1029/2003TC001526.

Sarti, M., Ardizzoni F. 1984. Tettonica triassica nel Gruppo di cima Pape-Pale di Sanson (Dolomiti Bellunesi). Mem. Sc. Geol. Padova, 36, 353-370.

Schaltegger, U., Brack, P., 2007. Crustal-scale magmatic systems during intracontinental strike-slip tectonics: U, Pb and Hf isotopic constraints from Permian magmatic rocks of the Southern Alps. Int. J. Earth Sci. 96, 1131–1151. doi:10.1007/s00531-006-0165-8.

Sloman, L., 1989. Triassic shoshonites from the Dolomites, northern Italy: alkaline arc rocks in a strike-slip setting. J. Geophys. Res. 94, 4655–4666.

Sparks, R.S.J., 2003. Forecasting volcanic eruptions. Earth and Planet. Sci. Lett. 210, 1-15.

Staehle, V., Frenzel, G., Hess, J. C., Saup, F., Schmidt, S. T. & Schneider, W., 2001. Permian metabasalt and Triassic alkaline dykes in the northern Ivrea zone: clues to the post-Variscan geodynamic evolution of the Southern Alps. Schweizerische Mineralogische und Petrographische Mitteilungen 81, 1–21.

Stefani, M., Furin, S., Gianolla, P., 2010. The changing climate framework and depositional dynamics of Triassic carbonate platforms from the Dolomites, Pal. Pal. Pal., 290, 43–57.

Talbot, J.Y., Chen, Y., Faure, M., 2005. A magnetic fabric study of the Aigoual-Saint Guiral-Liron granite pluton (French Massif Central) and relationships with its associated dikes. J. Geophys. Res. Solid Earth. 110, 1–14. doi:10.1029/2005JB003699.

Tarling, D.H., Hrouda, F., 1993. The Magnetic Anisotropy of Rocks. Chapman & Hall, London, pp. 217.

Tibaldi, A., Pasquarè, F.A., 2008. A new mode of inner volcano growth: The “flower intrusive structure”. Earth and Planet. Sci. Lett. 271, 202-208.

Tikoff, B., Teyssier, C., 1992. Crustal-scale, en echelon "P-shear’ tensional bridges: a possible solution to the batholithic room problem. Geology 20, 927–930. doi:10.1130/0091-7613(1992)020<0927:CSEEPS>2.3.CO;2.

Tomek, F., Žák, J., Chadima, M., 2014. Magma flow paths and strain patterns in magma chambers growing by floor subsidence: a model based on magnetic fabric study of shallow-level plutons in the Štiavnica volcano-plutonic complex, Western Carpathians. Bull. Volcanol. 76. doi:10.1007/s00445-014-0873-z.

Tomek, F., Žák, J., Verner, K., Holub, F. V., Sláma, J., Paterson, S. R., Memeti, V., 2017. Mineral fabrics in high-level intrusions recording crustal strain and volcano–tectonic interactions: the Shellenbarger pluton, Sierra Nevada, California. J. Geol. Soc. 174, 193-208.

Van der Voo, R., Klootwijk, C.T., 1972. Paleomagnetic reconnaissance study of the Flamanville granite with a special reference to the anisotropy of its susceptibility. Geol. Mijnbouw 51, 609-617.

Vardabasso, S., 1929. Rapporti tra attività magmatica e vicende tettoniche nella provincia petrografica di Predazzo: Studi Trentini Di Scienze Naturali, 11, 49–64.

Vardabasso, S., 1930. Carta geologica del territorio eruttivo di Predazzo e Monzoni: Ufficio Idrografico del Magistrato alle Acque di Venezia. scale 1:25000, 2 sheet.

Viel G., 1979. Litostratigrafia ladinica: una revisione. Ricostruzione paleogeografica e paleostrutturale dell'area Dolomitica-Cadorina (Alpi Meridionali). Riv. It. Paleont. Strat. 85(1), 85–125, 85(2), 297–352.

Viel, G., 1982. Polarità tettonica e vulcanismo ladino-carnici del Sudalpino. Rend. Soc. Geol. Ital. v. 4 (1981), pp.261-262, Roma.

Visonà, D., 1997. The Predazzo multipulse intrusive body (Western Dolomites, Italy). Field and mineralogical studies. Mem. Sci. Geol. 49, 117– 125.

Visonà, D., Fioretti, A.M., Poli, M.E., Zanferrari, A., Fanning, M., 2007. U-Pb SHRIMP zircon dating of andesite from the Dolomite area (NE Italy): geochronological evidence for the early onset of Permian Volcanism in the eastern part of the southern Alps. Swiss J. Geosci. 100, 313–324. doi:10.1007/s00015-007-1219-z.

Von Richthofen, F.F., 1860. Geognostische Beschreibung der Umgebung von Predazzo, Sanct Cassian und der Seiser Alpe in Süd-Tyrol. Verlag von Justus Perthes, Gotha.

Zanetti, A., Mazzucchelli, M., Sinigoi, S., Giovanardi, T., Peressini, G., Fanning, M., 2013. SHRIMP U-Pb ZirconTriassic Intrusion Age of the Finero Mafic Complex (Ivrea-Verbano Zone, Western Alps) and its Geodynamic Implications. J. Petrol. 54, 2235–2265. doi:10.1093/petrology/egt046.

Wotzlaw, J. F., Brack, P., & Storck, J. C., 2018. High-resolution stratigraphy and zircon U–Pb geochronology of the Middle Triassic Buchenstein Formation (Dolomites, northern Italy): precession-forcing of hemipelagic carbonate sedimentation and calibration of the Anisian–Ladinian boundary interval. Journal of the Geological Society, 175(1), 71-85.

Figures

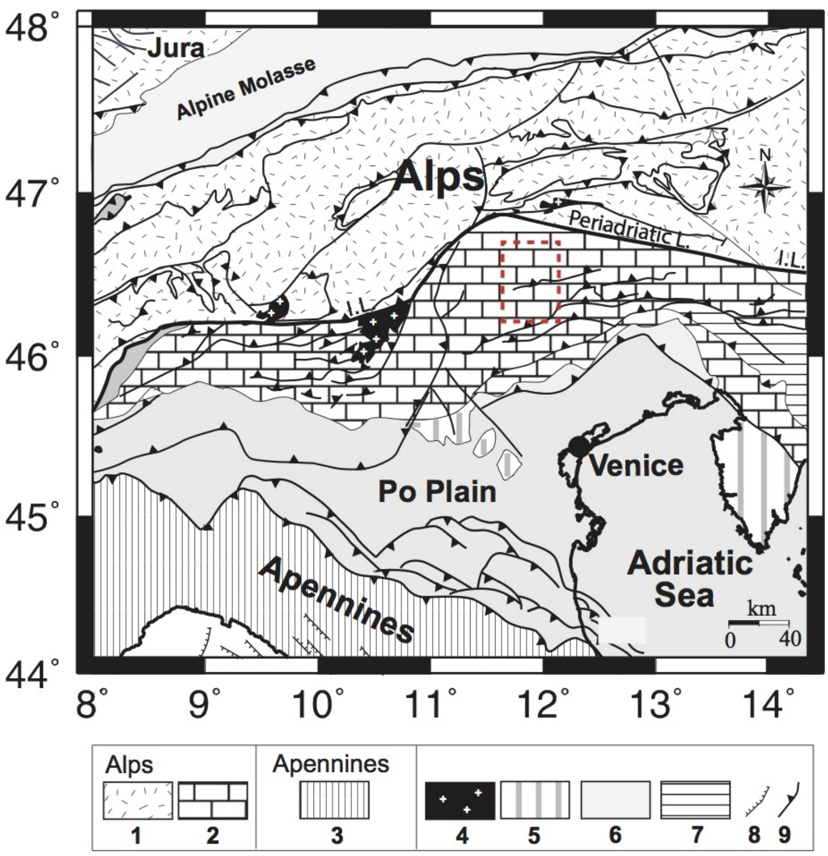

Figure 1: Simplified geological map of the Southern Alps. Alps: 1) Australpine, Penninic and Helvetic units; 2) Southern Alps units. Apennines: 3) Apenninic units; 4) ~~Tertiary and Quaternary~~Cenozoic volcanic and plutonic bodies; 5) foreland units; 6) foreland basin units; 7) Dinaric units; 8) normal faults; 9) thrust faults. Redrawn and simplified from Bigi et al. (1990). The dashed rectangle shows the location of the map of Figure 2. I.L.: Insubric line.

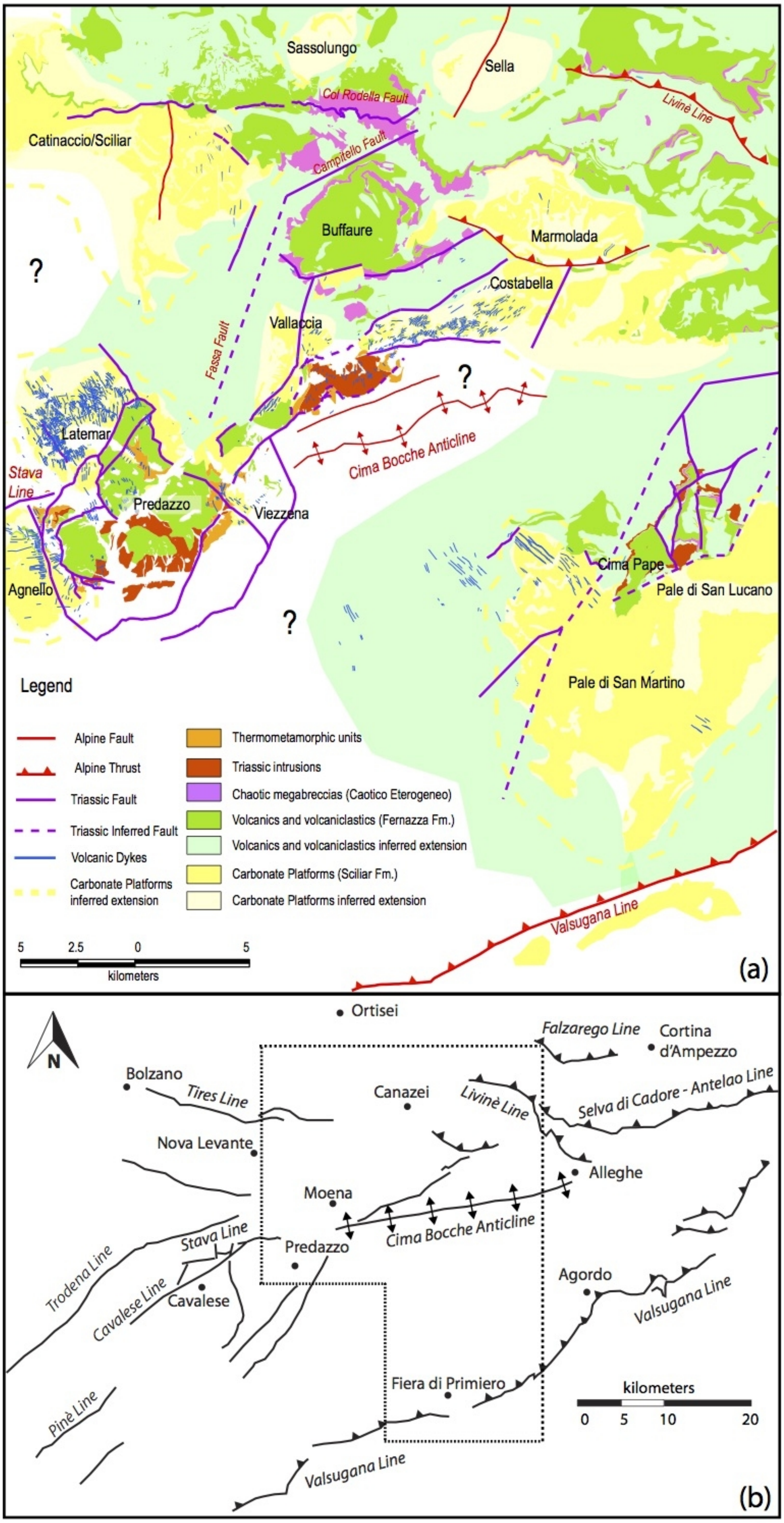

Sassolungo
Sella
Col Rodella Fault
Livinè Line
Catinaccio/Sciliar
Campitello Fault
Buffaure
Marmolada
?
Costabella
Fassa Fault
Vallaccia
?
Latemar
Cima Bocche Anticline
Stava Line
Predazzo
Viezzena
Cima Pape
Agnello
Pale di San Lucano
?
Pale di San Martino
Legend
Alpine Fault
Alpine Thrust
Triassic Fault
Triassic Inferred Fault
Volcanic Dykes
Carbonate Platforms inferred extension
Thermometamorphic units
Triassic intrusions
Chaotic megabreccias (Caotico Eterogeneo)
Volcanics and volcaniclastics (Fernazza Fm.)
Volcanics and volcaniclastics inferred extension
Carbonate Platforms (Sciliar Fm.)
Carbonate Platforms inferred extension
5 2.5 0 5
kilometers
Valsugana Line
(a)
Ortisei
Falzarego Line
Cortina d'Ampezzo
N
Bolzano
Tires Line
Canazei
Livinè Line
Selva di Cadore - Antelao Line
Nova Levante
Alleghe
Moena
Stava Line
Cima Bocche Anticline
Predazzo
Trodena Line
Cavalese Line
Agordo
Cavalese
Valsugana Line
Fiera di Primiero
kilometers
0 5 10 20
Pinè Line
Valsugana Line
(b)

Figure 2: a) Unrestored paleogeographic map at Ladinian times of the central-western region of the Dolomites. Notice the regional extent of volcanics and the continuity of plutonic bodies and associated thermometamorphic rocks for more than 20 km in a SW-NE direction, i.e., parallel to major Triassic faults. Cenozoic faults and structures are shown for reference. The location of the map is shown in Fig. 1. b) Simplified tectonic map of the Dolomites, showing only major faults, not differentiated by their age. The dashed area represents the location of panel a.

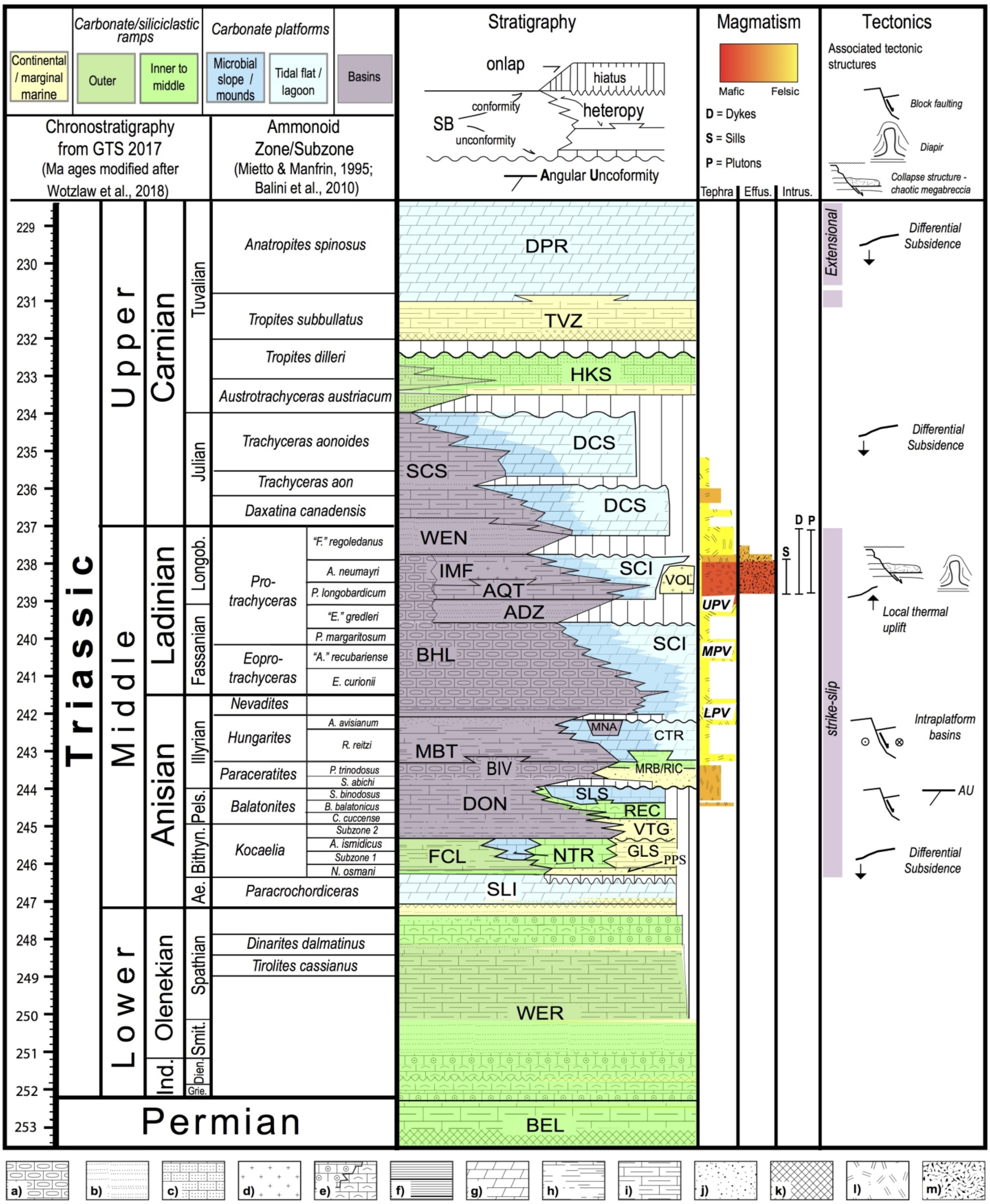

Figure 3: Schematic bio-chrono-stratigraphic scheme of the Middle-Upper Triassic succession of the Dolomites with the most important magmatic pulse recorded as ash falls, tefhras or effusives. The position of the known possible source volcanic areas from the Southern Alps is indicated. In the subsurface of Venetian Plain, a significant number of volcanic products (mainly effusve and

intrusive) is known (e.g., Brusca et al., 1981) Lithostratigraphic abbreviations: BEL: Bellerophon Formation; WER: Werfen Formation; SLI: Lower Serla Dolomite; PPS: Piz da Peres Conglomerate; FCL: Coll'Alto dark Limestones~~Collalto Formation~~; NTR: Monte Rite Formation; GLS: Gracilis Formation; VTG: Voltago Conglomerate; DON: Dont Formation; REC: Recoaro Limestone; SLS Upper Serla Dolomite/Formation; MRB/RIC: Richthofen Conglomerate and Morbiac dark Limestone; BIV: Bivera Formation; MBT: Ambata Formation; MNA: Moena Formation; CTR: Contrin Formation; BHL: Livinallongo Formation; SCI: Sciliar Formation; ADZ: Zoppè Sandstone; AQT: Aquatona Formation; IMF: Fernazza Volcanic Complex (Fernazza Formation); WEN: Wengen Formation; SCS: San Cassiano Formation; DCS: Cassian Dolomite; HKS: Heiligkreuz Formation; TVZ: Travenanzes Formation; DPR: Dolomia Principale. Lithologies: a) cherty limestone; b) sandstone; c) sandy limestone; d) volcanics and volcaniclastics; e) oolitic-bioclastic limestone; f) black platy limestone or dolostone, black shale; g) dolostone; h) marlstone, claystone and shale; i) marly limestone; j) conglomerate; k) evaporates; l) tuffs, pyroclastics; m) lava, pillow-lava-pillow breccia; ~~m) volcanos with mainly explosive eruptions;~~ m) volcanos with mainly effusive eruptions. LPV, MPV, UPV= Lower -Middle - Upper Pietra Verde. ~~Ages from GTS 2012 modified after Wotzlaw et al. (2018).~~

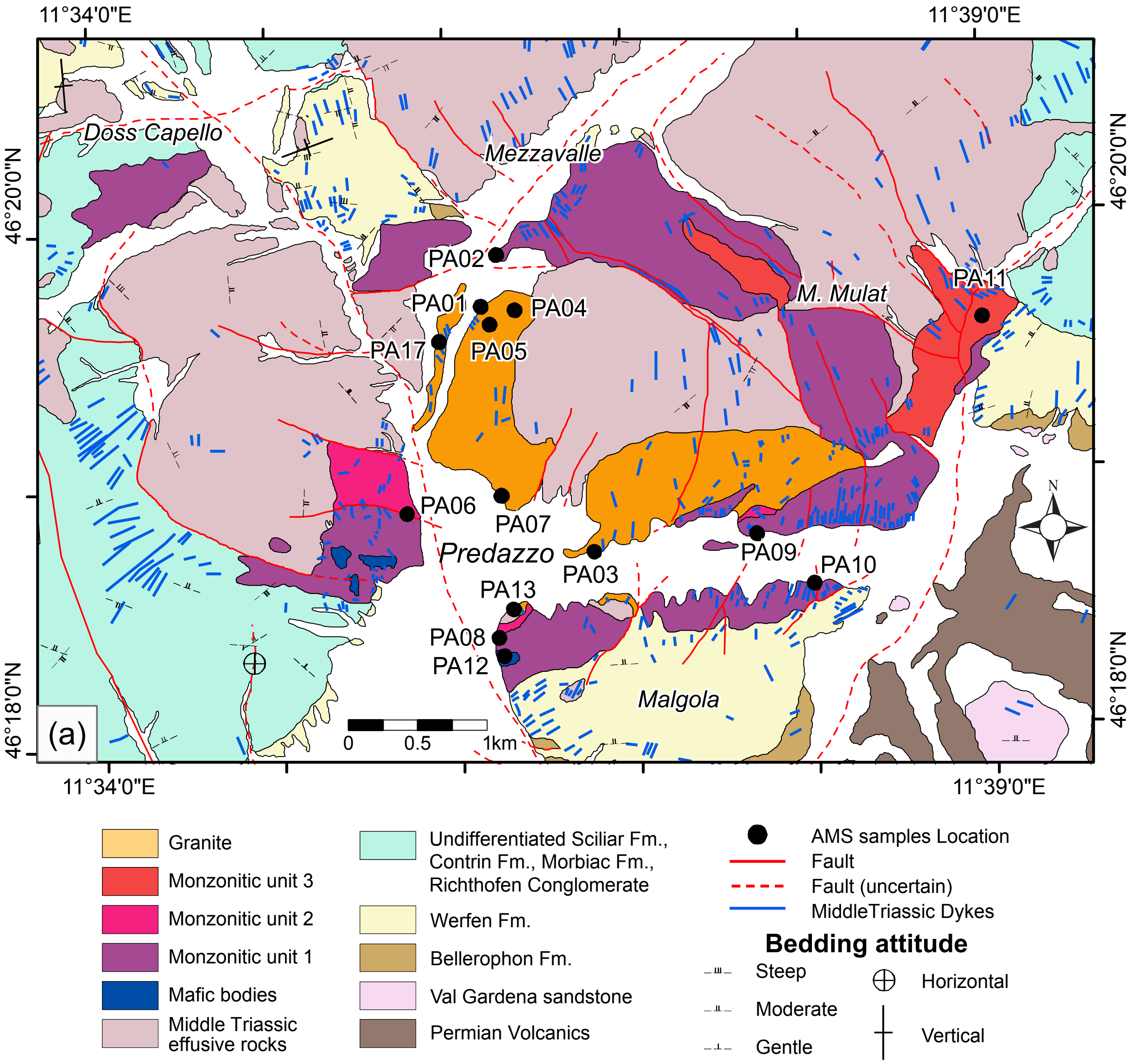

11°34'0"E
11°39'0"E
46°20'0"N
46°18'0"N
Doss Capello
Mezzavalle
M. Mulat
Predazzo
Malgola
PA01
PA02
PA03
PA04
PA05
PA06
PA07
PA08
PA09
PA10
PA11
PA12
PA13
PA17
(a)
0
0.5
1km
N
Granite
Monzonitic unit 3
Monzonitic unit 2
Monzonitic unit 1
Mafic bodies
Middle Triassic effusive rocks
Undifferentiated Sciliar Fm., Contrin Fm., Morbiac Fm., Richthofen Conglomerate
Werfen Fm.
Bellerophon Fm.
Val Gardena sandstone
Permian Volcanics
AMS samples Location
Fault
Fault (uncertain)
MiddleTriassic Dykes
Bedding attitude
Steep
Moderate
Gentle
Horizontal
Vertical

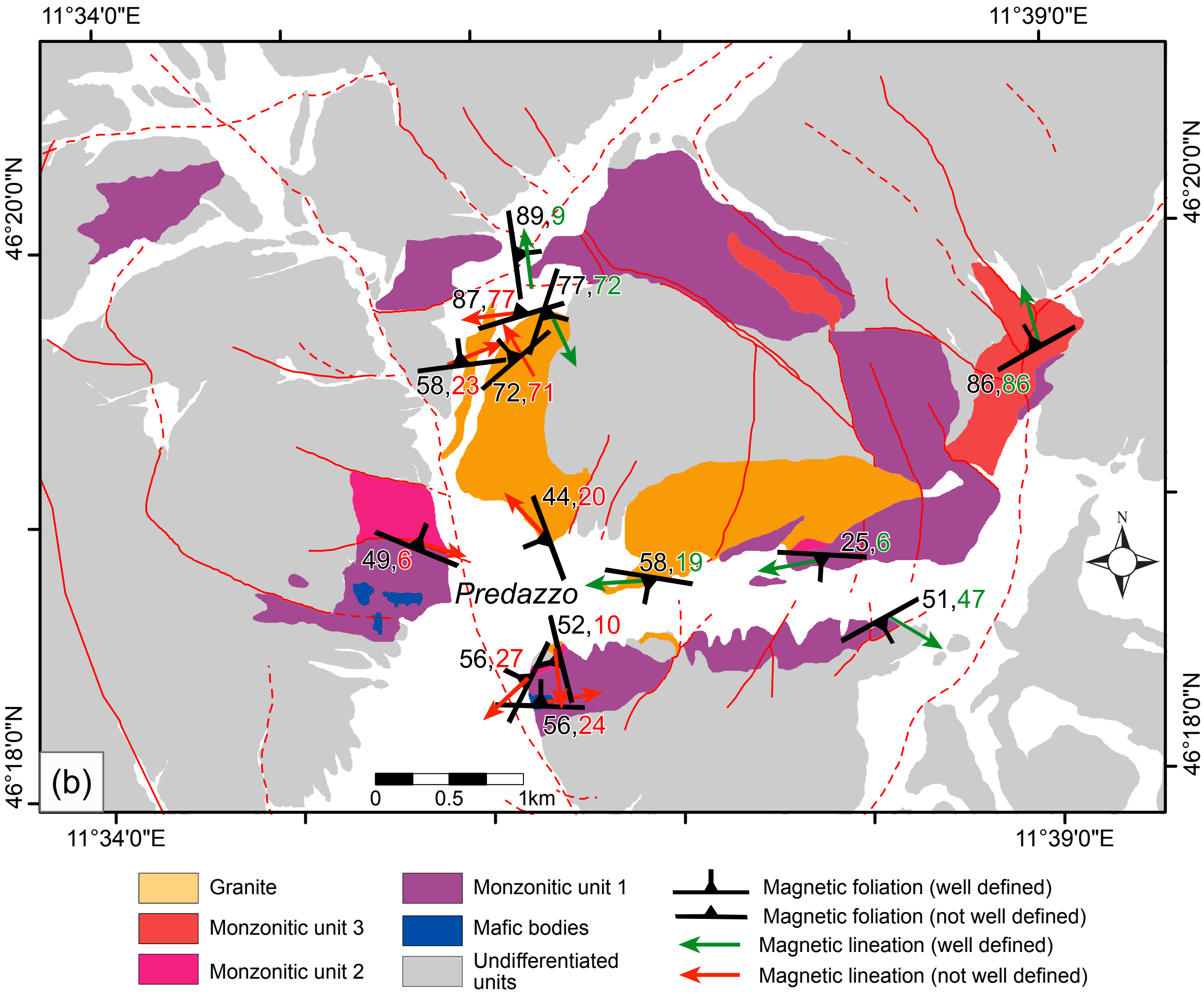

Figure 4: Geological map of the pre-Quaternary units of the Predazzo area (from Visonà, 1997), showing the location of the samplig sites (a) and ~~relative~~ measured magnetic foliations and lineations (b). The two numbers besides each site indicate the magnetic foliation and lineation dips, respectively.

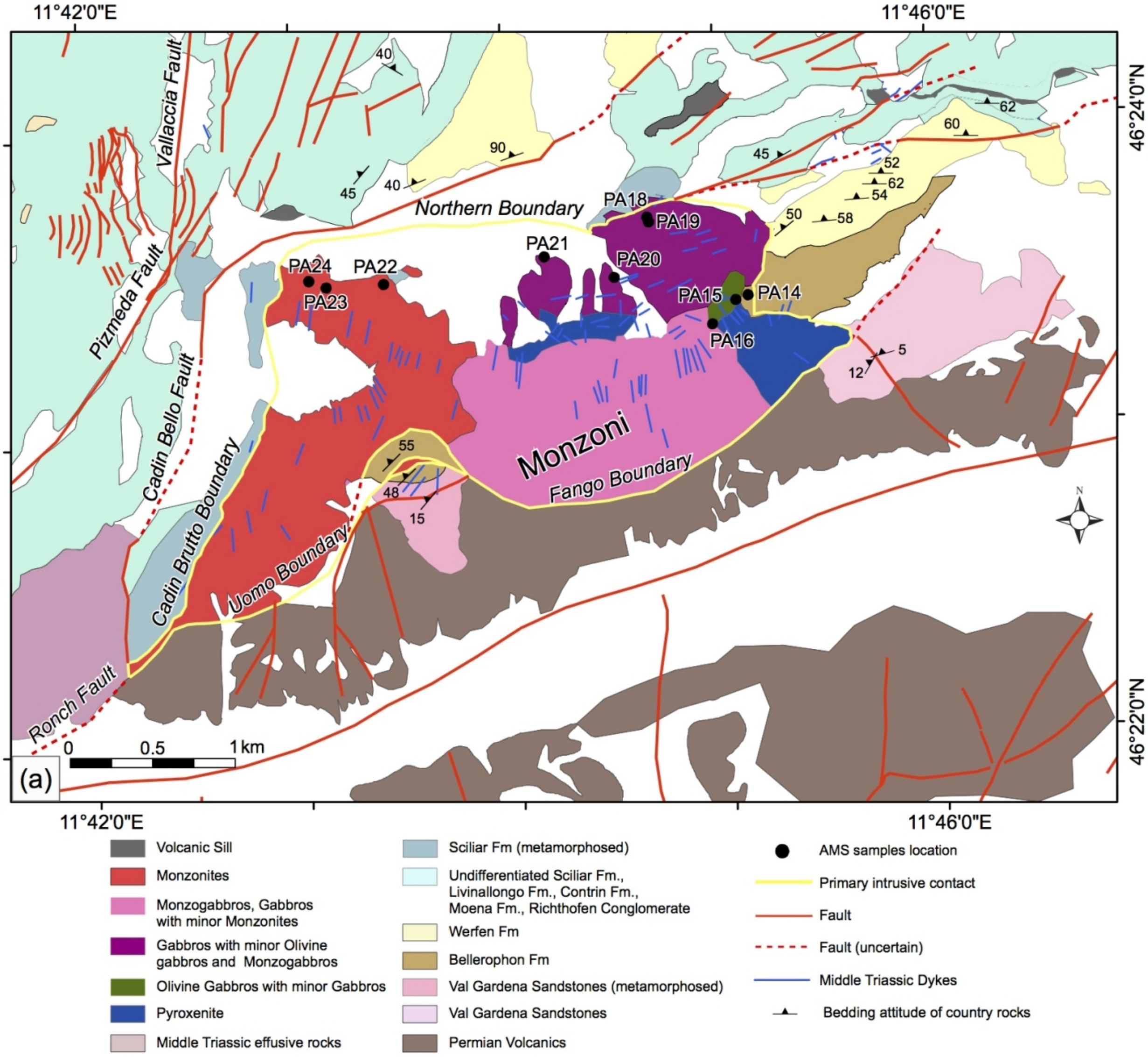

11°42'0"E
11°46'0"E
46°24'0"N
46°22'0"N
Vallaccia Fault
Pizmeda Fault
Cadin Bello Fault
Cadin Brutto Boundary
Uomo Boundary
Ronch Fault
Northern Boundary
Fango Boundary
Monzoni
PA14
PA15
PA16
PA18
PA19
PA20
PA21
PA22
PA23
PA24
0
0.5
1 km
(a)
N
Volcanic Sill
Monzonites
Monzogabbros, Gabbros with minor Monzonites
Gabbros with minor Olivine gabbros and Monzogabbros
Olivine Gabbros with minor Gabbros
Pyroxenite
Middle Triassic effusive rocks
Sciliar Fm (metamorphosed)
Undifferentiated Sciliar Fm., Livinallongo Fm., Contrin Fm., Moena Fm., Richthofen Conglomerate
Werfen Fm
Bellerophon Fm
Val Gardena Sandstones (metamorphosed)
Val Gardena Sandstones
Permian Volcanics
AMS samples location
Primary intrusive contact
Fault
Fault (uncertain)
Middle Triassic Dykes
Bedding attitude of country rocks

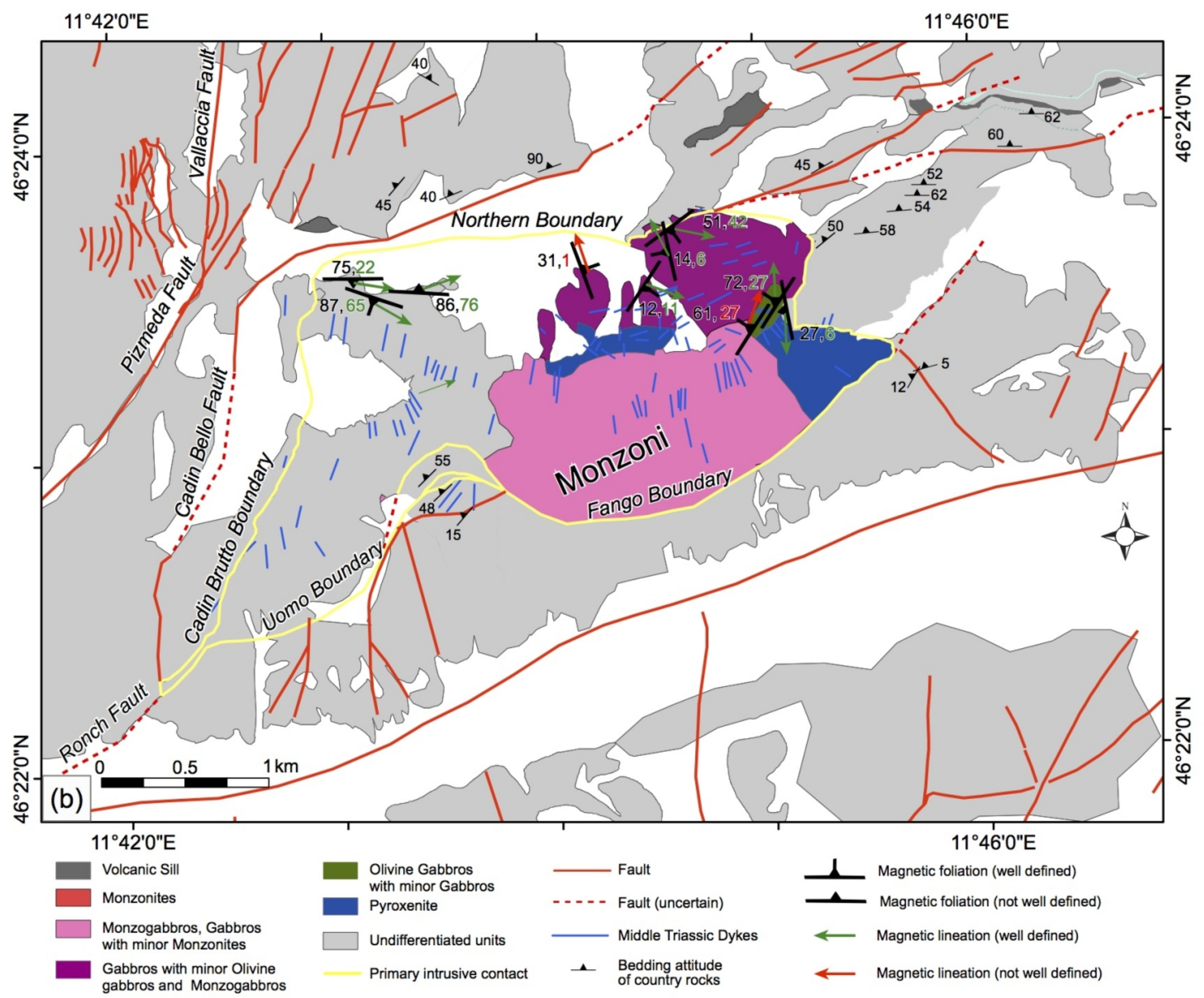

Figure 5: Geological map of the pre-Quaternary units of the Monzoni area, showing the location of the sampling sites (a) and ~~relative~~ measured magnetic foliations and lineations (b). The two numbers ~~besides~~at each site indicate the magnetic foliation and lineation dips, respectively.

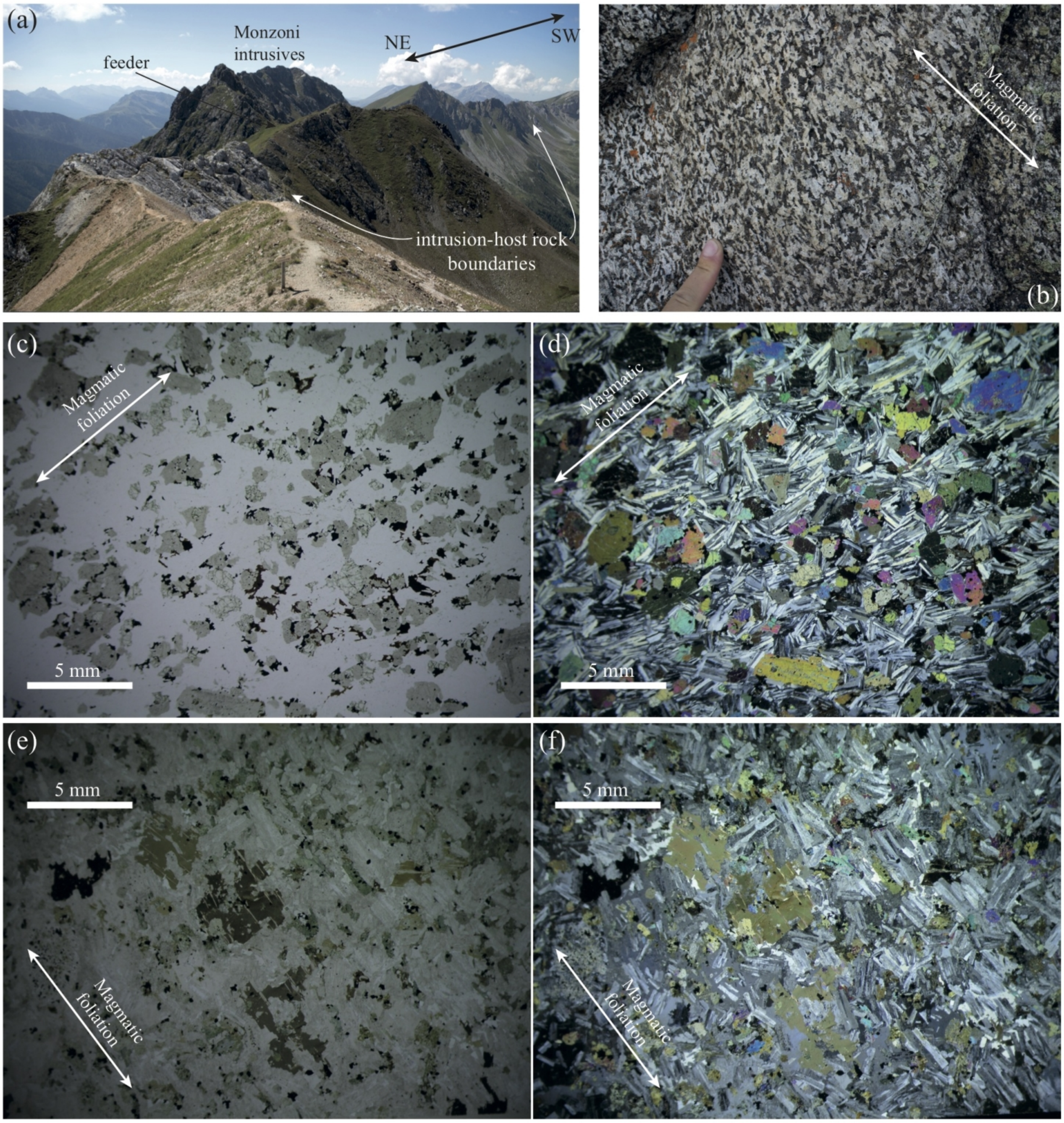

Figure 6: a) Monte Monzoni crest, showing the contacts between intrusive and host rocks. The location of the feeder area is also shown. b) Granite from the Predazzo body showing a well defined magmatic foliation; c) Olivine gabbro showing preferred orientation of plagioclase and pyroxene crystals (sample PA20); c) Monzonite showing preferred orientation of plagioclase and biotite crystals (sample PA22A, same location of sample 22).

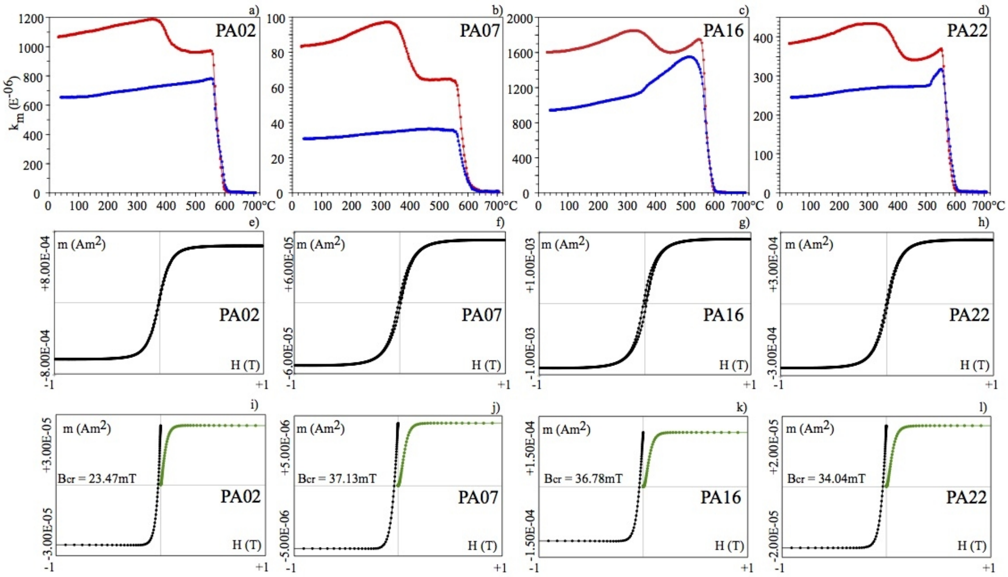

Figure 76: Magnetic mineralogy results for selected samples from Predazzo and Monzoni plutons. a-d) Thermomagnetic curves; red and blue lines represent the heating □-cooling cycle respectively. e-h) Hysteresis loops, corrected for the paramagnetic linear trend. i-l) IRM acquisition curves (green lines) and backfield applications (black lines).

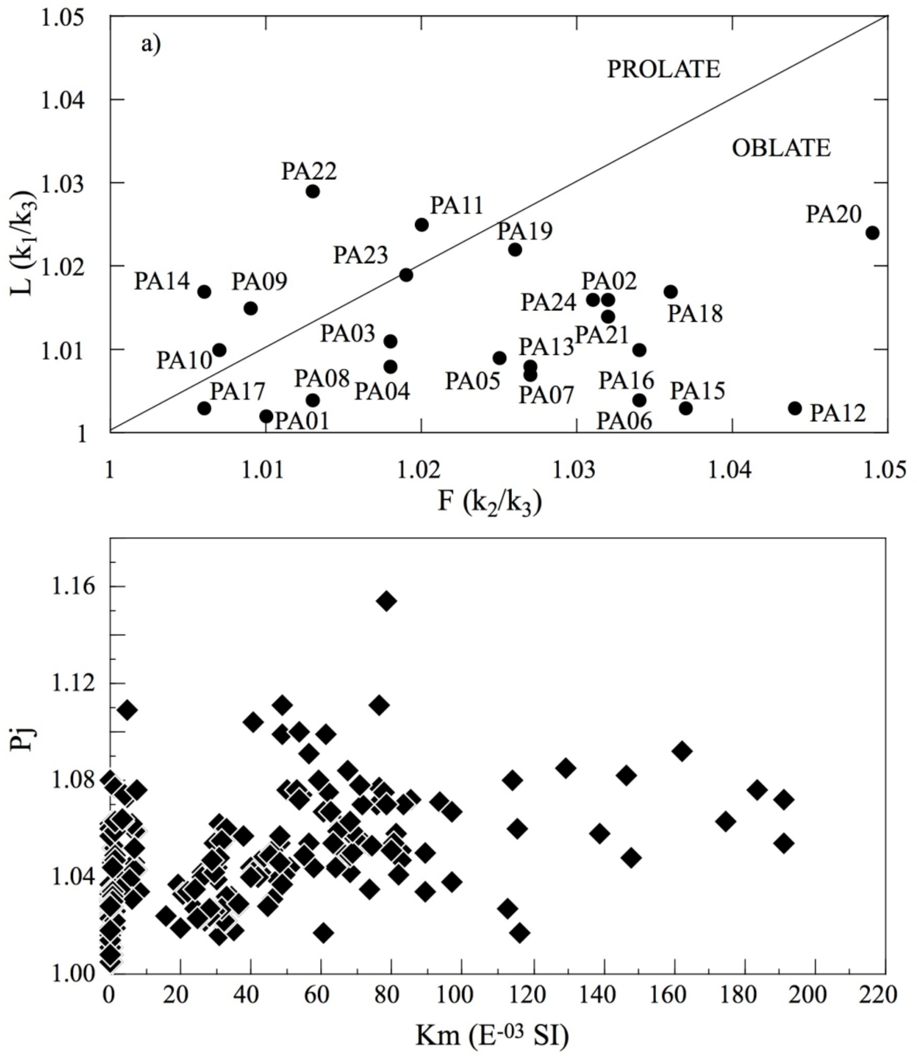

Figure 87: Shape parameters for the analyzed sites: a) F-L diagram; b) K-Pj' -T diagram.

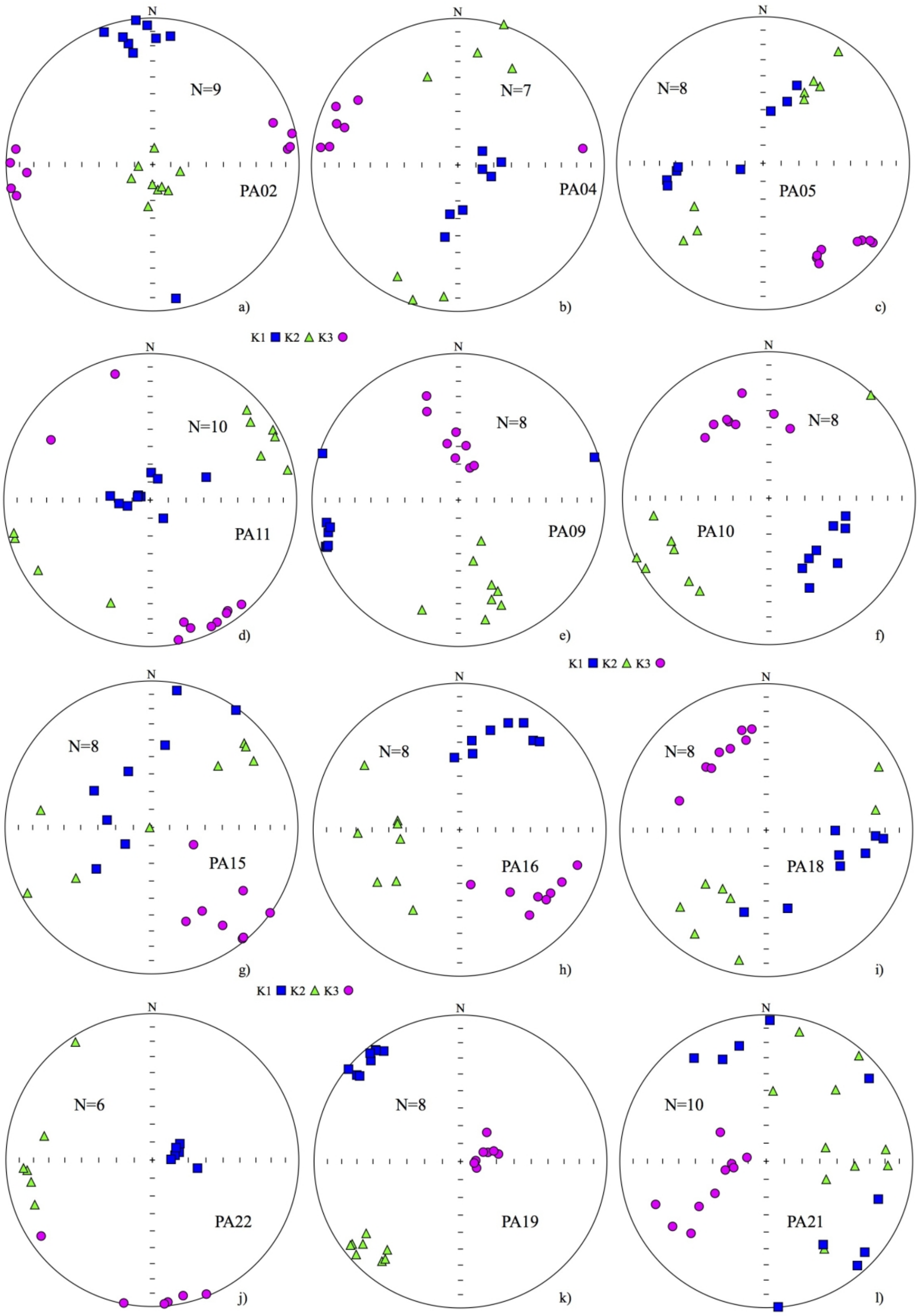

Figure 98: Low-field AMS plots for representative sites in the Predazzo (a-f) and Monzoni (ig-l) intrusive bodies. Data are plotted on lower hemisphere, equal area projections. Squares, triangles and circles represent maximum, intermediate and minimum axes, respectively, plotted relative to paleo-geographic coordinates.

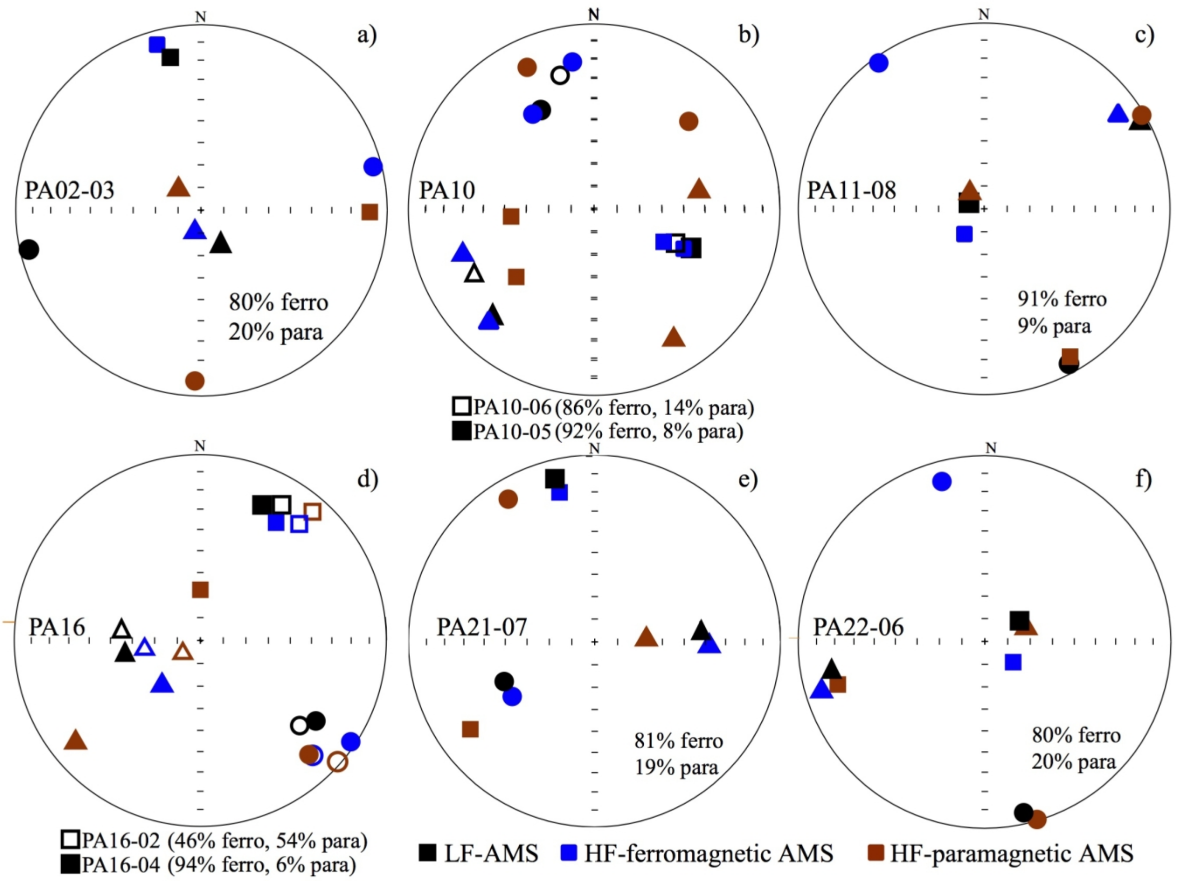

Figure 10~~9~~: Lower hemisphere equal area projections of the principal axes of the low-field/room temperature (black symbols), high-field paramagnetic (red symbols) and high-field ferromagnetic (blu symbols) susceptibility ellipsoids. Percentages of the relative contribution of ferromagnetic and paramagnetic susceptibility to the magnetic fabric is also reported for each specimen.

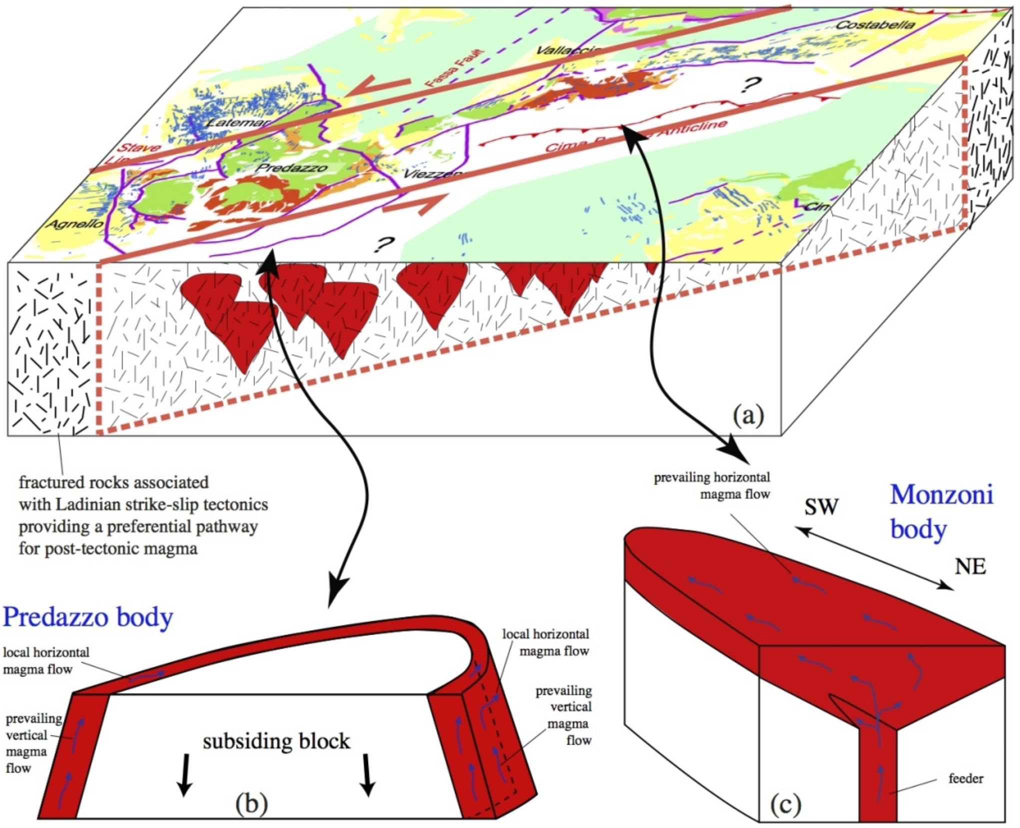

Figure 11: a) Sketch showing the emplacement of Ladinian intrusive bodies along a wide fractured zone associated with previous strike-slip tectonics. b) Sketch of the emplacement mode for the Predazzo body; c) Sketch of the emplacement mode for the Monzoni body.

TABLES

Site	Lithology	Lat	Long	N	Km	std	L	std	F	std	Pj	std	T	std	D,I (k_1)	E_{2-3}	D,I (k_3)	E_{1-2}
PA01	Albitized granite	46°19'41"N	11°36'09"E	10	4.04E^{-04}	3.75 E^{-04}	1.002	0.01	1.010	0.011	1.013	0.018	0.667	0.461	263,77	74.7/36.4	162,3	40.9/21.3
PA02	Monzonites	46°19'53"N	11°36'15"E	8	6.90E^{-02}	2.70E^{-03}	1.016	0.006	1.032	0.006	1.049	0.006	0.318	0.217	353,9	11.3/7.8	262,1	9.4/5.4
PA03	Biotite granite	46°18'42"N	11°36'45"E	8	4.48E^{-03}	3.3E^{-03}	1.011	0.009	1.018	0.013	1.030	0.01	0.256	0.443	266,19	23.7/20.5	9,32	24.1/18.5
PA04	Albitized granite	46°19'39"N	11°36'21"E	6	1.03E^{-04}	1.01 E^{-05}	1.008	0.002	1.018	0.005	1.026	0.006	0.394	0.188	154,72	23.5/3.6	288,13	11.2/5.6
PA05	Albitized granite	46°19'36"N	11°36'13"E	7	8.43E^{-05}	3.88 E^{-05}	1.009	0.01	1.025	0.015	1.035	0.02	0.483	0.329	329,71	35.9/8.2	139,18	18.1/5.9
PA06	Diorite	46°18'52"N	11°35'44"E	9	4.41E^{-02}	8.80 E^{-03}	1.004	0.006	1.034	0.008	1.042	0.008	0.809	0.284	107,6	37.2/4.7	202,41	6.3/4.1
PA07	Biotite granite	46°18'56"N	11°36'14"E	5	6.37E^{-03}	3.99 E^{-04}	1.007	0.008	1.027	0.006	1.036	0.012	0.577	0.184	317,20	45.8/13.3	70,46	16.1/9.3
PA08	Monzodiorite	46°18'23"N	11°36'09"E	8	3.72E^{-02}	3.13 E^{-03}	1.004	0.003	1.013	0.006	1.018	0.006	0.496	0.286	227,27	39.4/7.7	116,34	10.2/8.1
PA09	Monzodiorite	46°18'46"N	11°37'40"E	8	3.11E^{-02}	1.47 E^{-03}	1.015	0.003	1.009	0.004	1.024	0.003	-0.244	0.283	260,6	12.6/4.1	3,65	12.3/3.7
PA10	Monzonites	46°18'38"N	11°37'59"E	8	7.39E^{-03}	9.51 E^{-03}	1.01	0.007	1.007	0.005	1.017	0.012	-0.204	0.262	121,47	13.1/4	331,39	9.2/5.2
PA11	Monzonites to Syenite	46°18'52"N	11°39'26"E	9	2.91E^{-02}	2.00 E^{-02}	1.025	0.01	1.02	0.09	1.046	0.012	-0.099	0.265	344,86	18.9/7.4	151,4	16.6/7.1
PA12	Clinopyroxenite	46°18'16"N	11°36'11"E	8	1.63E^{-01}	2.33 E^{-02}	1.003	0.01	1.044	0.015	1.052	0.015	0.858	0.318	79,24	68.5/18.3	182,26	18.4/12.6
PA13	Biotite granite	46°18'29"N	11°36'17"E	4	1.63E^{-03}	7.49 E^{-04}	1.008	0.007	1.027	0.017	1.037	0.015	0.542	0.423	174,10	37.2/11.8	76,38	17.6/9.4
PA14	Monzodiorite	46°19'33"N	11°35'54"E	9	2.57E^{-02}	3.13 E^{-03}	1.017	0.004	1.006	0.009	1.024	0.006	-0.495	0.409	177,6	13.9/6.9	75,63	40.1/9.6
PA15	Gabbros	46°23'25"N	11°45'07"E	9	7.34E^{-02}	2.53 E^{-02}	1.003	0.013	1.037	0.039	1.045	0.046	0.850	0.55	357,67	70.6/14.9	137,18	24.5/15.0
PA16	Gabbros (cumulate)	46°23'25"N	11°45'04"E	9	1.63E^{-03}	1.64 E^{-03}	1.01	0.012	1.034	0.025	1.047	0.028	0.532	0.36	26,27	25.4/6.5	132,29	12.0/4.8
PA17	Albitized granite	46°23'20"N	11°44'57"E	9	1.02E^{-04}	1.32 E^{-05}	1.003	0.004	1.006	0.004	1.010	0.007	0.334	0.413	68,23	35.2/15.9	173,32	24.7/17.8
PA18	Olivine gabbros	46°23'41"N	11°44'39"E	8	7.68E^{-02}	1.12 E^{-02}	1.017	0.009	1.036	0.01	1.055	0.011	0.351	0.272	107,42	18.4/6.3	331,39	16.4/3.8
PA19	Olivine gabbros	46°23'40"N	11°44'40"E	8	3.07E^{-02}	1.30 E^{-03}	1.022	0.005	1.026	0.003	1.049	0.006	0.084	0.12	317,6	7.3/3.2	73,76	6.4/3.8
PA20	Olivine gabbros	46°23'30"N	11°44'30"E	9	5.26E^{-02}	6.07 E^{-03}	1.024	0.01	1.049	0.017	1.075	0.015	0.344	0.239	108,11	17.8/11.0	310,78	18.6/7.6
PA21	Monzogabbros	46°23'34"N	11°44'10"E	9	6.22E^{-02}	2.19 E^{-02}	1.014	0.014	1.032	0.018	1.048	0.01	0.383	0.481	336,1	19.1/11.9	244,59	25.0/10.1

Site	Lithology	Lat	Long	N	Km	std	L	std	F	std	Pj	std	T	std	D,I (k_1)	E_{2-3}	D,I (k_3)	E_{1-2}
PA22	Monzonites	46°23'30"N	11°43'24"E	6	$3.73E^{-02}$	$1.54\ E^{-02}$	1.029	0.007	1.013	0.011	1.043	0.016	-0.364	0.185	76,76	5.7/4.4	184,4	37.6/2.8
PA23	Monzonites	46°23'30"N	11°43'08"E	8	$7.36E^{-02}$	$2.79\ E^{-02}$	1.019	0.007	1.019	0.015	1.038	0.013	-0.02	0.47	121,65	10.8/7.1	25,3	14.8/7.8
PA24	Monzonites	46°23'31"N	11°43'03"E	9	$8.14E^{-02}$	$2.10\ E^{-02}$	1.016	0.007	1.031	0.014	1.049	0.021	0.325	0.149	97,22	22.4/11.7	0,15	17.3/11.0

Table I: Location of sampling sites in the Predazzo and Monzoni plutons and measured magnetic parameters. N = number of specimens; $K_m = (k_{max} + k_{int} + k_{min}) / 3$ (mean susceptibility, in SI units); $L=k_1/k_2$; $F=k_3/k_1$ $Pj = \exp\{2[(\eta_1 - \eta)^2 + (\eta_2 - \eta)^2 + (\eta_3 - \eta)^2]\}^{1/2}$ (corrected anisotropy degree; Jelinek, 1981); $T = 2(\eta_2 - \eta_3) / (\eta_1 - \eta_3) - 1$ (shape factor; Jelinek, 1981); $\eta_1 = \ln k_1$; $\eta_2 = \ln k_2$; $\eta_3 = \ln k_3$; $\eta = (\eta_1 + \eta_2 + \eta_3) / 3$; D, I ($k_1$) = declination and inclination of the maximum susceptibility axis (paleo-geographic coordinates); D,I (k_3) = declination and inclination of the minimum susceptibility axis (paleo-geographic coordinates); α_{95}: confidence angles; std: standard deviation.